# 8 DMFT for Linear Response Functions

Eva Pavarini
Institute for Advanced Simulation
Forschungszentrum Jülich

## Contents



E. Pavarini, E. Koch, A. Lichtenstein, and D. Vollhardt (eds.)
Dynamical Mean-Field Theory of Correlated Electrons
Modeling and Simulation Vol. 12
Forschungszentrum Jülich, 2022, ISBN 978-3-95806-619-9
http://www.cond-mat.de/events/correl22

# 1 Introduction: the many-body problem

The electronic many-body problem, in the non-relativistic limit and in the Born-Oppenheimer approximation, is described by the Hamiltonian

$$\hat{H}_e = -\frac{1}{2}\sum_i \nabla_i^2 - \sum_i \sum_\alpha \frac{Z_\alpha}{|\boldsymbol{r}_i - \boldsymbol{R}_\alpha|} + \sum_{i>j} \frac{1}{|\boldsymbol{r}_i - \boldsymbol{r}_j|} + \sum_{\alpha>\alpha'} \frac{Z_\alpha Z_{\alpha'}}{|\boldsymbol{R}_\alpha - \boldsymbol{R}_{\alpha'}|}, \tag{1}$$

where $\{\boldsymbol{r}_i\}$ are electron coordinates, $\{\boldsymbol{R}_\alpha\}$ nuclear coordinates and $Z_\alpha$ the nuclear charges. Using a complete one-electron basis, for example the basis $\{\varphi_a(\boldsymbol{r})\}$, where $\{a\}$ are the quantum numbers, we can write this Hamiltonian in second quantization as

$$\hat{H}_e = \underbrace{-\sum_{ab} t_{ab} c_a^\dagger c_b}_{\hat{H}_0} + \underbrace{\frac{1}{2}\sum_{aa'bb'} U_{aa'bb'}\; c_a^\dagger c_{a'}^\dagger c_{b'} c_b}_{\hat{H}_U}.$$

Here the hopping integrals are given by

$$t_{ab} = -\int d\mathbf{r}\; \overline{\varphi_a}(\boldsymbol{r}) \left( -\frac{1}{2}\nabla^2 \underbrace{- \sum_\alpha \frac{Z_\alpha}{|\boldsymbol{r} - \boldsymbol{R}_\alpha|}}_{v_{\rm en}(\boldsymbol{r})} \right) \varphi_b(\boldsymbol{r}),$$

while the elements of the Coulomb tensor are

$$U_{aa'bb'} = \int d\mathbf{r}_2 \int d\mathbf{r}_2\; \overline{\varphi_a}(\boldsymbol{r}_1)\, \overline{\varphi_{a'}}(\boldsymbol{r}_2)\; \frac{1}{|\boldsymbol{r}_1 - \boldsymbol{r}_2|}\; \varphi_{b'}(\boldsymbol{r}_2)\, \varphi_b(\boldsymbol{r}_1).$$

In principle, all complete one-electron bases are equivalent. In practice, since, in the general case, we cannot solve the $N$-electron problem exactly, some bases are better than others. One possible choice for the basis are the Kohn-Sham orbitals, $\left\{\varphi_a^{\rm KS}(\boldsymbol{r})\right\}$, obtained, e.g., in the local density approximation (LDA).[1] In this case, it is useful to replace the electron-nuclei interaction $v_{\rm en}(\boldsymbol{r})$ with the DFT potential $v_R(\boldsymbol{r})$, which includes in addition the Hartree term $v_{\rm H}(\boldsymbol{r})$ and the (approximate) exchange-correlation potential $v_{\rm xc}(\boldsymbol{r})$

$$v_{\rm R}(\boldsymbol{r}) = v_{\rm en}(\boldsymbol{r}) + \underbrace{\int d\mathbf{r}'\; \frac{n(\boldsymbol{r}')}{|\boldsymbol{r} - \boldsymbol{r}'|}}_{v_{\rm H}(\boldsymbol{r})} + v_{\rm xc}(\boldsymbol{r}),$$

so that

$$\tilde{t}_{ab} = -\int d\mathbf{r}\; \overline{\varphi_a^{\rm KS}}(\boldsymbol{r}) \left( -\frac{1}{2}\nabla^2 + v_{\rm R}(\boldsymbol{r}) \right) \varphi_b^{\rm KS}(\boldsymbol{r}). \tag{2}$$

To avoid double counting (DC), we have however to subtract from $\hat{H}_U$ the term $\hat{H}_{\rm DC}$, which describes the Coulomb terms already included in the hopping integrals

$$\hat{H}_e = \underbrace{-\sum_{ab} \tilde{t}_{ab}\, c_a^\dagger c_b}_{\hat{H}_0 = \hat{H}_e^{\rm LDA}} + \underbrace{\frac{1}{2}\sum_{aba'b'} \tilde{U}_{aa'bb'}\; c_a^\dagger c_{a'}^\dagger c_{b'} c_b - \hat{H}_{\rm DC}}_{\Delta \hat{H}_U}.$$

[1] For the purpose of many-body calculations the differences between LDA, GGA, or their plain extensions are in practice negligible; for simplicity, in the rest of the lecture, we thus adopt LDA as representative functional.

For weakly-correlated systems, in the Kohn-Sham basis, the effects included in $\Delta\hat{H}_U$ can, in first approximation, either be neglected or treated as a perturbation. This implies that $\hat{H}_e^{\rm LDA} \sim \hat{H}_{\rm eff}$, where $\hat{H}_{\rm eff}$ is the effective model which provides a good description of the system (at least) at low energy, and which describes emergent effective "elementary particles" and their interactions. Hypothetically, one could imagine that $\hat{H}_{\rm eff}$ is obtained via a canonical transformation, so that $\hat{H}_{\rm eff} \sim \hat{S}^{-1}\hat{H}_e\,\hat{S}$, although the exact form of the operator $\hat{S}$ is unknown.

A defining feature of strong-correlation effects is that they cannot be described via a single-electron Hamiltonian. An effective model $\hat{H}_{\rm eff}$ of form $\hat{H}_e^{\rm LDA}$ does not capture the Mott metal-insulator transition, no matter what the specific values of the parameters $\tilde{t}_{ab}$ are.[2] Thus for strongly-correlated materials the low-energy effective model must be different. The canonical Hamiltonian used to describe the Mott transition is the Hubbard model

$$\hat{H} = -\sum_{\sigma}\sum_{ii'} t^{i,i'} c^{\dagger}_{i\sigma} c_{i'\sigma} + U\sum_{i} \hat{n}_{i\uparrow}\hat{n}_{i\downarrow}, \tag{3}$$

which includes, in addition to a single-electron term, the on-site Coulomb repulsion. This model captures the essence of the Mott transition. At half filling, for $U{=}0$ it describes a paramagnetic metal, and for $t^{i,i'}(1{-}\delta_{i,i'}){=}0$ an insulating set of paramagnetic atoms. Unfortunately, differently from Hamiltonians of type $\hat{H}_e^{\rm LDA}$, Hubbard-like models cannot be solved exactly in the general case. Remarkably, till 30 years ago, no method for describing the complete phase diagram of (3) in a single coherent framework, including the paramagnetic insulating phase, was actually known. This changed between 1989 and 1992, when the dynamical mean-field theory (DMFT) was developed [1–4]. The key idea of DMFT consists in mapping the Hubbard model onto a self-consistent *auxiliary quantum-impurity problem*, which can be solved exactly. The mapping is based on the *local dynamical self-energy approximation*, very good for realistic three-dimensional lattices—and becoming exact in the infinite coordination limit [1, 2].

DMFT was initially applied only to simple cases, due to limitations in model building, computational power, and numerical methods for solving the auxiliary impurity problem (the quantum-impurity solvers). In the last twenty years remarkable progress lifted many of these limitations. First, reliable schemes to build realistic low-energy materials-specific Hubbard-like models have been devised, in particular using Kohn-Sham localized Wannier functions. This is astonishing, given that we do not know the exact operator $\hat{S}$ which gives the effective low-energy Hamiltonian, and thus a truly systematic derivation is not possible. Second, key advances in quantum-impurity solvers and increasingly more powerful supercomputers made it possible to study always more complex many-body Hamiltonians. The approach which emerged, consisting in solving, within DMFT, materials-specific many-body Hamiltonians constructed via LDA, is known as the LDA+DMFT method [5–7]. This technique (and its extensions) is now the state-of-the-art for describing strongly-correlated materials. In this lecture I will outline the basic ideas on which the method is based, its successes and its limitations. This manuscript extends the one of last year's school—in which more details on the model building aspects can be found—to the calculation of linear response functions.

[2] One can obtain an insulator by reducing the symmetry, e.g, by increasing the size of the primitive cell. This Slater-type insulator has however different properties than a Mott-type insulator.

# 2 From DMFT to LDA+DMFT

In this section we introduce the basics of dynamical mean-field theory. We start from a case for which we can perform analytic calculations, the two-site Hubbard Hamiltonian. This is a toy model, useful to illustrate how the method works, but for which, as we will see, DMFT is not a good approximation. Indeed, the Hubbard dimer is the worst case for DMFT, since the coordination number is the lowest possible. Next we extend the formalism to the one-band and then to the multi-orbital Hubbard Hamiltonian. For three-dimensional lattices the coordination number is typically large and thus DMFT is an excellent approximation. Finally, we summarize the modern schemes to construct materials-specific many-body models. They are based on Kohn-Sham Wannier orbitals, calculated, e.g, using the LDA functional. The solution of such models via DMFT defines the LDA+DMFT method.

## 2.1 DMFT for a toy model: The Hubbard dimer

The two-site Hubbard model is given by

$$\hat{H} = \varepsilon_d \sum_{i\sigma} \hat{n}_{i\sigma} - t \sum_{\sigma} \left( c^\dagger_{1\sigma} c_{2\sigma} + c^\dagger_{2\sigma} c_{1\sigma} \right) + U \sum_i \hat{n}_{i\uparrow} \hat{n}_{i\downarrow}, \tag{4}$$

with $i = 1, 2$. The ground state for $N = 2$ electrons (half filling) is the singlet[3]

$$|G\rangle_H = \frac{a_2(t,U)}{\sqrt{2}} \left( c^\dagger_{1\uparrow} c^\dagger_{2\downarrow} - c^\dagger_{1\downarrow} c^\dagger_{2\uparrow} \right) |0\rangle + \frac{a_1(t,U)}{\sqrt{2}} \left( c^\dagger_{1\uparrow} c^\dagger_{1\downarrow} + c^\dagger_{2\uparrow} c^\dagger_{2\downarrow} \right) |0\rangle \tag{5}$$

with

$$a_1^2(t,U) = \frac{1}{\Delta(t,U)} \frac{\Delta(t,U) - U}{2}, \qquad a_2^2(t,U) = \frac{4t^2}{\Delta(t,U)} \frac{2}{\Delta(t,U) - U}, \tag{6}$$

and

$$\Delta(t,U) = \sqrt{U^2 + 16t^2}. \tag{7}$$

The energy of this state is

$$E_0(2) = 2\varepsilon_d + \frac{1}{2}\big(U - \Delta(t,U)\big). \tag{8}$$

In the $T \to 0$ limit, using the Lehmann representation (see Appendix B), one can show that the local Matsubara Green function for spin $\sigma$ takes then the form

$$\begin{aligned} G^\sigma_{i,i}(i\nu_n) = & \frac{w_+(t,U)}{i\nu_n - \big(\underbrace{E_0(2) - \varepsilon_d + t - \mu}_{E_0(2) - E_-(1) - \mu}\big)} + \frac{w_-(t,U)}{i\nu_n - \big(\underbrace{-E_0(2) + U + 3\varepsilon_d + t - \mu}_{E_+(3) - E_0(2) - \mu}\big)} \\ & + \frac{w_-(t,U)}{i\nu_n - \big(\underbrace{E_0(2) - \varepsilon_d - t - \mu}_{E_0(2) - E_+(1) - \mu}\big)} + \frac{w_+(t,U)}{i\nu_n - \big(\underbrace{-E_0(2) + U + 3\varepsilon_d - t - \mu}_{E_-(3) - E_0(2) - \mu}\big)}, \end{aligned} \tag{9}$$

[3] Eigenstates and eigenvalues of the Hubbard dimer for arbitrary filling can be found in Appendix A.

where $\nu_n = \pi(2n+1)/\beta$ are fermionic Matsubara frequencies and $\mu = \varepsilon_d + U/2$ is the chemical potential. The weights are

$$w_\pm(t,U) = \frac{1}{4}\big(1 \pm w(t,U)\big), \qquad \text{with} \qquad w(t,U) = 2a_1(t,U)a_2(t,U) = \frac{4t}{\Delta(t,U)}. \tag{10}$$

The local Green function can be rewritten as the average of the Green function for the bonding ($k=0$) and the anti-bonding state ($k=\pi$), i.e.,

$$G^\sigma_{i,i}(i\nu_n) = \frac{1}{2}\left( \underbrace{\frac{1}{i\nu_n + \mu - \varepsilon_d + t - \Sigma^\sigma(0;i\nu_n)}}_{G^\sigma(0;i\nu_n)} + \underbrace{\frac{1}{i\nu_n + \mu - \varepsilon_d - t - \Sigma^\sigma(\pi;i\nu_n)}}_{G^\sigma(\pi;i\nu_n)} \right). \tag{11}$$

The self-energy is given by

$$\Sigma^\sigma(k;i\nu_n) = \frac{U}{2} + \frac{U^2}{4}\frac{1}{i\nu_n + \mu - \varepsilon_d - \frac{U}{2} - e^{ik}\,3t}. \tag{12}$$

The self-energies $\Sigma^\sigma(0;i\nu_n)$ and $\Sigma^\sigma(\pi;i\nu_n)$ differ due to the phase $e^{ik} = \pm 1$ in their denominators. The local self-energy is, by definition, the average of the two

$$\begin{aligned}\Sigma^\sigma_l(i\nu_n) = \frac{1}{2}\Big(\Sigma^\sigma(\pi;i\nu_n) + \Sigma^\sigma(0;i\nu_n)\Big) &= \frac{U}{2} + \frac{U^2}{4}\,\frac{i\nu_n + \mu - \varepsilon_d - \frac{U}{2}}{\big(i\nu_n + \mu - \varepsilon_d - \frac{U}{2}\big)^2 - (3t)^2} \\ &= \frac{U}{2} + \frac{U^2}{4}\,\frac{i\nu_n}{(i\nu_n)^2 - (3t)^2}.\end{aligned} \tag{13}$$

The difference

$$\begin{aligned}\Delta\Sigma^\sigma_l(i\nu_n) = \frac{1}{2}\Big(\Sigma^\sigma(\pi;i\nu_n) - \Sigma^\sigma(0;i\nu_n)\Big) &= -\frac{U^2}{4}\,\frac{3t}{\big(i\nu_n + \mu - \varepsilon_d - \frac{U}{2}\big)^2 - (3t)^2} \\ &= -\frac{U^2}{4}\,\frac{3t}{(i\nu_n)^2 - (3t)^2},\end{aligned} \tag{14}$$

thus measures the importance of non-local effects; it would be zero if the self-energy was independent of $k$. Next we define the hybridization function

$$F^\sigma(i\nu_n) = \frac{\big(t + \Delta\Sigma^\sigma_l(i\nu_n)\big)^2}{i\nu_n + \mu - \varepsilon_d - \Sigma^\sigma_l(i\nu_n)} \tag{15}$$

which for $U{=}0$ becomes

$$F^\sigma_0(i\nu_n) = \frac{t^2}{i\nu_n}. \tag{16}$$

By using these definitions, we can rewrite the local Green function as

$$G^\sigma_{i,i}(i\nu_n) = \frac{1}{i\nu_n + \mu - \varepsilon_d - F^\sigma(i\nu_n) - \Sigma^\sigma_l(i\nu_n)}. \tag{17}$$

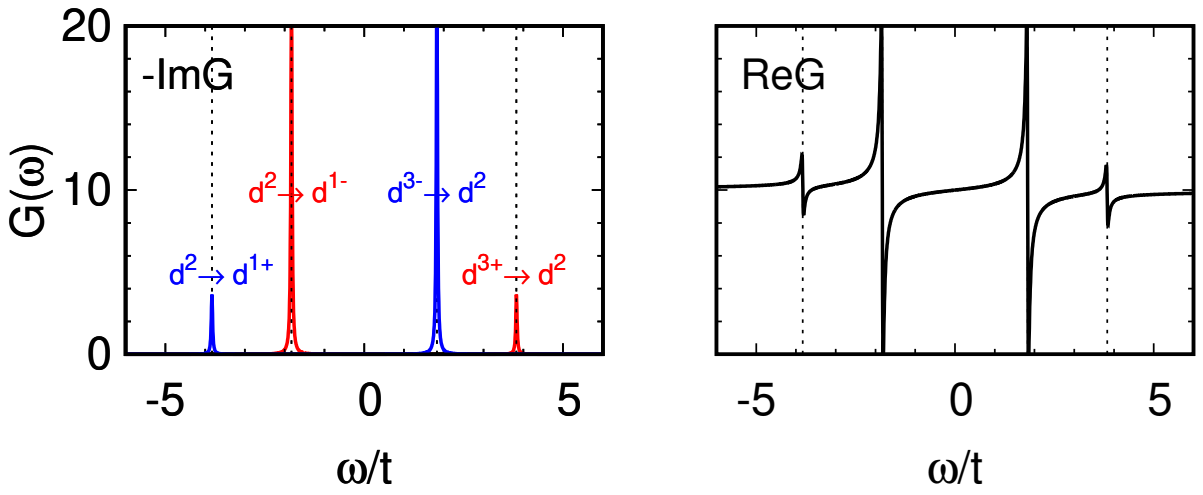


**Fig. 1:** *Hubbard dimer: Imaginary (left) and real (right) part of the retarded Green function, obtained setting $i\nu_n \to \omega + i\delta$ (analytic continuation) in Eq. (9). Red lines: $k = 0$ contribution. Blue lines: $k = \pi$ contribution. Dashed lines: Poles of the retarded Green function. Parameters: $t = 1$, $U = 4$. The weight of the poles yielding the smaller peaks, $w_-(t, U)$, defined in Eq. (10), goes to zero for $U \to 0$. In the atomic limit, instead, all four poles have the same weight; the energies of the two positive (negative) poles become identical, however.*

The associated retarded Green function, obtained via analytic continuation ($i\nu_n \to \omega + i\delta$), is shown in Fig. 1. It is important to point out that, as one may see from the formulas just discussed, the local Green function and the local self-energy satisfy the *local Dyson equation*

$$\Sigma_l^\sigma(i\nu_n) = \frac{1}{\mathfrak{G}_{i,i}^\sigma(i\nu_n)} - \frac{1}{G_{i,i}^\sigma(i\nu_n)}, \tag{18}$$

where $\mathfrak{G}_{i,i}^\sigma(i\nu_n)$ is given by

$$\mathfrak{G}_{i,i}^\sigma(i\nu_n) = \frac{1}{i\nu_n + \mu - \varepsilon_d - F^\sigma(i\nu_n)}. \tag{19}$$

Thus, one could think of mapping the Hubbard dimer into an auxiliary quantum-impurity model, chosen such that, within certain approximations, the impurity Green function is as close as possible to the local Green function of the original problem. How can we do this? Let us adopt as auxiliary model the Anderson molecule

$$\hat{H}^{\rm A} = \varepsilon_s \sum_\sigma \hat{n}_{s\sigma} - t \sum_\sigma \left( c_{d\sigma}^\dagger c_{s\sigma} + c_{s\sigma}^\dagger c_{d\sigma} \right) + \varepsilon_d \sum_\sigma \hat{n}_{d\sigma} + U \hat{n}_{d\uparrow} \hat{n}_{d\downarrow} \,, \tag{20}$$

where $s$ labels the uncorrelated bath site and $d$ the correlated quantum-impurity site. The first constraint would be that Hamiltonian (20) has a ground state with the same occupations of the 2-site Hubbard model, i.e., at half filling, $n_d = n_s = 1$. Such a *self-consistency condition* is satisfied if $\varepsilon_s = \mu = \varepsilon_d + U/2$. This can be understood by comparing the Hamiltonian matrices of the two models in the Hilbert space with $N = 2$ electrons. To this end, we first order the

two-electron states of the Hubbard dimer as

$$\begin{aligned} |1\rangle &= c^\dagger_{1\uparrow}c^\dagger_{2\uparrow}|0\rangle, & |4\rangle &= \tfrac{1}{\sqrt{2}}(c^\dagger_{1\uparrow}c^\dagger_{2\downarrow} - c^\dagger_{1\downarrow}c^\dagger_{2\uparrow})|0\rangle, \\ |2\rangle &= c^\dagger_{1\downarrow}c^\dagger_{2\downarrow}|0\rangle, & |5\rangle &= c^\dagger_{1\uparrow}c^\dagger_{1\downarrow}|0\rangle, \\ |3\rangle &= \tfrac{1}{\sqrt{2}}(c^\dagger_{1\uparrow}c^\dagger_{2\downarrow} + c^\dagger_{1\downarrow}c^\dagger_{2\uparrow})|0\rangle, & |6\rangle &= c^\dagger_{2\uparrow}c^\dagger_{2\downarrow}|0\rangle. \end{aligned} \tag{21}$$

In this basis the Hamiltonian of the Hubbard dimer has the matrix form

$$\hat{H}_2(\varepsilon_d, U, t) = \begin{pmatrix} 2\varepsilon_d & 0 & 0 & 0 & 0 & 0 \\ 0 & 2\varepsilon_d & 0 & 0 & 0 & 0 \\ 0 & 0 & 2\varepsilon_d & 0 & 0 & 0 \\ 0 & 0 & 0 & 2\varepsilon_d & -\sqrt{2}t & -\sqrt{2}t \\ 0 & 0 & 0 & -\sqrt{2}t & 2\varepsilon_d{+}U & 0 \\ 0 & 0 & 0 & -\sqrt{2}t & 0 & 2\varepsilon_d{+}U \end{pmatrix}. \tag{22}$$

The ground state, the singlet given in Eq. (5), can be obtained by diagonalizing the lower $3{\times}3$ block. For the Anderson molecule, ordering the basis in the same way ($1 \to d, 2 \to s$), this Hamiltonian becomes

$$\hat{H}^A_2(\varepsilon_d, U, t; \varepsilon_s) = \begin{pmatrix} \varepsilon_d{+}\varepsilon_s & 0 & 0 & 0 & 0 & 0 \\ 0 & \varepsilon_d{+}\varepsilon_s & 0 & 0 & 0 & 0 \\ 0 & 0 & \varepsilon_d{+}\varepsilon_s & 0 & 0 & 0 \\ 0 & 0 & 0 & \varepsilon_d{+}\varepsilon_s & -\sqrt{2}t & -\sqrt{2}t \\ 0 & 0 & 0 & -\sqrt{2}t & 2\varepsilon_d{+}U & 0 \\ 0 & 0 & 0 & -\sqrt{2}t & 0 & 2\varepsilon_s \end{pmatrix}. \tag{23}$$

Comparing the lower $3{\times}3$ block of $\hat{H}^A_2(\varepsilon_d, U, t; \varepsilon_s)$ with the corresponding block of $\hat{H}_2(\varepsilon_d, U, t)$ we can see that, unless $\varepsilon_s = \mu = \varepsilon_d + U/2$, the two doubly occupied states $|5\rangle$ and $|6\rangle$ have different energies and thus the two sites $i = 1, 2$ are differently occupied in the ground state. By setting $\varepsilon_s = \mu$ we find that

$$\hat{H}^A_2(\varepsilon_d, U, t; \mu) = \hat{H}_2(\varepsilon_d{+}\tfrac{U}{4}, \tfrac{U}{2}, t). \tag{24}$$

The $N = 2$ ground state of $\hat{H}^A_2(\varepsilon_d, U, t; \mu)$ has thus the form of the ground-state for the Hubbard dimer

$$|G\rangle_A = \frac{a_2(t, U/2)}{\sqrt{2}}\left(c^\dagger_{d\uparrow}c^\dagger_{s\downarrow} - c^\dagger_{d\downarrow}c^\dagger_{s\uparrow}\right)|0\rangle + \frac{a_1(t, U/2)}{\sqrt{2}}\left(c^\dagger_{d\uparrow}c^\dagger_{d\downarrow} + c^\dagger_{s\uparrow}c^\dagger_{s\downarrow}\right)|0\rangle, \tag{25}$$

and the condition $n_s = n_d = 1$ is satisfied. Since $\varepsilon_s \neq \varepsilon_d$, however, the eigenstates of $\hat{H}^{\mathrm{A}}$ for one electron ($N = 1$) or one hole ($N = 3$) are not the bonding and antibonding states of the

Hubbard dimer.[4] The impurity Green function is then given by

$$G^{\sigma}_{d,d}(i\nu_n) = \frac{1}{4}\Bigg( \frac{1+w'(t,U)}{i\nu_n - (E_0(2) - E_-(1) - \mu)} + \frac{1-w'(t,U)}{i\nu_n - (E_+(3) - E_0(2) - \mu)} \\ \frac{1-w'(t,U)}{i\nu_n - (E_0(2) - E_+(1) - \mu)} + \frac{1+w'(t,U)}{i\nu_n - (E_-(3) - E_0(2) - \mu)} \Bigg), \tag{26}$$

where

$$E_0(2) - E_\pm(1) - \mu = -\Big( E_\pm(3) - E_0(2) - \mu \Big) = -\frac{1}{4}\Big( 2\Delta(t,U/2) \pm \Delta(t,U) \Big) \tag{27}$$

and

$$w'(t,U) = \frac{1}{2}\frac{32t^2 - U^2}{\Delta(t,U)\Delta(t,U/2)}\,. \tag{28}$$

After some rearrangement we obtain a much simpler expression

$$G^{\sigma}_{d,d}(i\nu_n) = \frac{1}{i\nu_n + \mu - \varepsilon_d - \mathcal{F}^{\sigma}_0(i\nu_n) - \Sigma^{\sigma}_A(i\nu_n)}\,. \tag{29}$$

The impurity self-energy equals the local self-energy of the Hubbard dimer

$$\Sigma^{\sigma}_A(i\nu_n) = \frac{U}{2} + \frac{U^2}{4}\frac{i\nu_n}{(i\nu_n)^2 - (3t)^2}\,, \tag{30}$$

as one may see comparing it to equation (13). The hybridization function is given by

$$\mathcal{F}^{\sigma}_0(i\nu_n) = \frac{t^2}{i\nu_n}\,, \tag{31}$$

as for the non-interacting Hubbard dimer, Eq. (16). For $U = 0$, $G^{\sigma}_{d,d}(i\nu_n)$ equals the non-interacting impurity Green function

$$G^{0\sigma}_{d,d}(i\nu_n) = \frac{1}{i\nu_n + \mu - \varepsilon_d - \mathcal{F}^{\sigma}_0(i\nu_n)}\,. \tag{32}$$

The impurity Green function thus satisfies the *impurity Dyson equation*

$$\Sigma^{\sigma}_A(i\nu_n) = \frac{1}{G^{0\sigma}_{d,d}(i\nu_n)} - \frac{1}{G^{\sigma}_{d,d}(i\nu_n)}\,. \tag{33}$$

In Fig. 2 we show the retarded impurity Green function of the Anderson molecule (orange, right panels) and the retarded local Green function of the 2-site Hubbard model, both in the local self-energy approximation (blue, right panels) and exact (blue, left panels). Comparing left and right panels we can see that setting $\Delta\Sigma^{\sigma}_l(\omega) = 0$ yields large errors. The right panels demonstrate, however, that the spectral function of the Hubbard dimer with $\Delta\Sigma^{\sigma}_l(\omega) = 0$ is quite similar to the one of the Anderson molecule. The small remaining deviations come from the fact that,

[4] The complete list of eigenvalues and eigenvectors of the Anderson molecule for $\varepsilon_s = \varepsilon_d + U/2$ and arbitrary electron number $N$ can be found in Appendix A.

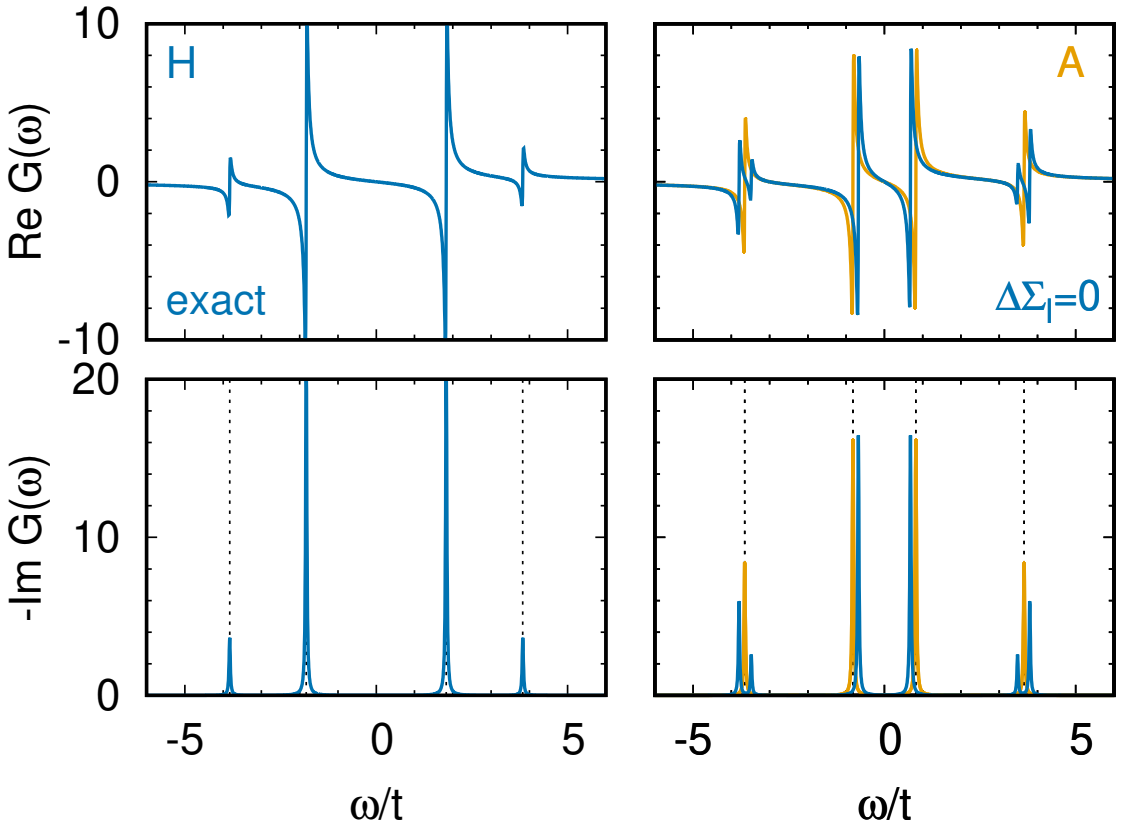


**Fig. 2:** *Retarded Green function of the Hubbard dimer ($t = 1$, $U = 4$) and of the Anderson molecule ($\varepsilon_s = \varepsilon_d + U/2$) in the zero temperature limit. Left panels: Hubbard dimer, exact Green function. Right panels, blue: Hubbard dimer in the local self-energy approximation, i.e., with $\Delta\Sigma_l^\sigma(\omega) = 0$. Right panels, orange: Anderson molecule. Dashed lines: Poles for the Hubbard dimer (left) or the Anderson molecule (right).*

for the Hubbard dimer, in the impurity Dyson equation, the non-interacting impurity Green function is replaced by $\mathfrak{G}^\sigma_{i,i}(i\nu_n)$ in the local self-energy approximation, i.e., by the *bath* Green function

$$\mathcal{G}^\sigma_{i,i}(i\nu_n) = \frac{1}{i\nu_n + \mu - \varepsilon_d - \mathcal{F}^\sigma_l(i\nu_n)}\,, \tag{34}$$

where

$$\mathcal{F}^\sigma_l(i\nu_n) = \frac{t^2}{i\nu_n + \mu - \varepsilon_d - \Sigma^\sigma_A(i\nu_n)}\,. \tag{35}$$

We are now in the position of explaining how DMFT works for the Hamiltonian of the Hubbard dimer, choosing the Anderson molecule Hamiltonian (20) as the auxiliary quantum-impurity model. The procedure can be split in the following steps

1. Build the initial quantum impurity model with $G^{0\sigma}_{d,d}(i\nu_n) = G^{0\sigma}_{i,i}(i\nu_n)$. The initial bath is thus defined by energy $\varepsilon_s = \varepsilon_d$ and hopping $t$.

2. Calculate the local Green function $G^\sigma_{d,d}(i\nu_n)$ for the auxiliary model.

3. Use the local Dyson equation to calculate the impurity self-energy

$$\Sigma_A^\sigma(i\nu_n) = \frac{1}{G_{d,d}^{0\sigma}(i\nu_n)} - \frac{1}{G_{d,d}^{\sigma}(i\nu_n)}.$$

4. Calculate the local Green function of the Hubbard dimer setting the self-energy equal to the one of the quantum-impurity model

$$G_{i,i}^\sigma(i\nu_n) \sim \frac{1}{2}\left(\frac{1}{i\nu_n + \mu - \varepsilon_d + t - \Sigma_A^\sigma(i\nu_n)} + \frac{1}{i\nu_n + \mu - \varepsilon_d - t - \Sigma_A^\sigma(i\nu_n)}\right).$$

5. Calculate a new bath Green function $\mathcal{G}_{i,i}^\sigma(i\nu_n)$ from the local Dyson equation

$$\mathcal{G}_{i,i}^\sigma(i\nu_n) = \frac{1}{\Sigma_A^\sigma(i\nu_n) + 1/G_{i,i}^\sigma(i\nu_n)}.$$

6. Build a new $G_{d,d}^{0\sigma}(i\nu_n)$ from $\mathcal{G}_{i,i}^\sigma(i\nu_n)$.

7. Restart from the second step.

8. Iterate till self-consistency, i.e., here till $n_d^\sigma = n_i^\sigma$ and $\Sigma_A^\sigma(i\nu_n)$ does not change any more.

The Anderson molecule satisfies the self-consistency requirements for $\varepsilon_s = \mu$. The remaining difference between $G_{d,d}^\sigma(i\nu_n)$, the impurity Green function, and $G_{i,i}^\sigma(i\nu_n)$, the local Green function of the Hubbard dimer in the local self-energy approximation, arises from the difference in the associated hybridization functions

$$\Delta\mathcal{F}_l(i\nu_n) = \mathcal{F}_l^\sigma(i\nu_n) - \mathcal{F}_0^\sigma(i\nu_n) = t^2p^2\left(-\frac{2}{i\nu_n} + \frac{1}{i\nu_n - \varepsilon_a} + \frac{1}{i\nu_n + \varepsilon_a}\right), \tag{36}$$

where $p^2 = U^2/8\varepsilon_a^2$ and $\varepsilon_a = \sqrt{9t^2 + U^2/4}$. The error made is small, however, as shown in the right panels of Fig. 2. To further improve we would have to modify the auxiliary model adding more bath sites. Staying with the Anderson molecule, in Fig. 3 we compare in more detail its spectral function with the exact spectral function of the Hubbard dimer. The figure emphasizes several important conclusions. The top right panel reminds us that DMFT is not a good approximation for molecular complexes with two (or few) correlated sites. This is because in such systems the coordination number is the lowest possible, the worst case for dynamical mean-field theory. In three-dimensional crystals, instead, the coordination number is typically large enough to make dynamical mean-field theory an excellent approximation. The bottom left panel of Fig. 3 shows that, in the local-self-energy approximation, the agreement between Anderson and Hubbard Green functions remains very good for any $U$ value. This indicates that when the local-self-energy approximation works well, as in the case of three-dimensional crystals, it can be successfully used to study the behavior of a given system as a function of $U$. Leaving for a moment DMFT aside, the two bottom panels of Fig. 3 show that the evolution with $U$ is different for the impurity Green function of the Anderson molecule and the exact local Green function of the Hubbard dimer. Anticipating the discussion of later sections, if we compare to

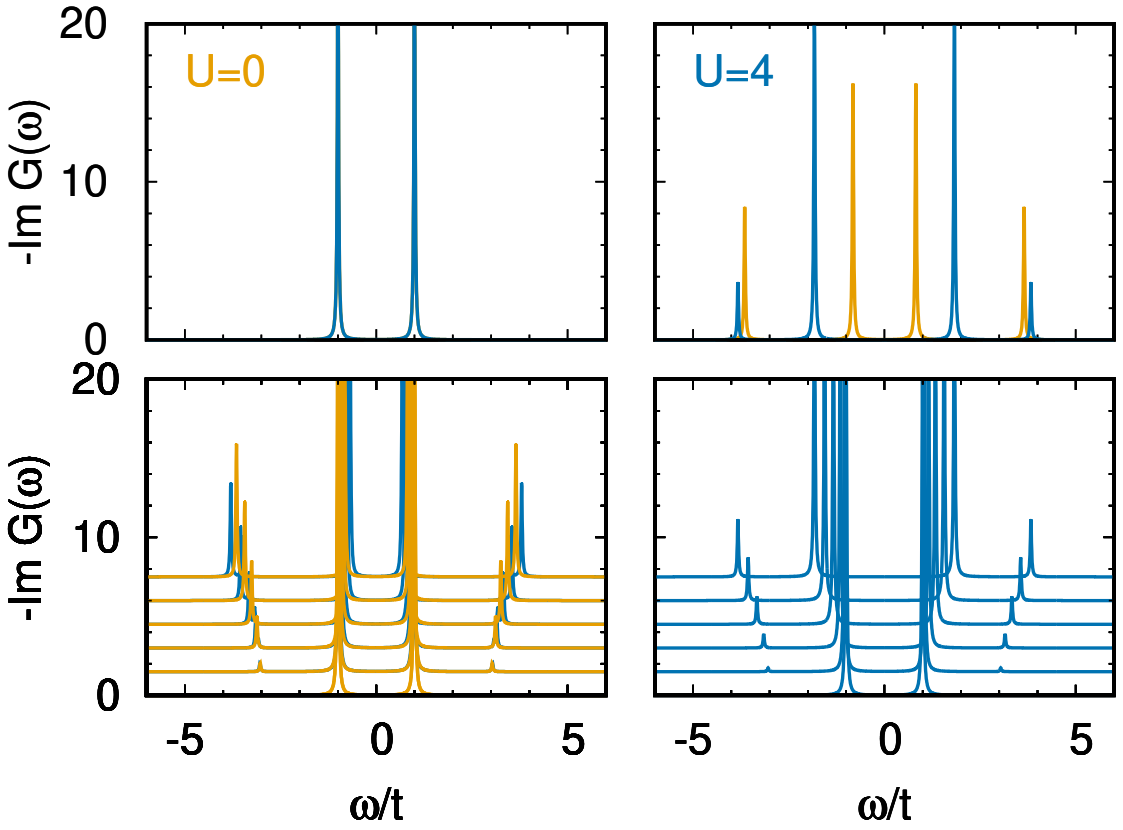


**Fig. 3:** *Imaginary part of the retarded Green function of the Anderson molecule (orange) and Hubbard dimer (blue) in the zero temperature limit. In the bottom left panel the local self-energy approximation is adopted for the Hubbard dimer; in all other cases the exact Green function of the Hubbard dimer is shown. Parameters:* $t = 1$, $\varepsilon_s = \mu$. *Top:* $U = 0$ *(left) and* $U = 4t$ *(right). Bottom: Evolution with increasing* $U$ *from* $0$ *to* $4t$ *in equal steps.*

the spectral function of the actual *lattice* Hubbard model, we could say that the Hubbard dimer captures well the evolution of the Hubbard bands and the gap in the large-$U$ limit. On the other hand, the Anderson molecule partially captures the behavior of the central "quasi-particle" or "Kondo" peak, although the Kondo effect itself is unrealistically described; as a matter of fact, the Kondo energy gain (the "Kondo temperature") is perturbative ($\propto t^2/U$) in the case of the Anderson molecule, while it is exponentially small for a Kondo impurity in a metallic bath. Going back to DMFT, this also points to the possible shortcomings of calculations in which the quantum-impurity model for the lattice Hubbard model is solved via exact diagonalization, however using a single bath site or very few; this might perhaps be sufficient in the large-gap limit,[5] but is bound to eventually fail approaching the metallic regime. Indeed, this failure is one of the reasons why the solution of the Kondo problem required the development of—at the time new—non-perturbative techniques such as the numerical renormalization group.

[5]For a discussion of bath parametrization in exact diagonalization and the actual convergence with the number of bath sites for the lattice Hubbard model see Ref. [8].

## 2.2 Non-local Coulomb interaction

In Sec. 2.1 we have seen that the local Coulomb interaction gives rise, *alone*, to non-local self-energy terms, which can be very important. What is, instead, the effect of the non-local part of the Coulomb interaction? For a Hubbard dimer, extending the Coulomb interaction to first neighbors leads to the Hamiltonian

$$\begin{aligned}\hat{H} =&\varepsilon_d \sum_{i\sigma} \hat{n}_{i\sigma} - t \sum_{\sigma} \left( c^\dagger_{1\sigma} c_{2\sigma} + c^\dagger_{2\sigma} c_{1\sigma} \right) + U \sum_{i=1,2} \hat{n}_{i\uparrow} \hat{n}_{i\downarrow} \\ &+ \sum_{\sigma\sigma'} \left( V - 2J_V - J_V\, \delta_{\sigma\sigma'} \right) \hat{n}_{1\sigma} \hat{n}_{2\sigma'} - J_V \sum_{i\neq i'} \left( c^\dagger_{i\uparrow} c_{i\downarrow} c^\dagger_{i'\downarrow} c_{i'\uparrow} + c^\dagger_{i'\uparrow} c^\dagger_{i'\downarrow} c_{i\uparrow} c_{i\downarrow} \right), \end{aligned} \tag{37}$$

where the parameters in the last two terms are the intersite direct ($V$) and exchange ($J_V$) Coulomb interaction. For two electrons the Hamiltonian, in a matrix form, becomes

$$\hat{H}_2^{\rm NL} = \begin{pmatrix} 2\varepsilon_d + V - 3J_V & 0 & 0 & 0 & 0 & 0 \\ 0 & 2\varepsilon_d + V - 3J_V & 0 & 0 & 0 & 0 \\ 0 & 0 & 2\varepsilon_d + V - 3J_V & 0 & 0 & 0 \\ 0 & 0 & 0 & 2\varepsilon_d + V - J_V & -\sqrt{2}t & -\sqrt{2}t \\ 0 & 0 & 0 & -\sqrt{2}t & 2\varepsilon_d + U & -J_V \\ 0 & 0 & 0 & -\sqrt{2}t & -J_V & 2\varepsilon_d + U \end{pmatrix},$$

where the basis is defined in Eq. (21). In the atomic ($t = 0$) limit, the triplet states, $|1\rangle$, $|2\rangle$ and $|3\rangle$, have lower energy than the singlet states, $|4\rangle$, $|5\rangle$ and $|6\rangle$, as one can see by comparing the diagonal elements of the upper and lower $3 \times 3$ block of the matrix $\hat{H}_2^{\rm NL}$ here above. This is due to the fact that $J_V$ is positive (ferromagnetic) and $V < U$. The triplet can remain the ground multiplet even for finite $t$. If, however, $J_V$ is sufficiently small, the ground state is a singlet, as in the case $V{=}J_V{=}0$. Setting for simplicity $J_V = 0$, we notice that $\hat{H}_2^{\rm NL} = \hat{H}_2(\varepsilon'_d, U', t)$, where the right-hand-side term is the $N{=}2$-electron Hamiltonian of the $J_V{=}V{=}0$ Hubbard dimer, Eq. (22), with parameters $\varepsilon'_d = \varepsilon_d + V/2$ and $U'{=}U{-}V$. The $N{=}2$ ground state is thus still given by Eq. (5), provided that we replace $U$ with $U'$ in the coefficients. Eventually, in the limiting case $U{=}V$, $\hat{H}_2^{\rm NL}$ equals the corresponding Hamiltonian of an effective non-correlated dimer, $\hat{H}_2(\varepsilon'_d, 0, t)$. What happens away from half filling? For $N{=}1$ electrons, eigenvectors and eigenvalues are the same as in the $V{=}0$ case; for $N{=}3$ electrons all energies are shifted by $2V$. Summarizing, we can obtain the Green function for $V \neq 0$ from Eq. (9) setting

$$\begin{aligned} E_\pm(N{=}1, U; V) &= E_\pm(N{=}1, U; 0) &&= \varepsilon_d \pm t \\ E_\pm(N{=}3, U; V) &= E_\pm(N{=}3, U; 0) + 2V &&= 3\varepsilon_d \pm t + U + 2V \\ E_0(N{=}2, U; V) &= E_0(N{=}2, U{-}V; 0) + V &&= E_0(2, U{-}V) + V \\ \mu(U; V) &= \mu(U) + V &&= \mu + V \\ w_\pm(t, U; V) &= w_\pm(t, U{-}V; 0). \end{aligned}$$

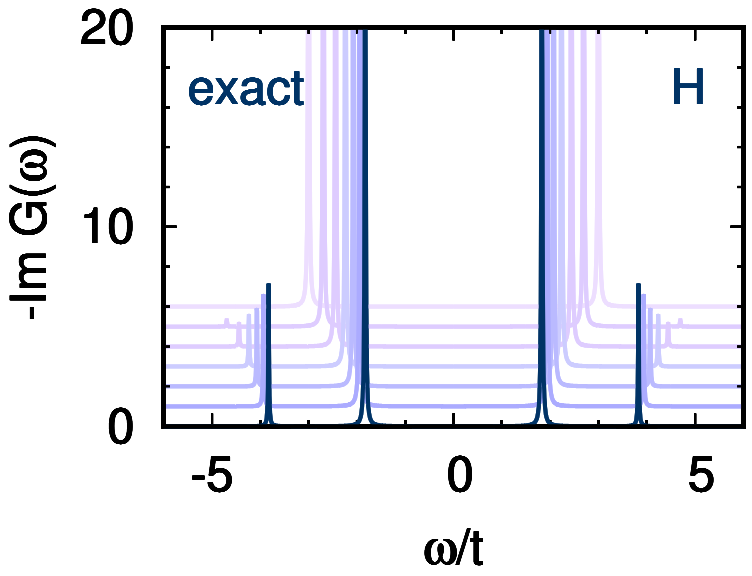


**Fig. 4:** *Imaginary part of the retarded Green function of the Hubbard dimer in the zero temperature limit ($U$=4, $t$=1), increasing the intersite Coulomb repulsion $V$ from 0 to $V$=$U$=4 in equal steps; we have set $J_V = 0$. The dark blue line corresponds to $V = 0$.*

Thus we have, recalling that $U' = U-V$,

$$G^{\sigma}_{i,i}(i\nu_n) = \frac{w_+(t,U')}{i\nu_n-\left(E'_0(2)-\frac{1}{2}V-\varepsilon_d+t-\mu'\right)}+\frac{w_-(t,U')}{i\nu_n-\left(-E'_0(2)+U'+\frac{1}{2}V+3\varepsilon_d+t-\mu'\right)}$$
$$+\frac{w_-(t,U')}{i\nu_n-\left(E'_0(2)-\frac{1}{2}V-\varepsilon_d-t-\mu'\right)}+\frac{w_+(t,U')}{i\nu_n-\left(-E'_0(2)+U'+\frac{1}{2}V+3\varepsilon_d-t-\mu'\right)}, \qquad (38)$$

where we set $\mu' = \mu-V/2 = \varepsilon_d+U'/2$ and $E'_0(2) = E_0(2,U')$. The associated spectral function is shown in Fig. 4. The figure illustrates that increasing $V$ from 0 to $U$ makes the spectra progressively closer to the one of a non-correlated system. Eventually, for $U$=$V$, only two poles contribute, since $w_-(t,U') = 0$. In this limit, the spectral function is identical to the one of the non-interacting Hubbard dimer, however with an enhanced effective hopping, $t \longrightarrow t + V/2$. We can thus say that, in first approximation, the (positive) intersite coupling $V$ effectively reduces the strength of correlations in the Hubbard dimer. In conclusion, the case of the Hubbard dimer explains why *strong-correlation* effects typically appear when the *local term of the electron-electron repulsion dominates*, i.e., when it is much larger than long-range terms. A hypothetical system in which the Coulomb interaction strength is independent on the distance between sites (for the dimer, $U$=$V$) is likely to be already well described via an *effective weakly correlated model*. Of course, in real materials, the effects of long-range Coulomb repulsion can be much more complicated than in the two-site model just discussed, but the general considerations made here remain true even in realistic cases.

## 2.3 Quantum-impurity solvers: Continuous-time quantum Monte Carlo

For the case of the Anderson molecule exact diagonalization is the simplest quantum-impurity solver and the one that provides most insights. Methods based on Quantum Monte Carlo (QMC) sampling are often, however, the only option for realistic multi-orbital and/or multi-site models. Thus, here we explain how to obtain the impurity Green function of the Anderson molecule via hybridization-expansion continuous-time QMC [9], a very successful QMC-based quantum-impurity solver. In this approach, the first step consists in splitting the Hamiltonian into bath ($\hat{H}_{\rm bath}$), hybridization ($\hat{H}_{\rm hyb}$), and local ($\hat{H}_{\rm loc}$) terms

$$\hat{H}^{\rm A} = \underbrace{\varepsilon_s \sum_\sigma \hat{n}_{s\sigma}}_{\hat{H}_{\rm bath}} \underbrace{-t \sum_\sigma \left( c^\dagger_{d\sigma} c_{s\sigma} + c^\dagger_{s\sigma} c_{d\sigma} \right)}_{\hat{H}_{\rm hyb}} + \underbrace{\varepsilon_d \sum_\sigma \hat{n}_{d\sigma} + U \hat{n}_{d\uparrow} \hat{n}_{d\downarrow}}_{\hat{H}_{\rm loc}} . \tag{39}$$

Next, we write the partition function $Z$ as a perturbation series in the hybridization. To this end, we define $\hat{H}_0 = \hat{H}_{\rm bath} + \hat{H}_{\rm loc}$ and rewrite the partition function as

$$Z = {\rm Tr} \left( e^{-\beta(\hat{H}_0 - \mu \hat{N})} \hat{V}(\beta) \right) \tag{40}$$

where the operator $\hat{V}(\beta)$ is given by

$$\hat{V}(\beta) = e^{\beta(\hat{H}_0 - \mu\hat{N})}\, e^{-\beta(\hat{H}_0 + \hat{H}_{\rm hyb} - \mu\hat{N})} = \sum_m \underbrace{\int_0^\beta d\tau_1 \cdots \int_{\tau_{m-1}}^\beta d\tau_m}_{\int d\boldsymbol{\tau}^m} \underbrace{(-1)^m \prod_{l=m}^1 \hat{H}_{\rm hyb}(\tau_l)}_{\hat{O}^m(\boldsymbol{\tau})} , \tag{41}$$

and

$$\hat{H}_{\rm hyb}(\tau_l) = e^{\tau_l(\hat{H}_0 - \mu\hat{N})}\, \hat{H}_{\rm hyb}\, e^{-\tau_l(\hat{H}_0 - \mu\hat{N})} = -t \sum_\sigma \left( c^\dagger_{d\sigma_l}(\tau_l) c_{s\sigma_l}(\tau_l) + c^\dagger_{s\sigma_l}(\tau_l) c_{d\sigma_l}(\tau_l) \right). \tag{42}$$

In this expansion, the only terms that contribute to the trace are even order ones ($m = 2k$) and they are products of impurity ($d$) and bath ($s$) creator-annihilator pairs. We can thus rewrite

$$\int d\boldsymbol{\tau}^{2k} \longrightarrow \int d\boldsymbol{\tau}^k \int d\bar{\boldsymbol{\tau}}^k \quad \text{and} \qquad \hat{O}^{2k}(\boldsymbol{\tau}) \longrightarrow \sum_{\boldsymbol{\sigma},\bar{\boldsymbol{\sigma}}} \hat{O}^{2k}_{\boldsymbol{\sigma},\bar{\boldsymbol{\sigma}}}(\boldsymbol{\tau}, \bar{\boldsymbol{\tau}}) \tag{43}$$

where

$$\hat{O}^{2k}_{\boldsymbol{\sigma},\bar{\boldsymbol{\sigma}}}(\boldsymbol{\tau}, \bar{\boldsymbol{\tau}}) = (t)^{2k} \prod_{i=1}^k \left( c^\dagger_{d\bar{\sigma}_i}(\bar{\tau}_i) c_{s\bar{\sigma}_i}(\bar{\tau}_i) c^\dagger_{s\sigma_i}(\tau_i) c_{d\sigma_i}(\tau_i) \right). \tag{44}$$

The vector $\boldsymbol{\sigma} = (\sigma_1, \sigma_2, ..., \sigma_k)$ gives the spins $\{\sigma_i\}$ associated with the $k$ impurity annihilators at imaginary times $\{\tau_i\}$, while $\bar{\boldsymbol{\sigma}} = (\bar{\sigma}_1, \bar{\sigma}_2, ..., \bar{\sigma}_k)$ gives the spins $\{\bar{\sigma}_i\}$ associated with the $k$ impurity creators at imaginary times $\{\bar{\tau}_i\}$. It follows that the local and bath traces can be

decoupled and the partition function can be rewritten as

$$\frac{Z}{Z_{\rm bath}} = \sum_k \int d\boldsymbol{\tau}^k \int d\bar{\boldsymbol{\tau}}^k \sum_{\boldsymbol{\sigma},\bar{\boldsymbol{\sigma}}} d^k_{\bar{\boldsymbol{\sigma}},\boldsymbol{\sigma}}(\boldsymbol{\tau},\bar{\boldsymbol{\tau}})\, t^k_{\boldsymbol{\sigma},\bar{\boldsymbol{\sigma}}}(\boldsymbol{\tau},\bar{\boldsymbol{\tau}}) \tag{45}$$

$$d^k_{\bar{\boldsymbol{\sigma}},\boldsymbol{\sigma}}(\boldsymbol{\tau},\bar{\boldsymbol{\tau}}) = \frac{t^{2k}}{Z_{\rm bath}}\, {\rm Tr}_{\rm bath}\left(e^{-\beta(\hat{H}_{\rm bath}-\mu\hat{N}_s)}\mathcal{T}\prod_{i=k}^{1} c^\dagger_{s\sigma_i}(\tau_i)c_{s\bar{\sigma}_i}(\bar{\tau}_i)\right) \tag{46}$$

$$t^k_{\boldsymbol{\sigma},\bar{\boldsymbol{\sigma}}}(\boldsymbol{\tau},\bar{\boldsymbol{\tau}}) = {\rm Tr}_{\rm loc}\left(e^{-\beta(\hat{H}_{\rm loc}-\mu\hat{N}_d)}\mathcal{T}\prod_{i=k}^{1} c_{d\sigma_i}(\tau_i)c^\dagger_{d\bar{\sigma}_i}(\bar{\tau}_i)\right), \tag{47}$$

where $Z_{\rm bath} = 1 + 2e^{-\beta(\varepsilon_s-\mu)} + e^{-2\beta(\varepsilon_s-\mu)}$ and

$$c_{d\sigma}(\tau) = e^{\tau(\hat{H}_{\rm loc}-\mu\hat{N}_d)}c_{d\sigma}e^{-\tau(\hat{H}_{\rm loc}-\mu\hat{N}_d)}, \qquad c_{s\sigma}(\tau) = e^{\tau(\hat{H}_{\rm bath}-\mu\hat{N}_s)}c_{s\sigma}e^{-\tau(\hat{H}_{\rm bath}-\mu\hat{N}_s)}.$$

The trace involving only bath operators is simple to calculate, since $\hat{H}_{\rm bath}$ describes an independent-electron problem for which Wick's theorem holds. It is given by the determinant

$$d^k_{\bar{\boldsymbol{\sigma}},\boldsymbol{\sigma}}(\boldsymbol{\tau},\bar{\boldsymbol{\tau}}) = \det\left(\mathcal{F}^k_{\bar{\boldsymbol{\sigma}},\boldsymbol{\sigma}}(\boldsymbol{\tau},\bar{\boldsymbol{\tau}})\right) \tag{48}$$

of the $k\times k$ non-interacting hybridization-function matrix, with elements

$$\left(\mathcal{F}^k_{\bar{\boldsymbol{\sigma}},\boldsymbol{\sigma}}(\boldsymbol{\tau},\bar{\boldsymbol{\tau}})\right)_{i',i} = \mathcal{F}^0_{\bar{\sigma}_{i'},\sigma_i}(\bar{\tau}_{i'}-\tau_i), \tag{49}$$

where

$$\mathcal{F}^0_{\bar{\sigma},\sigma}(\tau) = \delta_{\bar{\sigma},\sigma}\frac{t^2}{1+e^{-\beta(\varepsilon_s-\mu)}} \times \begin{cases} -e^{-\tau(\varepsilon_s-\mu)} & \tau > 0, \\ +e^{-(\beta+\tau)(\varepsilon_s-\mu)} & \tau < 0. \end{cases} \tag{50}$$

This is the imaginary time Fourier transform of the hybridization function introduced previously

$$\mathcal{F}^0_{\bar{\sigma},\sigma}(i\nu_n) = \frac{t^2}{i\nu_n - (\varepsilon_s-\mu)}\,\delta_{\bar{\sigma},\sigma}. \tag{51}$$

The calculation of the local trace is in general more complicated. In the case discussed here, the Hamiltonian does not flip spins. Thus only terms with an equal number of creation and annihilation operators *per spin* contribute to the local trace, and we can express the partition function in expansion orders per spin, $k_\sigma$. This yields [10]

$$\frac{Z}{Z_{\rm bath}} = \left(\prod_\sigma \sum_{k_\sigma=0}^{\infty}\int d\boldsymbol{\tau}_\sigma^{k_\sigma}\int d\bar{\boldsymbol{\tau}}_\sigma^{k_\sigma}\right) d^k_{\bar{\boldsymbol{\sigma}},\boldsymbol{\sigma}}(\boldsymbol{\tau},\bar{\boldsymbol{\tau}})t^k_{\boldsymbol{\sigma},\bar{\boldsymbol{\sigma}}}(\boldsymbol{\tau},\bar{\boldsymbol{\tau}}), \tag{52}$$

where the vectors $\boldsymbol{\sigma} = (\boldsymbol{\sigma}_\uparrow,\boldsymbol{\sigma}_\downarrow)$ and $\bar{\boldsymbol{\sigma}} = (\bar{\boldsymbol{\sigma}}_\uparrow,\bar{\boldsymbol{\sigma}}_\downarrow)$ have $(k_\uparrow,k_\downarrow)$ components, and for each $k_\sigma$ component $\sigma_i = \bar{\sigma}_i = \sigma$. Thus

$$t^k_{\boldsymbol{\sigma},\bar{\boldsymbol{\sigma}}}(\boldsymbol{\tau},\bar{\boldsymbol{\tau}}) = {\rm Tr}_{\rm loc}\left(e^{-\beta(\hat{H}_{\rm loc}-\mu\hat{N}_d)}\,\mathcal{T}\prod\nolimits_\sigma\prod\nolimits_{i=k_\sigma}^{1} c_{d\sigma}(\tau_{\sigma_i})c^\dagger_{d\sigma}(\bar{\tau}_{\bar{\sigma}_i})\right). \tag{53}$$

The latter can be calculated analytically. To do this, first we parametrize all configurations for a given spin via a timeline $[0,\beta)$ plus a number of creator/annihilator pairs which define segments

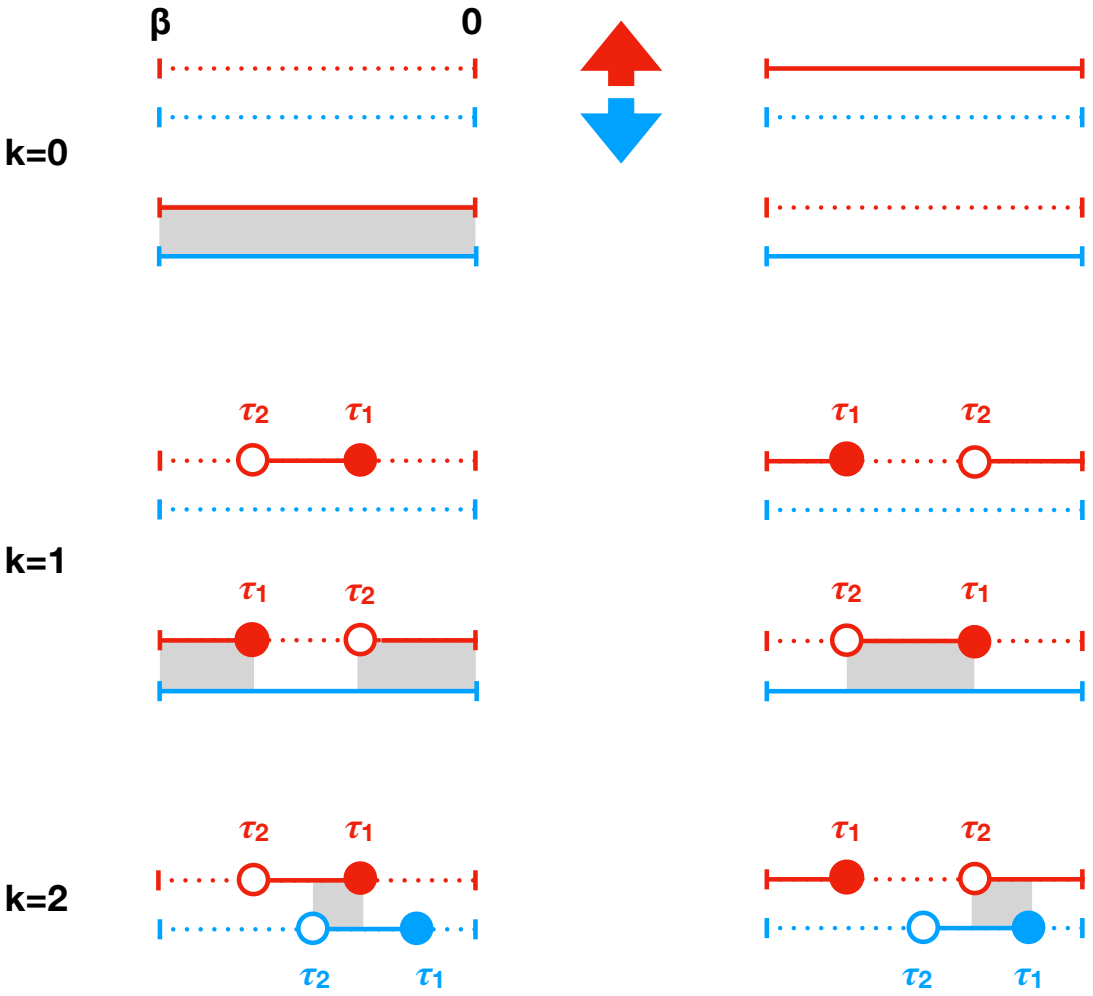


**Fig. 5:** *Representative configurations contributing to the local trace at zeroth, first and second order. The timelines for spin up are red and those for spin down are blue. The filled circles correspond to the insertion of a creator (time $\tau_1$), and the empty circles to the insertion of an annihilator (time $\tau_2$). Dotted lines represent the vacuum state for a given spin, full lines the occupied state. The grey boxes indicate the regions in which $l_{\uparrow,\downarrow} \neq 0$.*

on the timeline. At zeroth order two possible configurations exist per spin, an empty timeline, which corresponds to the vacuum state $|0\rangle$, and a full timeline, which corresponds to the state $c^\dagger_{d\sigma}|0\rangle$. A given configuration yields, at order $k = k_\uparrow + k_\downarrow$

$$t^k_{\sigma,\bar{\sigma}}(\boldsymbol{\tau},\bar{\boldsymbol{\tau}}) = \left(\prod_\sigma s^{k_\sigma}_\sigma\right) e^{-\sum_{\sigma\sigma'}((\varepsilon_d-\mu)\delta_{\sigma\sigma'}+\frac{U}{2}(1-\delta_{\sigma,\sigma'}))l_{\sigma,\sigma'}}, \tag{54}$$

where $l_{\sigma,\sigma'}$ is the length of the overlap of the $\tau$ segments for spins $\sigma$ and $\sigma'$, respectively, while $s_\sigma = \mathrm{sign}(\tau_{\sigma_1} - \bar{\tau}_{\sigma_1})$ is the fermionic sign. Possible configurations at order $k = 0, 1, 2$ are shown in Fig. 5. At order $k = 0$, summing up the contribution of the four configurations shown in Fig. 5 yields the local partition function $Z_{\rm loc} = 1 + 2e^{-\beta(\varepsilon_d-\mu)} + e^{-\beta(2(\varepsilon_d-\mu)+U)}$. Order $k = 1$ is already more complicated. Setting $\varepsilon_s = \mu$ as in the self-consistent solution, the contribution

to the bath trace in this case is

$$d^1_{\bar\sigma\sigma}(\tau_1,\tau_2) = \mathcal{F}^0_{\bar\sigma\sigma}(\tau_1,\tau_2) = -\frac{t^2}{2}\delta_{\sigma,\bar\sigma}\ \mathrm{sign}(\tau_1-\tau_2). \tag{55}$$

The local trace at the same order is instead given by

$$t^1_{\sigma\bar\sigma}(\tau_2,\tau_1) = \mathrm{Tr}_{\mathrm{loc}}\Big(e^{-\beta(\hat H_{\mathrm{loc}}-\mu\hat N_d)}\mathcal{T}c_{d\sigma}(\tau_2)c^\dagger_{d\sigma}(\tau_1)\Big). \tag{56}$$

We can now calculate the contribution at half filling of the four $k=1$ configurations shown in Fig. 5. In the case $k_\uparrow = 1$ and $k_\downarrow = 0$ we have, going from left to right in each row

$$t^1_{\uparrow\uparrow}(\tau_2,\tau_1) = \begin{cases} +e^{-(\tau_2-\tau_1)(\varepsilon_d-\mu)} & = +e^{+\tau_{21}U/2} \\ -e^{-(\beta-(\tau_1-\tau_2))(\varepsilon_d-\mu)} & = -e^{(\beta+\tau_{21})U/2} \\ -e^{-\beta(2(\varepsilon_d-\mu)+U)+(\tau_1-\tau_2)(\varepsilon_d-\mu+U)} & = -e^{-\tau_{21}U/2} \\ +e^{-(\tau_2-\tau_1)(\varepsilon_d-\mu+U)-\beta(\varepsilon_d-\mu)} & = +e^{(\beta-\tau_{21})U/2} \end{cases} \tag{57}$$

where $\tau_{21} = \tau_2 - \tau_1$ and $\mu = \varepsilon_d + U/2$. Similar results can be obtained for $k_\uparrow = 0$ and $k_\downarrow = 1$. Summing up all terms up to order one we find

$$\begin{aligned} \frac{Z}{Z_{\mathrm{bath}}} &\sim Z_{\mathrm{loc}} + \sum_\sigma \int_0^\beta d\tau_2 \int_0^\beta d\tau_1\, d^1_{\sigma\sigma}(\tau_1,\tau_2)\, t^1_{\sigma\sigma}(\tau_2,\tau_1) \\ &\sim Z_{\mathrm{loc}}\left(1 - \beta\frac{1-e^{\frac{\beta U}{2}}}{1+e^{\frac{\beta U}{2}}}\frac{2t^2}{U}\right). \end{aligned} \tag{58}$$

The exact formula of the partition function can be obtained from the eigenvalues and eigenvectors in Appendix A

$$\frac{Z}{Z_{\mathrm{bath}}} = Z_{\mathrm{loc}}\frac{3(1+e^{\frac{\beta U}{2}}) + e^{\frac{\beta U}{4}}\left(4e^{-\frac{\beta\Delta(t,U)}{4}} + 4e^{+\frac{\beta\Delta(t,U)}{4}} + e^{+\frac{\beta\Delta(t,U/2)}{2}} + e^{-\frac{\beta\Delta(t,U/2)}{2}}\right)}{8\big(1+e^{\frac{\beta U}{2}}\big)}. \tag{59}$$

Its Taylor expansion in powers of $t/U$ yields, at second order, the expression above. Going back to Eq. (56), one can observe that, for $k=1$, the local trace is proportional to the local Green function, $G^\sigma_{d,d}(\tau)$. Indeed, $G^\sigma_{d,d}(\tau)$ can be calculated using the configurations just described—provided that we start from $k=1$ and we divide by the hybridization function. More specifically, for $k=1$ and $\tau > 0$ we have

$$G^\sigma_{d,d}(\tau) \sim -\frac{1}{\beta}\int_0^\beta\int_0^\beta \underbrace{d\tau_2 d\tau_1\, d^1_{\sigma\sigma}(\tau_1,\tau_2)t^1_{\sigma\sigma}(\tau_2,\tau_1)}_{w^1}\ \delta\big(\tau-(\tau_2-\tau_1)\big)\ \frac{1}{\mathcal{F}^0_{\sigma\sigma}(\tau_1-\tau_2)}. \tag{60}$$

We are now ready to generalize to arbitrary order. Taking all $k$ values into account, the partition function can be expressed as the sum over all configurations $\{c\}$, i.e., in short

$$Z = \sum_c w_c = \sum_c |w_c|\ \mathrm{sign}\ w_c. \tag{61}$$

In a compact form, we can write $w_c = d\boldsymbol{\tau}_c \; d_c \; t_c$ where $d\boldsymbol{\tau}_c = \prod_\sigma \prod_i^{k_\sigma} d\tau_{\sigma_i} d\bar{\tau}_{\bar{\sigma}_i}$, and $d_c$ and $t_c$ are the bath and local traces for the configuration $c$. This expression of the partition function shows that we can interpret $|w_c|$ as the sampling weight of configuration $c$. A generic observable $\hat{O}$ can then be obtained as the Monte Carlo average on a finite number of configurations $N_c$

$$\langle \hat{O} \rangle = \frac{\sum_c \langle \hat{O} \rangle_c |w_c| \,\mathrm{sign}\; w_c}{\sum_c |w_c| \,\mathrm{sign}\; w_c} = \frac{\sum_c \mathrm{sign}\; w_c \langle \hat{O} \rangle_c \; |w_c| / \sum_c |w_c|}{\sum_c \mathrm{sign}\; w_c \; |w_c| / \sum_c |w_c|} \approx \frac{\frac{1}{N_c} \sum_c^{N_c} \langle \hat{O} \,\rangle_c \,\mathrm{sign}\; w_c}{\frac{1}{N_c} \sum_c \mathrm{sign}\; w_c}. \quad (62)$$

The term $\frac{1}{N_c} \sum_c \mathrm{sign}\; w_c$ in the denominator is the average fermionic sign. When this is small, much longer runs are required to obtain data of the same quality; eventually the computational time can become so long that the calculation is unfeasible—in these cases we have a sign problem. In practice, the QMC simulation starts from a random configuration $c$. Next we propose an update $c \to c'$. Within the Metropolis-Hastings algorithm, the acceptance ratio is

$$R_{c\to c'} = \min\left(1, \frac{p_{c'\to c}}{p_{c\to c'}} \frac{|w_{c'}|}{|w_c|}\right), \quad (63)$$

where $p_{c\to c'}$ is the proposal probability for the update $c \to c'$. In the approach described here, known as *segment solver*, the basic updates are addition and removal of segments, antisegments (segments winding over the borders of the timeline, see Fig. 5), or complete lines. As example, let us consider the insertion of a segment for spin $\sigma$. A segment is made by a creator and an annihilator. The creator is inserted at time $\tau_{\rm in}$; the move is rejected if $\tau_{\rm in}$ is in a region where a segment exists. If created, the segment can have at most length $l_{\rm max}$, given by the distance between $\tau_{\rm in}$ and the time at which the next creator is, hence

$$p_{c\to c'} = \frac{d\bar{\tau}}{\beta} \frac{d\tau}{l_{\rm max}} \,. \quad (64)$$

The proposal probability of the reverse move (removing a segment) is instead given by the inverse of the number of existing segments

$$p_{c'\to c} = \frac{1}{k_\sigma + 1} \,. \quad (65)$$

The acceptance ratio for the insertion of a segment becomes then

$$R_{c\to c'} = \min\left(1, \frac{\beta l_{max}}{k_\sigma + 1} \left| \frac{d_{c'}}{d_c} \frac{t_{c'}}{t_c} \right| \right). \quad (66)$$

For the impurity Green function, here the most important observable, the direct average yields

$$\langle \hat{O} \rangle_c = \langle G^\sigma_{d,d} \rangle_c = \sum_{\sigma'} \sum_{i=1}^{k_\sigma} \sum_{j=1}^{k_\sigma} \Delta(\tau, \tau_{\sigma' j} - \bar{\tau}_{\sigma' j}) \left(M^{k'_\sigma}\right)_{\sigma' j, \sigma' i} \delta_{\sigma, \sigma_{\sigma' j}} \delta_{\sigma, \bar{\sigma}_{\sigma' i}} \quad (67)$$

where $M^k = \left(\mathcal{F}^k\right)^{-1}$ is the inverse of the hybridization matrix and

$$\Delta(\tau, \tau') = -\frac{1}{\beta} \begin{cases} \delta(\tau - \tau') & \tau' > 0 \\ -\delta(\tau - (\tau' + \beta)) & \tau' < 0 \end{cases} . \quad (68)$$

One can verify that at order $k = 1$ this indeed returns Eq. (60).

## 2.4 DMFT for the single- and multi-orbital Hubbard model

The Hubbard Hamiltonian (3) is in principle the simplest model for the description of the Mott metal-insulator transition. In the tight-binding approximation it becomes

$$\hat{H} = \varepsilon_d \sum_{\sigma i} \hat{n}_{i\sigma} - t \sum_{\sigma \langle ii' \rangle} c^\dagger_{i\sigma} c_{i'\sigma} + U \sum_i \hat{n}_{i\uparrow} \hat{n}_{i\downarrow}, \tag{69}$$

where $\langle ii' \rangle$ is a sum over first neighbors. As discussed in the introduction, for $U = 0$, at half-filling, this Hamiltonian describes a metallic band. For $t = 0$ it describes an insulating collection of disconnected atoms. Somewhere in-between, at a critical value of $t/U$, a metal to insulator transition must occur. In this section we will discuss the DMFT solution of (69) and the picture of the metal-insulator transition emerging from it. The first step consists in mapping the original many-body Hamiltonian into an effective quantum-impurity model, such as the Anderson Hamiltonian

$$\hat{H}^A = \underbrace{\sum_{\boldsymbol{k}\sigma} \varepsilon^s_{\boldsymbol{k}} \hat{n}_{\boldsymbol{k}\sigma}}_{\hat{H}_{\rm bath}} + \underbrace{\sum_{\boldsymbol{k}\sigma} \left( V^s_{\boldsymbol{k}} c^\dagger_{\boldsymbol{k}\sigma} c_{d\sigma} + \text{h.c.} \right)}_{\hat{H}_{\rm hyb}} + \underbrace{\varepsilon_d \sum_\sigma \hat{n}_{d\sigma} + U \hat{n}_{d\uparrow} \hat{n}_{d\downarrow}}_{\hat{H}_{\rm imp}}. \tag{70}$$

In this model the on-site Coulomb repulsion $U$ appears only in the impurity Hamiltonian, $\hat{H}_{\rm imp}$, while the terms $\hat{H}_{\rm bath}$ and $\hat{H}_{\rm hyb}$, describe, respectively, the bath and the bath-impurity hybridization. In the next step, the quantum-impurity model is solved. Differently from the case of the Anderson molecule, this cannot be done analytically. It requires non-perturbative numerical methods, such as exact diagonalization, the numerical renormalization group, density-matrix renormalization group or QMC. Here we describe the DMFT self-consistency loop for a QMC quantum-impurity solver. Solving the quantum-impurity model yields the impurity Green function $G^\sigma_{d,d}(i\nu_n)$. From the impurity Dyson equation we can calculate the impurity self-energy

$$\Sigma^\sigma_A(i\nu_n) = \left( G^{0\sigma}_{d,d}(i\nu_n) \right)^{-1} - \left( G^\sigma_{d,d}(i\nu_n) \right)^{-1}. \tag{71}$$

Next, we adopt the local self-energy approximation, i.e., we assume that the self-energy of the Hubbard model equals the impurity self-energy. Then, the local Green function is given by

$$G^\sigma_{i_c,i_c}(i\nu_n) = \frac{1}{N_{\boldsymbol{k}}} \sum_{\boldsymbol{k}} \frac{1}{i\nu_n + \mu - \varepsilon_{\boldsymbol{k}} - \Sigma^\sigma_A(i\nu_n)}, \tag{72}$$

where $N_{\boldsymbol{k}}$ is the number of $\boldsymbol{k}$ points. The local Dyson equation is used once more, this time to calculate the bath Green function $\mathcal{G}^\sigma(i\nu_n)$, which in turn defines a new quantum-impurity model. This procedure is repeated until self-consistency is reached, i.e., the number of electrons is correct and the self-energy does not change anymore (within a given numerical accuracy). In this situation we have

$$G^\sigma_{i_c,i_c}(i\nu_n) \sim G^\sigma_{d,d}(i\nu_n). \tag{73}$$

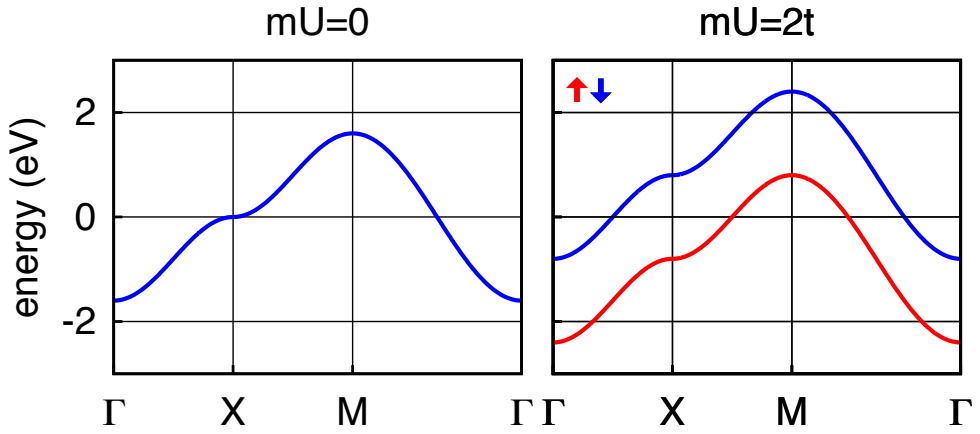


**Fig. 6:** *The metal-insulator transition in ferromagnetic Hartree-Fock. The calculation is for a square lattice tight-binding model with dispersion* $\varepsilon_{\boldsymbol{k}} = -2t(\cos k_x + \cos k_y)$.

It is important to underline that self-consistency is key to the success of DMFT in describing the metal-to-insulator transition. This can, perhaps, be best understood looking once more at the effects of self-consistency in a simpler approach, the static mean-field Hartree-Fock method.[6] If we chose the same primitive cell as in DMFT, the Hartree-Fock self-energy matrix is

$$\Sigma^{\sigma}_{i,i'}(i\nu_n) = U\left(\frac{n}{2} - s_\sigma m\right)\delta_{i,i'}, \tag{74}$$

where $s_\sigma = +1$ for spin up and $s_\sigma = -1$ for spin down and $m = m_+ = (n_\uparrow - n_\downarrow)/2$, with $n_\sigma = n_{i\sigma}$. The approximation is then identical to replacing the Hubbard Hamiltonian with

$$\hat{H}_{\rm HF} = \sum_{\boldsymbol{k}\sigma}\left(\varepsilon_{\boldsymbol{k}} + U\left(\frac{1}{2} - s_\sigma m\right)\right)\hat{n}_{\boldsymbol{k}\sigma}. \tag{75}$$

This shows that $h_{\rm eff} = 2Um$ plays the role of an effective magnetic field (Weiss field). The self-consistency criterion is

$$\bar{n}_\sigma = \bar{n}_{i\sigma} = \langle \hat{n}_{i\sigma}\rangle_{\rm HF}\,, \tag{76}$$

where the expectation value $\langle \hat{n}_{i\sigma}\rangle_{\rm HF}$ is calculated using the Hamiltonian $\hat{H}_{\rm HF}$, which in turn depends on $\bar{n}_\sigma$ via $m$. This gives the self-consistency equation

$$m = \frac{1}{2}\frac{1}{N_{\boldsymbol{k}}}\sum_{\boldsymbol{k}\sigma}\frac{\sigma e^{-\beta(\varepsilon_{\boldsymbol{k}} + U(\frac{1}{2} - s_\sigma m) - \mu)}}{1 + e^{-\beta(\varepsilon_{\boldsymbol{k}} + U(\frac{1}{2} - s_\sigma m) - \mu)}}\,. \tag{77}$$

If we set $m = 0$ the equation is satisfied; for such a trivial solution the static mean-field correction in Eq. (75) merely redefines the chemical potential and has therefore no effect. For sufficiently large $U$, however, a non-trivial solution ($m \neq 0$) can be found. If $m \neq 0$ the spin up and spin down bands split, and eventually a gap can open. This is shown in Fig. 6. The static mean-field correction in Eq. (75) equals the contribution of the Hartree diagram to the self-energy, $\Sigma^{\sigma}_{\rm H}(i\nu_n) = U\bar{n}_{-\sigma}$. In many-body perturbation theory, however, $\bar{n}_\sigma = 1/2$, i.e., $m = 0$.

[6] Keeping in mind that many self-consistent solutions obtained with the Hartree-Fock method are spurious.

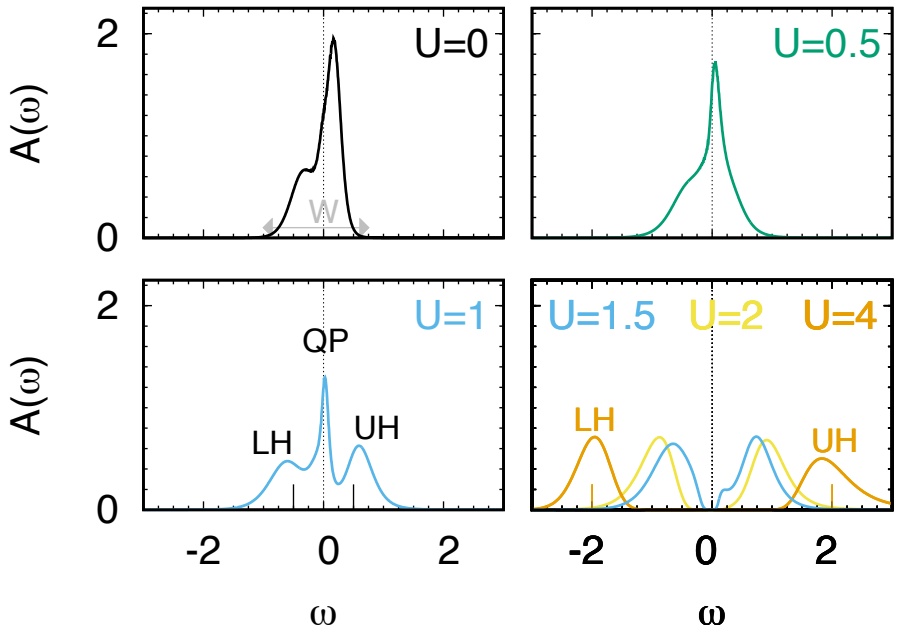


**Fig. 7:** *$VOMoO_4$: LDA+DMFT spectral function at finite temperature for $0 \leq U \leq 4$. Energies are in eV and spectral functions in states/spin/eV. The calculations have been done using a continuous-time hybridization-expansion QMC solver [10]. A detailed LDA+DMFT study of the electronic and magnetic properties $VOMoO_4$ can be found in Ref. [11].*

In the self-consistent static mean-field approximation, instead, $m$ can differ from zero, and a phenomenon not described by the mere Hartree diagram can be captured, ferromagnetism in a correlated metal. If the band splitting, given by $h_{\rm eff}{=}2Um$, is larger than the bandwidth, the system can even become an insulator.

In DMFT the role of the Weiss mean field is played by the bath Green function $\mathcal{G}^{\sigma}_{i,i}(i\nu_n)$. The emerging picture of the Mott transition is described in Fig. 7 for a representative single-band material. In the $U = 0$ limit, the spectral function $A_0(\omega)$ is metallic at half filling (top left panel). For finite $U$, if we set $\Sigma^{\sigma}_A(\omega) = 0$ as initial guess, the DMFT self-consistency loop starts with $A(\omega) = A_0(\omega)$. For small $U/t$, the *converged* spectral function $A(\omega)$ is still similar to $A_0(\omega)$. This can be seen comparing the $U = 0.5$ and $U = 0$ panels in Fig. 7. Further increasing $U/t$, sizable spectral weight is transferred from the zero-energy quasi-particle peak to the lower (LH) and upper (UH) Hubbard bands, centered at $\omega \sim \pm U/2$. This can be observed in the $U = 1$ panel of Fig. 7. The system is still metallic, but with strongly renormalized masses and short lifetimes, reflected in the narrow quasi-particle (QP) peak. Finally, for $U$ larger than a critical value ($U \geq 1.5$ in the figure) a gap opens and the system becomes a Mott insulator. When this happens the self-energy diverges at low frequency, where

$$\Sigma^{\sigma}_A(\omega + i0^+) \sim \frac{U}{2} + \frac{U^2}{4}\frac{a(t,U)}{\omega + i0^+}. \tag{78}$$

In the large $U/t$ limit the gap increases linearly with the Coulomb repulsion, i.e., $E_g(1) \sim U - W$, where $W$ is the bandwidth.

The single-band Hubbard model describes the essence of the metal-insulator transition. In order to understand this phenomenon in materials, however, we have to study multi-orbital Hubbard-like Hamiltonians. These have the form

$$\hat{H} = \hat{H}_0 + \hat{H}_U$$
$$\hat{H}_0 = -\sum_{ii'}\sum_{\sigma}\sum_{mm'} t^{i,i'}_{m\sigma,m'\sigma'}\, c^{\dagger}_{im\sigma} c_{i'm'\sigma'}$$
$$\hat{H}_U = \frac{1}{2}\sum_{i}\sum_{\sigma\sigma'}\sum_{mm'}\sum_{pp'} U_{mpm'p'}\, c^{\dagger}_{im\sigma} c^{\dagger}_{ip\sigma'} c_{ip'\sigma'} c_{im'\sigma},$$

where $m, m'$ and $p, p'$ are different orbitals and the Coulomb tensor is local. The DMFT approach can be extended to solve models of this type, mapping them to multi-orbital quantum-impurity models. The main changes with respect to the formalism introduced in the previous section are then the following

$$\varepsilon_{\boldsymbol{k}} \to (H_{\boldsymbol{k}})_{m\sigma,m'\sigma'} \qquad (i\nu_n+\mu) \to (i\nu_n+\mu)\,\hat{1}_{m\sigma,m'\sigma'}$$
$$t^{i,i'} \to t^{i,i'}_{m\sigma,m'\sigma'} \qquad \varepsilon_d \to \varepsilon^{i,i'}_{m\sigma,m'\sigma'} = -t^{i,i}_{m\sigma,m'\sigma'}$$

where $\hat{1}$ is the identity matrix. As a consequence, the local Green function, the bath Green function, the hybridization function and the self-energy also become matrices

$$\mathcal{G}^{\sigma}(i\nu_n) \to \mathcal{G}^{\sigma,\sigma'}_{m,m'}(i\nu_n) \qquad G^{\sigma}(i\nu_n) \to G^{\sigma,\sigma'}_{m,m'}(i\nu_n) \qquad \Sigma^{\sigma}(i\nu_n) \to \Sigma^{\sigma,\sigma'}_{m,m'}(i\nu_n).$$

The corresponding generalization of the self-consistency loop is shown schematically in Fig. 8. Although the extension of DMFT to Hubbard models with many orbitals might appear straightforward, in practice it is not. The bottleneck is the solution of the generalized multi-orbital quantum-impurity problem. The most flexible solvers available so far are all based on QMC. Despite being flexible, QMC-based approaches have limitations. These can be classified in two types. First, with increasing the number of degrees of freedom, calculations become very quickly computationally too expensive—how quickly depends on the specific QMC algorithm used and the actual implementation. Thus, going beyond a rather small number of orbitals and reaching the zero-temperature limit is unfeasible in practice. The second type of limitation is more severe. Increasing the number of degrees of freedom leads, eventually, to the infamous sign problem; when this happens, QMC calculations cannot be performed at all. In order to deal with limitations of the first type, it is crucial to restrict QMC calculations to the essential degrees of freedom; furthermore, we should exploit symmetries, develop fast algorithms and use the power of massively parallel supercomputers to reduce the actual computational time. For the second type of problems not a lot can be done; nevertheless, it has been shown that a severe sign problem might appear earlier with some basis choices than with others [10]. Although eventually we cannot escape it, this suggests that the model set up can be used as a tool to expand the moderate sign-problem zone. For what concerns symmetries, in the paramagnetic

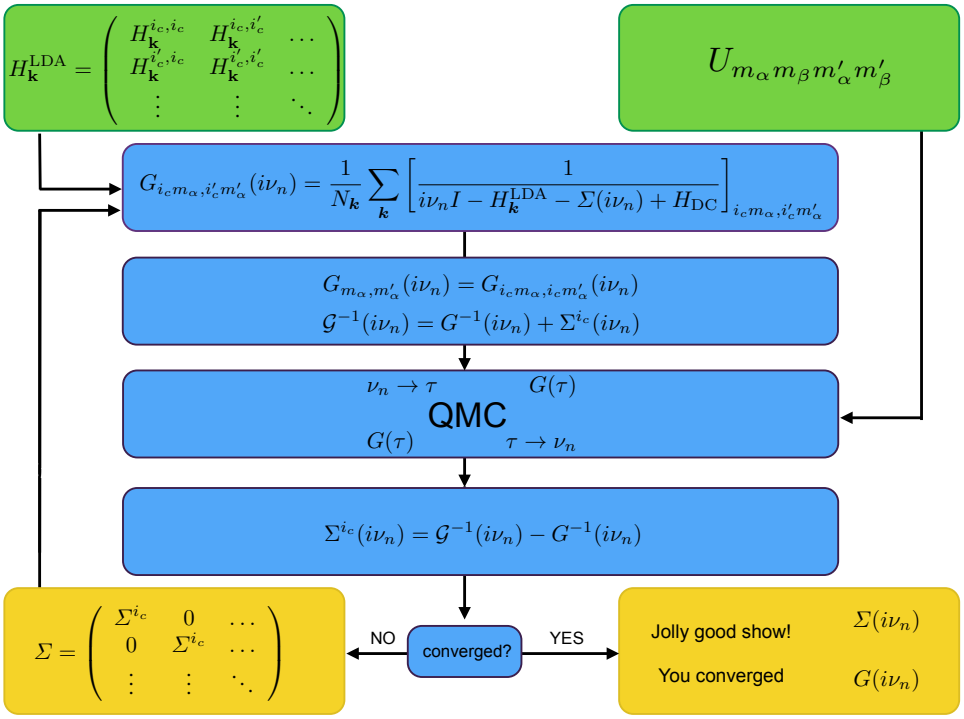


**Fig. 8:** *LDA+DMFT self-consistency loop. The one-electron Hamiltonian is built in the basis of Bloch states obtained from localized Wannier functions, for example in the local-density approximation (LDA); this gives* $H_{\boldsymbol{k}}^{\mathrm{LDA}}$*. The set* $\{i_c\}$ *labels the equivalent correlated sites inside the unit cell. The local Green-function matrix is at first calculated using an initial guess for the self-energy matrix. The bath Green-function matrix is then obtained via the Dyson equation and used to construct an effective quantum-impurity model. The latter is solved via a quantum-impurity solver, here quantum Monte Carlo (QMC). This yields the impurity Green-function matrix. Through the Dyson equation the self-energy is then obtained, and the procedure is repeated until self-consistency is reached.*

case and in absence of spin-orbit interaction or external fields, an obvious symmetry to exploit is the rotational invariance of spins, from which follows

$$X^{\sigma,\sigma'}_{m,m'}(i\nu_n) = \delta_{\sigma,\sigma'}\, X_{m,m'}(i\nu_n),$$

where $X = \mathcal{G}, G, \Sigma$. In addition, if we use a basis of real functions, the local Green-function matrices are real and symmetric in imaginary time $\tau$, hence

$$X^{\sigma,\sigma'}_{m,m'}(i\nu_n) = \delta_{\sigma,\sigma'}\, X_{m,m'}(i\nu_n) = \delta_{\sigma,\sigma'}\, X_{m',m}(i\nu_n).$$

Finally, often the unit cell contains several equivalent correlated sites, indicated as $\{i_c\}$ in Fig. 8. In order to avoid expensive cluster calculations, we can use space-group symmetries to construct the matrices $\mathcal{G}, G, \Sigma$ at a given site $i'_c$ from the corresponding matrices at an equivalent site, e.g., $i_c = 1$. Space-group symmetries also tell us if some matrix elements are zero. For example, for a model with only $t_{2g}$ (or only $e_g$) states, in cubic symmetry, in the paramagnetic case and in absence of spin-orbit interaction or external fields, we have

$$X^{\sigma,\sigma'}_{m,m'}(i\nu_n) = \delta_{\sigma,\sigma'}\, X_{m,m}(i\nu_n)\, \delta_{m,m'}.$$

## 2.5 LDA+DMFT: Model building

The state-of-the art approach for building realistic Hubbard-like models relies on constructing, for a given system, *materials-specific* Kohn-Sham Wannier functions $\varphi^{\rm KS}_{im\sigma}(\boldsymbol{r})$. These can be obtained via electronic structure calculations based on density-functional theory [5–7], e.g., in the LDA approximation.[7] After we have built the complete one-electron basis, the first steps in model-building are those already described in the introduction. We recall here the essential points and then discuss the next stage. The many-body Hamiltonian can be expressed as $\hat{H} = \hat{H}_0 + \hat{H}_U - \hat{H}_{\rm DC}$, with

$$\hat{H}_0 = \hat{H}^{\rm LDA} = -\sum_{\sigma}\sum_{ii'}\sum_{mm'} t^{i,i'}_{m,m'} c^{\dagger}_{im\sigma} c_{i'm'\sigma},$$

$$\hat{H}_U = \frac{1}{2}\sum_{ii'jj'}\sum_{\sigma\sigma'}\sum_{mm'pp'} U^{iji'j'}_{mp\,m'p'} c^{\dagger}_{im\sigma} c^{\dagger}_{jp\sigma'} c_{j'p'\sigma'} c_{i'm'\sigma}.$$

The double-counting correction $\hat{H}_{\rm DC}$ arises from the fact that the hopping integrals are calculated replacing the electron-nuclei interaction $v_{\rm en}(\boldsymbol{r})$ with the self-consistent DFT reference potential

$$v_{\rm R}(\boldsymbol{r}) = v_{\rm en}(\boldsymbol{r}) + \underbrace{\int d\boldsymbol{r}'\, \frac{1}{|\boldsymbol{r}-\boldsymbol{r}'|}}_{v_{\rm H}(\boldsymbol{r})} + v_{\rm xc}(\boldsymbol{r}),$$

which includes the long-range Hartree term $v_{\rm H}(\boldsymbol{r})$ and the exchange-correlation contribution $v_{\rm xc}(\boldsymbol{r})$. We thus have to subtract from $\hat{H}_U$ the effects already included in $\hat{H}_0$

$$\hat{H}_U \to \Delta\hat{H}_U = \hat{H}_U - \hat{H}_{\rm DC}.$$

Unfortunately we do not know which important correlation effects are indeed included in $\hat{H}_0$ via $v_{\rm R}(\boldsymbol{r})$, and therefore the exact expression of $\Delta\hat{H}_U$ is also unknown. The remarkable successes of the LDA suggest, however, that in many materials the LDA is overall a good approximation, and therefore, in those systems at least, the term $\Delta\hat{H}_U$ can be completely neglected. What about strongly-correlated materials? Even in correlated systems, most likely the LDA works rather well for the delocalized electrons or in describing the average or the long-range Coulomb effects. Thus one can think of separating the electrons into *uncorrelated* and *correlated*; only for the latter we do take the correction $\Delta\hat{H}_U$ into account explicitly, assuming furthermore that $\Delta\hat{H}_U$ is local or almost local [5], since we know that it is the local term which is responsible for most non-trivial many-body effects. Typically, correlated electrons are those that partially retain their atomic character, e.g., those that originate from localized $d$ and $f$ shells; for convenience, here we assume that in a given system they stem from a single atomic shell $l$ (e.g., $d$ for

[7] Using GGA or similar functionals in place of LDA yields minor differences in the many-body Hamiltonian; instead, using LDA+$U$ or similar approximations yields Hartree-Fock-like effects that would have to be subtracted via the double-counting correction.

transition-metal oxides or $f$ for heavy-fermion systems) and label their states with the atomic quantum numbers $l$ and $m = -l, \ldots, l$ of that shell. Thus

$$U^{iji'j'}_{mp\,m'p'} \sim \begin{cases} U^l_{mp\,m'p'} & iji'j' = iiii \quad \wedge \quad mp, m'p' \in l \\ 0 & iji'j' \neq iiii \quad \vee \quad mp, m'p' \notin l. \end{cases}$$

Within this approximation $\Delta\hat{H}_U$ is replaced by $\Delta\hat{H}^l_U = \hat{H}^l_U - \hat{H}^l_{\rm DC}$, where $\hat{H}^l_{\rm DC}$ is, e.g., given by the static mean-field contribution of $\hat{H}^l_U$. There is a drawback in this procedure, however. By splitting electrons into correlated and uncorrelated we implicitly assume that the main effect of the latter is the renormalization or *screening* of parameters for the former, in particular of the Coulomb interaction. The computation of screening effects remains, unfortunately, a challenge. The calculation of exact screening would require the solution of the original many-body problem, taking all degrees of freedom into account, an impossible task. Commonly-used approximate schemes are the constrained LDA approximation (cLDA) and the constrained random-phase approximation (RPA) [5–7]. Both methods give reasonable estimates of screened Coulomb parameters for DMFT calculations. Typically cRPA calculations include more screening channels and are performed for less localized bases than cLDA calculations; thus cRPA parameters turn out to be often smaller than cLDA ones. To some extent, the difference can be taken as an estimate of the error bar.

After we have selected the electrons for which we think it is necessary to include explicitly the Hubbard correction, we have to build the final Hamiltonian for DMFT calculations. To this end, it is often convenient to integrate out or *downfold*, in part or completely, the weakly correlated states. There are different degrees of downfolding. The two opposite extreme limits are (i) *no downfolding*, i.e., keep explicitly in the Hamiltonian all weakly-correlated states (ii) *massive downfolding*, i.e., downfold all weakly correlated states. If we perform massive downfolding, e.g., downfold to the $d$ (or $e_g$ or $t_{2g}$) bands at the Fermi level, the Hamiltonian relevant for DMFT takes a simpler form. The LDA part is limited to the selected orbitals or bands, which, in the ideal case, are decoupled from the rest

$$\hat{H}^{\rm LDA} = -\sum_{\sigma} \sum_{ii'} \sum_{m_\alpha m'_\alpha} t^{i,i'}_{m_\alpha, m'_\alpha}\, c^\dagger_{im_\alpha\sigma}\, c_{i'm'_\alpha\sigma}.$$

The local *screened* Coulomb interaction for this set of orbitals is the on-site tensor

$$\hat{H}^l_U = \frac{1}{2} \sum_i \sum_{\sigma\sigma'} \sum_{m_\alpha m'_\alpha} \sum_{m_\beta m'_\beta} U_{m_\alpha m_\beta m'_\alpha m'_\beta}\, c^\dagger_{im_\alpha\sigma} c^\dagger_{im_\beta\sigma'} c_{im'_\beta\sigma'} c_{im'_\alpha\sigma}.$$

It is important to point out that the level of downfolding does not modify the hardness of the quantum-impurity problem. If, for example, in studying a transition-metal oxide, we plan to treat only $3d$ bands as correlated, it does not matter if we perform calculations with a Hamiltonian containing also, e.g., O $p$ states, or we rather downfold all states but the $3d$ and work with a set of Wannier basis spanning the $3d$-like bands only. The number of correlated orbitals in the quantum-impurity problem is the same.[8]

[8] The choice might influence how severe the QMC sign problem is, however.

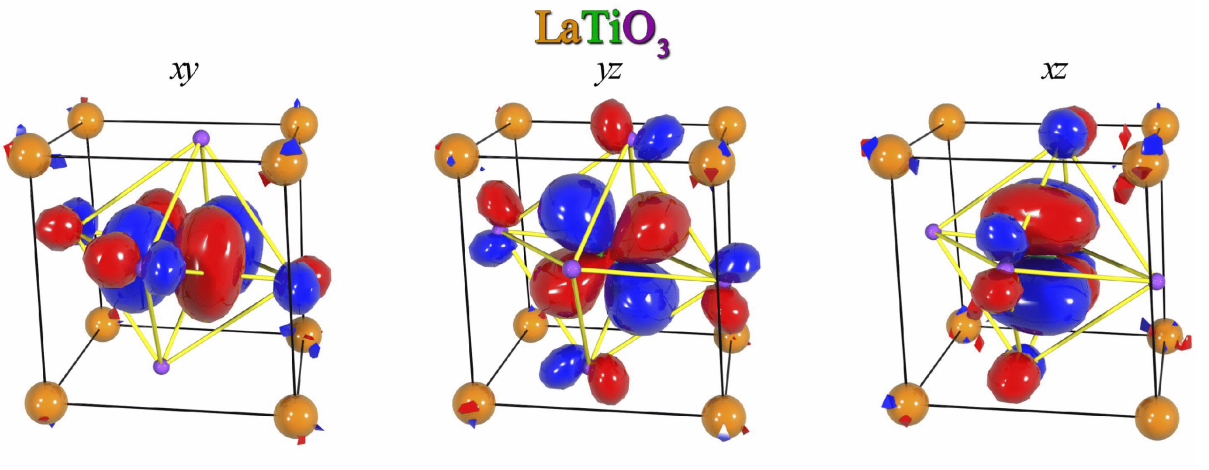


**Fig. 9:** *NMTO Wannier-like orbitals for $t_{2g}$ states in $LaTiO_3$ obtained via massive downfolding to the $t_{2g}$ bands. The $t_{2g}$-like orbitals have O $p$ tails at the neighboring O sites reflecting the distortions of the lattice. The figure has been taken from Ref. [12].*

One advantage of massive downfolding is that the double-counting correction typically becomes a shift of the chemical potential, and it is therefore not necessary to calculate it explicitly. A second important advantage is that the interpretation of the final results is simpler. Instead, a disadvantage is that the basis functions are less localized, and therefore the approximation of the Coulomb interaction to a local operator might be less justified, and in some cases it might be necessary to include non-local Coulomb terms. The effect of downfolding on the localization of Wannier functions is illustrated for example in Fig. 9. Finally, another disadvantage of massive downfolding is that the energy window in which the model is valid is more narrow.

All advantages and disadvantages considered, what is then the best way of performing DMFT calculations? There is no universal answer to this question; it depends on the problem we are trying to solve and the system we are studying. Independently of the degree of downfolding we choose, it is important to point out that a clear advantage of Wannier functions in general is that they carry information about the lattice, bonding, chemistry, and distortions. This can be seen once more in Fig. 9, where orbitals are tilted and deformed by the actual structure and chemistry of the compound. Indeed, one might naively think of using a "universal" basis, for example atomic functions, the same for all systems, and thus calculating the hopping integrals using simply the electron-nuclear interaction $v_{en}(\boldsymbol{r})$. Besides the complications arising from the lack of orthogonality, such a basis has no built-in materials-specific information, except lattice positions. It is therefore a worse starting point for describing the electronic structure, even in the absence of correlations: larger basis sets are required to reach the same accuracy. From the point of view of LDA+DMFT, an advantage of an universal basis would be that it is free from double-counting corrections; on the other hand, however, exactly because we do not use the LDA potential and LDA orbitals to calculate the hopping integrals, we also cannot count on the successes of LDA in the description of average and long-range Coulomb effects. The hopping integrals would not even include the long-range Hartree term. For these

reasons *ab-initio* Wannier functions remain so far the basis of choice. They can be built via the $N$th-Order Muffin-Tin Orbital (NMTO) method [12], the maximal-localization scheme [13], or projectors. Fig. 9 shows examples of NMTO-based Wannier functions. No matter what construction procedure is used, a common characteristic of *ab-initio* Wannier functions is that they are site-centered and localized.[9] A question naturally arises: How crucial is it to use localized functions as one-electron basis? This is an important point, since we have seen that strong-correlation effects arise in systems in which the on-site Coulomb interaction is much larger than longer-range terms. Let us consider therefore two opposite extreme limits. The first is the case in which the basis functions are independent of the lattice position (i.e., they are totally delocalized). For such a basis choice the Coulomb interaction parameters would be the same for every pair of lattice sites, no matter how distant. Thus a Hubbard-like model would be hard to justify. In the second extreme case, we adopt a hypothetical basis so localized that $\psi_{im\sigma}(\boldsymbol{r})\overline{\psi_{i'm'\sigma'}}(\boldsymbol{r}) \sim \delta_{i,i'}\,\delta(\boldsymbol{r}-\boldsymbol{T}_i)$. Even for such a basis choice, the unscreened Coulomb interaction is *not* local, but given by

$$U^{iji'j'}_{mp\,m'p'} \propto \frac{\delta_{i,i'}\delta_{j,j'}}{|\boldsymbol{T}_i-\boldsymbol{T}_j|},$$

hence it decays slowly with distance, although the (divergent) on-site term dominates. More generally, we can conclude that by increasing the localization of the basis we enhance the importance of the on-site Coulomb repulsion with respect to long-range terms; this better justifies Hubbard-like models—although we have to remember that most of the long-range part of the Coulomb interaction is in any case subtracted via the double-counting correction $\hat{H}_{\rm DC}$. The extreme case of the $\delta(\boldsymbol{r}-\boldsymbol{T}_i)$ functions also illustrates, however, how far we can go. A major problem with the extremely localized basis discussed above is that it would make it impossible to properly describe bonding, since the hopping integrals would be zero. Although such a basis is, of course, never used to build many-body models, there is a tempting approximation that has similar flaws. If one uses DFT-based electronic-structure techniques that tile the space in interstitial and non-overlapping atomic spheres (e.g., the LAPW method), it is tempting to use as basis for correlated electrons the atomic functions *defined inside the atomic spheres*. These functions are, by construction, much more localized than Wannier orbitals (even when no downfolding is performed in the Wannier construction). However, they *do not form a complete basis set* in the space of square-integrable functions. This is obvious because such a basis does not even span the LDA bands; to reproduce the bands we need, in addition, functions defined in the interstitial region. This is illustrated in Fig. 10 for a simple example of two quantum well potentials.[10] We therefore cannot use it to write the many-body Hamiltonian in the usual form, $\hat{H}_0 + \hat{H}_U$. In conclusion, a basis which, as *ab-initio* Wannier functions, is complete and indeed spans the bands, is better justified, although we somewhat lose in localization.

[9] Differences in localizations between the various construction procedures are actually small for the purpose of many-body calculations, provided that the same bands are spanned in the same way.

[10] Another, but less severe, problem of atomic sphere truncations is that the results will depend on the sphere size, in particular when atomic spheres are small.

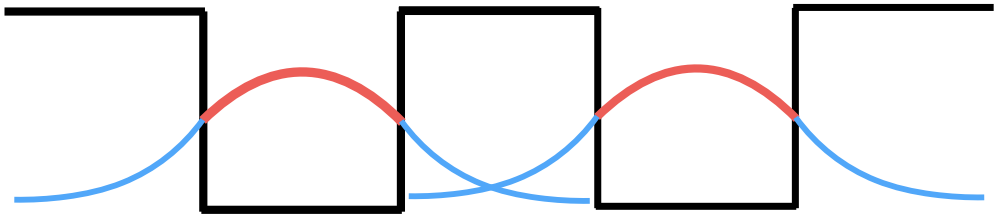

**Fig. 10:** *The problem of two quantum wells. The figure shows (schematically) for each well the wavefunction of a bound state. If we consider only the part of the wavefunction inside its own well (red in the figure), the differential overlap (and hence the hopping integral) between functions centered on different wells would be zero.*

# 3 Linear response functions

Linear response functions are key to understanding many experimental results. In this section we explain how to calculate them within the LDA+DMFT approach. First we introduce the generalized susceptibility, which yields the linear response to a given external perturbation. Next we present the method used to calculate it and discuss the approximations adopted. Last we analyze in detail the case of the magnetic susceptibility for the one-band Hubbard model.

## 3.1 Definitions

Let us start by introducing the site susceptibility in imaginary time. This is given by

$$\chi_{\hat{P}^i_\nu\,\hat{O}^{i'}_{\nu'}}(\boldsymbol{\tau}) = \left\langle \mathcal{T} \Delta\hat{P}^i_\nu(\tau_1,\tau_2)\Delta\hat{O}^{i'}_{\nu'}(\tau_3,\tau_4)\right\rangle_0, \tag{79}$$

where $\boldsymbol{\tau} = (\tau_1,\tau_2,\tau_3,\tau_4)$ and $\mathcal{T}$ is the time-ordering operator. The site-dependent operators are defined via the equations

$$\hat{P}^i_\nu(\tau_1,\tau_2) = \sum_{\boldsymbol{\alpha}} p^\nu_{\boldsymbol{\alpha}}\; c^\dagger_{i\alpha'}(\tau_2)c_{i\alpha}(\tau_1), \qquad \Delta\hat{P}^i_\nu(\tau_1,\tau_2) = \hat{P}^i_\nu(\tau_1,\tau_2) - \left\langle \hat{P}^i_\nu(\tau_1,\tau_2)\right\rangle$$
$$\hat{O}^{i'}_{\nu'}(\tau_3,\tau_4) = \sum_{\boldsymbol{\gamma}} o^{\nu'}_{\boldsymbol{\gamma}}\; c^\dagger_{i'\gamma'}(\tau_4)c_{i'\gamma}(\tau_3), \qquad \Delta\hat{O}^{i'}_{\nu'}(\tau_3,\tau_4) = \hat{O}^{i'}_{\nu'}(\tau_3,\tau_4) - \left\langle \hat{O}^{i'}_{\nu'}(\tau_3,\tau_4)\right\rangle.$$

The labels $\boldsymbol{\alpha} = (\alpha,\alpha')$, $\boldsymbol{\gamma} = (\gamma,\gamma')$ are collective flavors. For the multi-band Hubbard model they may include spin ($\sigma$) and orbital ($m$) quantum number, plus a fractional lattice vector identifying a correlated basis atom in the unit cell ($i_c$). The weight factors $o^\nu_{\boldsymbol{\alpha}}$ and $p^{\nu'}_{\boldsymbol{\gamma}}$, in general complex numbers, identify the type of response. We can then rewrite Eq. (79) as

$$\chi_{\hat{P}^i_\nu\,\hat{O}^{i'}_{\nu'}}(\boldsymbol{\tau}) = \sum_{\boldsymbol{\alpha\gamma}} p^\nu_{\boldsymbol{\alpha}} o^{\nu'}_{\boldsymbol{\gamma}}\; \chi_{i\boldsymbol{\alpha},i'\boldsymbol{\gamma}}(\boldsymbol{\tau}),$$

with

$$\chi_{i\boldsymbol{\alpha},i'\boldsymbol{\gamma}}(\boldsymbol{\tau}) = \left\langle \mathcal{T} c_{i\alpha}(\tau_1)c^\dagger_{i\alpha'}(\tau_2)c_{i'\gamma}(\tau_3)c^\dagger_{i'\gamma'}(\tau_4)\right\rangle - G_{i\alpha,i\alpha'}(\tau_1,\tau_2)G_{i'\gamma,i'\gamma'}(\tau_3,\tau_4). \tag{80}$$

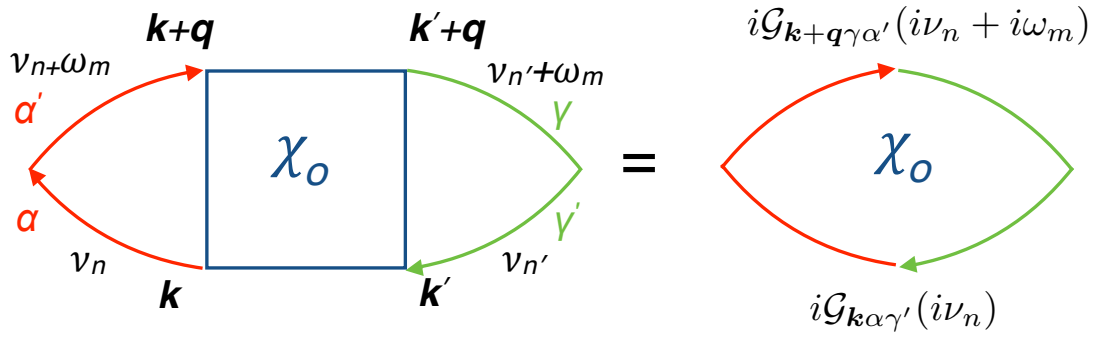


**Fig. 11:** *Diagram contributing to the linear susceptibility for a non-interacting system. The red lines indicates that the creator/annihilator is originally from the operator $\hat{P}_{\nu'}$ and the green lines indicate that the creator/annihilator is from the operator $\hat{O}_{\nu}$. The corresponding frequencies and momenta are explicitly assigned.*

Performing the Fourier transform from imaginary time to Matsubara frequencies we obtain

$$\chi_{i\boldsymbol{\alpha},i'\boldsymbol{\gamma}}(\boldsymbol{\nu}) = \frac{1}{16}\iiint d\boldsymbol{\tau}\; e^{i\boldsymbol{\nu}\cdot\boldsymbol{\tau}}\chi_{i\boldsymbol{\alpha},i'\boldsymbol{\gamma}}(\boldsymbol{\tau}), \tag{81}$$

where $\boldsymbol{\nu} = (\nu_1, -\nu_2, \nu_3, -\nu_4)$. Due to the conservation of energy, only three of the four $\nu_i$ frequencies are independent. Hence, for convenience we set $\nu_1 = \nu_n$, $\nu_2 = \nu_n + \omega_m$, $\nu_3 = \nu_{n'} + \omega_m$, and $\nu_4 = \nu_{n'}$. Next we perform the Fourier transform from site to momentum space. Due to the conservation of lattice momentum, only three of the four $\boldsymbol{k}_i$-vectors are independent. After redefining $\boldsymbol{k}_1 = \boldsymbol{k}$, $\boldsymbol{k}_2 = \boldsymbol{k}+\boldsymbol{q}$, $\boldsymbol{k}_3 = \boldsymbol{k}'+\boldsymbol{q}$ and $\boldsymbol{k}_4 = \boldsymbol{k}'$, we find the expression

$$\chi_{\hat{P}_\nu\,\hat{O}_{\nu'}}(\boldsymbol{q};\boldsymbol{\nu}) = \sum_{\boldsymbol{\alpha}\boldsymbol{\gamma}} p^{\nu}_{\boldsymbol{\alpha}} o^{\nu'}_{\boldsymbol{\gamma}} \sum_{ii'} e^{i(\boldsymbol{T}_i - \boldsymbol{T}_{i'})\cdot\boldsymbol{q}}\chi_{i\boldsymbol{\alpha},i'\boldsymbol{\gamma}}(\boldsymbol{\nu}) = \sum_{\boldsymbol{\alpha}\boldsymbol{\gamma}} p^{\nu}_{\boldsymbol{\alpha}} o^{\nu'}_{\boldsymbol{\gamma}} \underbrace{\frac{1}{N_{\boldsymbol{k}}^2}\sum_{\boldsymbol{k}\boldsymbol{k}'}[\chi(\boldsymbol{q};i\omega_m)]_{\boldsymbol{k}\nu_n\boldsymbol{\alpha},\boldsymbol{k}'\nu_{n'}\boldsymbol{\gamma}}}_{[\chi(\boldsymbol{q};\omega_m)]_{\nu_n\boldsymbol{\alpha},\nu_{n'}\boldsymbol{\gamma}}}.$$

In this expression, by summing over $\boldsymbol{k}$ and $\boldsymbol{k}'$ we obtained $[\chi(\boldsymbol{q};\omega_m)]_{\nu_n\boldsymbol{\alpha},\nu_{n'}\boldsymbol{\gamma}}$. The physical linear response function is given by the sum over the fermionic Matsubara frequencies

$$\chi_{\hat{P}_\nu\,\hat{O}_{\nu'}}(\boldsymbol{q};i\omega_m) = \sum_{\boldsymbol{\alpha}\boldsymbol{\gamma}} p^{\nu}_{\boldsymbol{\alpha}} o^{\nu'}_{\boldsymbol{\gamma}} \underbrace{\frac{1}{\beta^2}\sum_{nn'}\Big[\chi(\boldsymbol{q};\omega_m)\Big]_{\nu_n\boldsymbol{\alpha},\nu_{n'}\boldsymbol{\gamma}}}_{[\chi(\boldsymbol{q};\omega_m)]_{\boldsymbol{\alpha},\boldsymbol{\gamma}}}. \tag{82}$$

In this lecture we will consider the example of the magnetic susceptibility. In this case the operators $\hat{P}^i_\nu$ and $\hat{O}^{i'}_{\nu'}$ are the three components of the magnetization operator. In the single-orbital limit ($\alpha = \alpha' = \sigma$ and $\gamma = \gamma' = \sigma'$), we thus have, e.g.,

$$o^z_{\boldsymbol{\alpha}} = -g\mu_B\langle\sigma|\hat{\sigma}_z|\sigma\rangle, \qquad p^z_{\boldsymbol{\alpha}} = -g\mu_B\langle\sigma'|\hat{\sigma}_z|\sigma'\rangle.$$

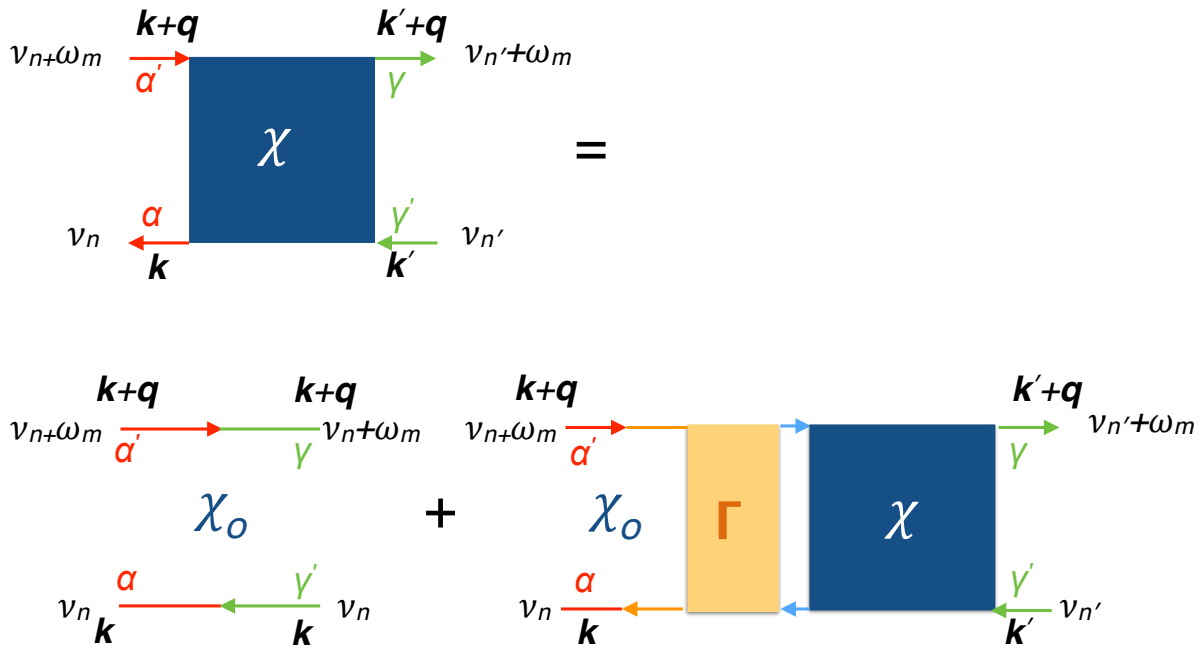


**Fig. 12:** *Diagrammatic representation of the Bethe-Salpeter equation for the linear susceptibility. The red lines indicate a creator/annihilator stemming from the operator $\hat{P}_\nu$ and the green lines from the operator $\hat{O}_{\nu'}$. The box labeled with $\Gamma$ is the vertex function, the one labeled with $\chi$ the full susceptibility, and $\chi_0$ is the pair-bubble term.*

## 3.2 DMFT and the Bethe-Salpeter equation

The linear response functions for the multi-band Hubbard model $\hat{H}_0 + \hat{H}_U$ can be in principle obtained via standard many-body perturbation theory, i.e., using the Coulomb interaction $U$ as the expansion parameter. In this approach the expansion point is the linear response function for the non-interacting Hamiltonian $\hat{H}_0$. This term, due to Wick's theorem, can be written as follows

$$\Big[\chi_0(\boldsymbol{q};i\omega_m)\Big]_{\nu_n\boldsymbol{\alpha},\nu_{n'}\boldsymbol{\gamma}} = \frac{1}{N_{\boldsymbol{k}}^2}\sum_{\boldsymbol{k}\boldsymbol{k}'}\underbrace{\Big[-\beta N_{\boldsymbol{k}}\mathcal{G}_{\boldsymbol{k}\alpha\gamma'}(i\nu_n)\,\mathcal{G}_{\boldsymbol{k}'+\boldsymbol{q}\alpha'\gamma}(i\nu_{n'}+i\omega_m)\,\delta_{n,n'}\delta_{\boldsymbol{k},\boldsymbol{k}'}\Big]}_{\Big[\chi_0(\boldsymbol{q};i\omega_m)\Big]_{\boldsymbol{k}\nu_n\boldsymbol{\alpha},\boldsymbol{k}'\nu_{n'}\boldsymbol{\gamma}}}. \quad (83)$$

The associated Feynman diagram is shown in Fig. 11, and we will refer to it as the bubble term. Once we switch on the Coulomb interaction, many-body perturbation theory leads to the Bethe-Salpeter equation, pictorially shown in Fig. 12. The susceptibility can then be expressed via the relation

$$\Big[\chi(\boldsymbol{q};i\omega_m)\Big]_{\nu_n\boldsymbol{\alpha},\nu_{n'}\boldsymbol{\gamma}} = \frac{1}{N_{\boldsymbol{k}}^2}\sum_{\boldsymbol{k}\boldsymbol{k}'}\Big[\chi_0(\boldsymbol{q};i\omega_m) + \frac{1}{N_{\boldsymbol{k}}^2}\chi_0(\boldsymbol{q};i\omega_m)\Gamma(\boldsymbol{q};i\omega_m)\chi(\boldsymbol{q};i\omega_m)\Big]_{\boldsymbol{k}\nu_n\boldsymbol{\alpha},\nu_{n'}\boldsymbol{k}'\boldsymbol{\gamma}}.$$

Replacing recursively $\chi(\boldsymbol{q};i\omega_m)$ one obtains an infinite series in the vertex $\Gamma(\boldsymbol{q};i\omega_m)$, which plays the role of the self-energy in the Dyson equation.

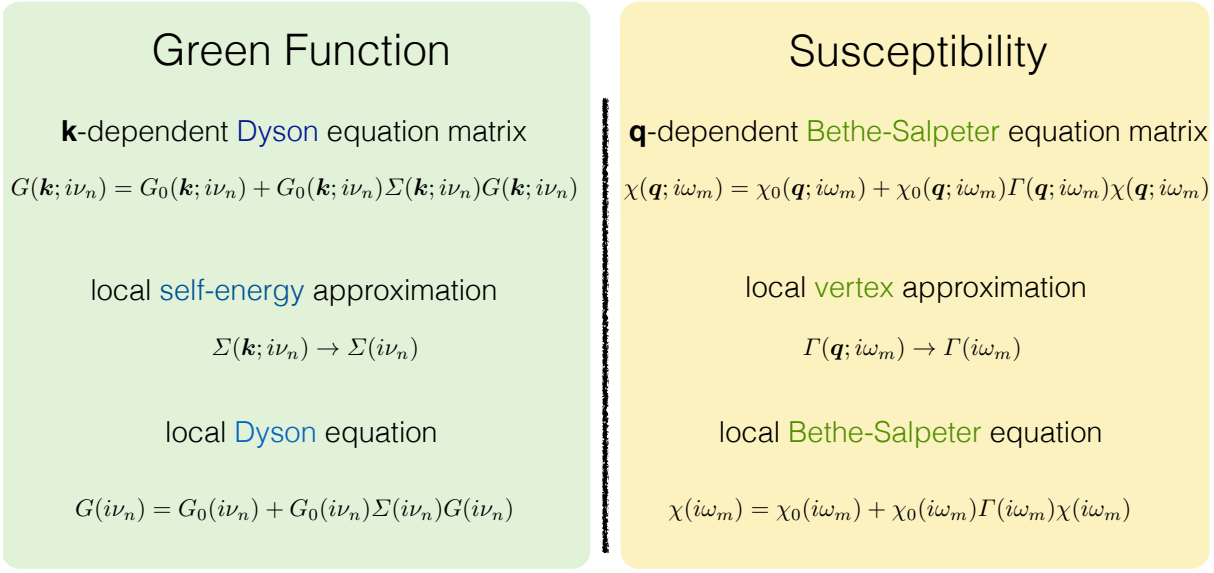


**Fig. 13:** *Analogies between the calculation of the Green function $G(\boldsymbol{k};i\nu_n)$ in the local-self-energy approximation (left) and the calculation of the response function $\chi(\boldsymbol{q};i\omega_m)$ in the local vertex approximation (right). Each term in the general Bethe-Salpeter equation can be viewed as a square matrix of dimension $N_{\boldsymbol{k}}N_nN_\alpha$, where $N_{\boldsymbol{k}}$ is the number of $\boldsymbol{k}$ points, $N_n$ the number of fermionic Matsubara frequencies, $N_\alpha$ the number of flavors.*

Instead of expanding around the non-interacting limit, for correlated systems it is more convenient to construct a diagrammatic series starting from the bubble term calculated using the DMFT Green functions, i.e., replacing $\mathcal{G} \longrightarrow G$ in Eq. (83). The result is

$$[\chi_0(\boldsymbol{q};i\omega_m)]_{\nu_n\boldsymbol{\alpha},\nu_{n'}\boldsymbol{\gamma}} = -\beta\delta_{nn'}\frac{1}{N_{\boldsymbol{k}}}\sum_{\boldsymbol{k}} G_{\alpha\gamma'}(\boldsymbol{k};i\nu_n)\, G_{\alpha'\gamma}(\boldsymbol{k}+\boldsymbol{q};i\nu_n+i\omega_m). \tag{84}$$

If we follow this approach, the unknown vertex $\Gamma(\boldsymbol{q};i\omega_m)$ in the Bethe-Salpeter equation differs from the one obtained in standard many-body perturbation theory. In order to calculate it we adopt two approximations. The first is that the vertex is approximately local. In the infinite dimension limit it has been shown that the vertex can be replaced by a local [4, 14] quantity, $\Gamma(i\omega_m)$. Assuming that, in the spirit of the dynamical mean-field approximation, for a real 3-dimensional system we can do the same, we thus set

$$\Gamma(\boldsymbol{q};i\omega_m) \longrightarrow \Gamma(i\omega_m). \tag{85}$$

Thus, dropping for simplicity the flavor indices, after performing the $\boldsymbol{k}$ sums, the Bethe-Salpeter equation becomes

$$\chi(\boldsymbol{q};i\omega_m) = \chi_0(\boldsymbol{q};i\omega_m) + \chi_0(\boldsymbol{q};i\omega_m)\Gamma(i\omega_m)\chi(\boldsymbol{q};i\omega_m). \tag{86}$$

By solving it we find, formally

$$\chi^{-1}(\boldsymbol{q};i\omega_m) = \chi_0^{-1}(\boldsymbol{q};i\omega_m) - \Gamma(i\omega_m). \tag{87}$$

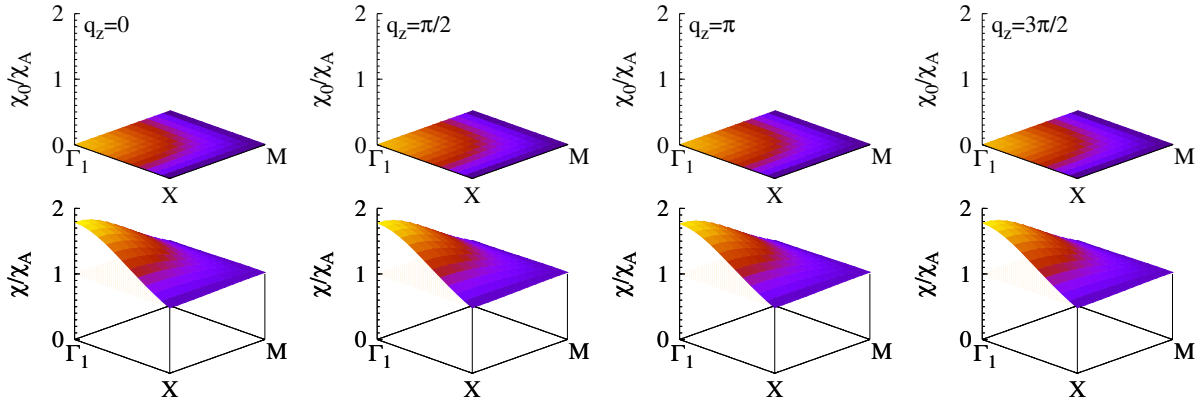


**Fig. 14:** *$VOMoO_4$: Static magnetic susceptibility $\chi(\boldsymbol{q};0)/\chi_A(0)$ in the $q_x, q_y$ plane for representative $q_z$ values, $T \sim 380$ K and $U = 5$ eV. The normalization $\chi_A(0) \sim \mu^2_{\rm eff}/k_BT$ is the atomic susceptibility in the large $\beta U$ limit. Top panels: $\Gamma = 0$. Bottom panels: $\Gamma \neq 0$. Special points: $\Gamma_1 = (2\pi, 0)$, X= $(\pi, 0)$ and M= $(\pi, \pi)$. Rearranged from Ref. [11].*

Next we assume that $\Gamma(i\omega_m)$ equals the vertex for the quantum impurity. We define $\chi(i\omega_m)$ the impurity susceptibility obtained via the quantum-impurity solver in the final iteration of the DMFT self-consistency loop, and $\chi_0(i\omega_m)$ the average of Eq. (84) over momenta

$$\chi_0(i\omega_m) = \frac{1}{N_{\boldsymbol{q}}} \sum_{\boldsymbol{q}} \chi_0(\boldsymbol{q}; i\omega_m). \tag{88}$$

The local vertex $\Gamma(i\omega_m)$ is then obtained by solving a local Bethe-Salpeter equation

$$\Gamma(i\omega_m) = \chi_0^{-1}(i\omega_m) - \chi^{-1}(i\omega_m). \tag{89}$$

Replacing $\Gamma(i\omega_m)$ into Eq. (87) finally yields the $\boldsymbol{q}$-dependent susceptibility. It has to be noticed that, although the two equations (87) and (89) look innocent, solving them numerically is a delicate task because the local susceptibility is in general not diagonal in $n, n'$ and does not decay very fast with the frequencies. There are, however, various ways to reduce the computational costs, e.g., via extrapolations [11] or using compact representations based on auxiliary polynomials [15, 16]. The method just illustrated for the calculation of linear response functions in the local vertex approximation bears resemblance with the approach adopted for the calculation of the Green functions in the local self-energy approximation. These analogies are schematically pointed out in Fig. 13. Instead, in Fig. 14 we show as an example the case of the static magnetic susceptibility for a one-band system, the $S$=1/2 frustrated Mott insulator $VOMoO_4$. The figure shows both the bubble term $\chi_0(\boldsymbol{q}; i\omega_m)$ (top panels) and the full susceptibility $\chi(\boldsymbol{q}; i\omega_m)$ (bottom panels). The two differ sizably in absolute value. In addition, as we will discuss later, the $\chi_0(\boldsymbol{q}; i\omega_m)$ term alone is very weakly dependent on the temperature. The expected Curie-Weiss-like behavior is only recovered when $\Gamma(i\omega_m)$ is taken into account.

## 3.3 The local susceptibility: Legendre representation

The core of the approach described in the previous section is the calculation of the local susceptibility tensor, $\chi_{\boldsymbol{\alpha\gamma}}(\boldsymbol{\tau})$. In DMFT all local observables $\langle\hat{O}\rangle$ are obtained via the quantum-impurity solver, for example the continuous-time hybridization expansion QMC technique presented in Section 2.3. Susceptibilities, however, require sizably longer computational time than Green-function matrices. Thus, instead of calculating directly $\chi_{\boldsymbol{\alpha\gamma}}(\boldsymbol{\tau})$, it is convenient to express the tensor elements in a basis of orthogonal functions $f_l^m(\tau)$, chosen such that the representation is as compact as possible. A successful choice [15, 16] is

$$f_l^m(\tau) = e^{-i\varphi_m(\tau)} \begin{cases} \sqrt{2l+1}\; p_l(x(\tau)), & \tau > 0 \\ -(-1)^m\sqrt{2l+1}\; p_l(x(\tau+\beta)), & \tau < 0 \end{cases}$$

where $p_l(x(\tau))$ is a Legendre polynomial of degree $l$, with $x(\tau) = 2\tau/\beta - 1$; here the factor $(-1)^m$ in the second row ensures anti-periodicity for all values of $m$, which is the index for the bosonic Matsubara frequency $\omega_m$. Via the orthogonality properties of the polynomials we obtain

$$\chi_{\boldsymbol{\alpha\gamma}}(i\omega_m) = \frac{1}{\beta^2}\sum_{ll'} f_l^{-m}(0^+)\; \chi^{l,l'}_{\boldsymbol{\alpha\gamma}}(i\omega_m)\; f_{l'}^{-m}(0^+). \tag{90}$$

The expansion coefficients in Eq. (90) take the form

$$\chi^{l,l'}_{\boldsymbol{\alpha\gamma}}(i\omega_m) = \int_0^\beta d\tau_{23}\int_0^\beta d\tau_{12}\int_0^\beta d\tau_{34}\; e^{-i\omega_m\tau_{23}} f_l^m(\tau_{12})\chi^{\alpha\alpha'}_{\gamma\gamma'}(\tau_{14},\tau_{24},\tau_{34},0) f_{l'}^m(\tau_{34}), \tag{91}$$

where $\tau_{ij} = \tau_i - \tau_j$, with $\tau_{14} = \tau_{12}+\tau_{23}+\tau_{34}$, and $\tau_{24} = \tau_{23}+\tau_{34}$. The phase defining the gauge is $\varphi_m(\tau) = \omega_m\tau/2$ and does not depend on $l$. As we have seen, in quantum Monte Carlo the observables are obtained as the average over the visited configurations $c$. Splitting (91) into two terms [16] we have

$$\left\langle \chi^{l,l'}_{\boldsymbol{\alpha\gamma}}(i\omega_m)\right\rangle_c = \left\langle \mathcal{C}^{l,l'}_{\boldsymbol{\alpha\gamma}}(i\omega_m)\right\rangle_c - \beta\delta_{m,0}\left\langle G^l_{\boldsymbol{\alpha}}\right\rangle_c\left\langle G^{l'}_{\boldsymbol{\gamma}}\right\rangle_c.$$

The first term can be expressed as

$$\left\langle C^{l,l'}_{\boldsymbol{\alpha\gamma}}(i\omega_m)\right\rangle_c = \frac{1}{\beta}\sum_{bb'dd'}^{N_B}\sum_{i,j}^{k_b,k_d}\sum_{i',j'}^{k_{b'},k_{d'}} f_l^m(\tau_{dj}-\bar\tau_{bi}) f_{l'}^m(\tau_{d'j'}-\bar\tau_{b'i'}) c^{db,d'b'}_{ji,j'i'}(i\omega_m)\delta_{\boldsymbol{\alpha},(\alpha_{dj},\bar\alpha_{bi})}\delta_{\boldsymbol{\gamma},(\alpha_{d'j'},\bar\alpha_{b'i'})}$$

where

$$c^{db,d'b'}_{ji,j'i'}(i\omega_m) = \left(w^{db}_{ji}w^{d'b'}_{j'i'} - w^{d'b}_{j'i}w^{db'}_{ji'}\right) e^{-i\omega_m(\bar\tau_{bi}-\tau_{d'j'})}.$$

Here the imaginary times $\tau_{bi}$ and $\bar\tau_{bi}$ all vary in the interval $[0,\beta)$. The letters $b$ and $d$ label the $N_B$ flavors decoupled by symmetry, e.g., $\{\uparrow,\downarrow\}$. Finally, $w^{db}_{ji} = \delta_{b,d}\mathcal{M}^{k_b}_{bj,bi}$, where the matrix $\mathcal{M}^{k_b} = [\mathcal{F}_0^{k_b}]^{-1}$ is the inverse of the hybridization function matrix $\mathcal{F}_0^{k_b}$ for expansion order $k_b$. The Green functions in the second term are instead given by

$$\left\langle G^l_{\boldsymbol{\alpha}}\right\rangle_c = -\frac{1}{\beta}\sum_{b}^{N_B}\sum_{ij}^{k_b} f_l^0(\tau_{bj}-\bar\tau_{bi})\; w^{bb}_{ji}\;\delta_{\boldsymbol{\alpha},(\alpha_{bj},\bar\alpha_{bi})}.$$

## 3.4 Magnetic susceptibility for the single-band Hubbard model

The magnetic susceptibility is the linear response to an external magnetic field applied along a direction, here defined as $\hat{z}$. The associated site susceptibility is

$$\chi^{i,i'}_{zz}(\boldsymbol{\tau}) = \left\langle \mathcal{T}\hat{M}^i_z(\tau)\hat{M}^{i'}_z(0)\right\rangle_0 - \left\langle \hat{M}^i_z\right\rangle_0\left\langle \hat{M}^{i'}_z\right\rangle_0,$$

where $\hat{M}^i_z = -g\mu_B\hat{S}^i_z$ is the magnetization for lattice site $i$. Its Fourier transform is

$$\begin{aligned}\chi_{zz}(\boldsymbol{q}; i\omega_m) &= \sum_{ii'} e^{i\boldsymbol{q}\cdot(\boldsymbol{T}_i-\boldsymbol{T}_{i'})}\int d\tau\; e^{i\omega_m\tau}\chi^{i,i'}_{zz}(\tau)\\ &= \left\langle \hat{M}_z(\boldsymbol{q};\omega_m)\hat{M}_z(-\boldsymbol{q};0)\right\rangle_0 - \left\langle \hat{M}_z(\boldsymbol{q})\right\rangle_0\left\langle \hat{M}_z(-\boldsymbol{q})\right\rangle_0, \end{aligned} \tag{92}$$

where $\omega_m$ is a bosonic Matsubara frequency. In this section we will discuss the example of the single-band Hubbard model on a hypercubic lattice and at half filling. Furthermore, unless differently specified, we will adopt the tight-binding dispersion

$$\varepsilon_{\boldsymbol{k}} = -2t\sum_{n=1}^{d}\cos k_d a, \tag{93}$$

where $d = 1, 2, 3$ is the dimension and $a$ the length of the unit vectors defining the lattice. For a single-band model the magnetization operator can be expressed in the Bloch basis as

$$\hat{M}_z(\boldsymbol{q}) = -\frac{g\mu_B}{2}\sum_{\boldsymbol{k}}\sum_{\sigma} s_\sigma c^\dagger_{\boldsymbol{k}+\boldsymbol{q}\sigma}c_{\boldsymbol{k}\sigma}, \tag{94}$$

where $s_\sigma = 1$ for $\sigma =\uparrow$ and $s_\sigma = -1$ for $\sigma =\downarrow$. To obtain the magnetic response function we thus have to calculate the imaginary-time tensor with elements

$$\begin{aligned}\left[\chi(\boldsymbol{q};\boldsymbol{\tau})\right]_{\boldsymbol{k}\sigma,\boldsymbol{k}'\sigma'} &= \left\langle \mathcal{T}c_{\boldsymbol{k}\sigma}(\tau_1)c^\dagger_{\boldsymbol{k}+\boldsymbol{q}\sigma}(\tau_2)c_{\boldsymbol{k}'+\boldsymbol{q}\sigma'}(\tau_3)c^\dagger_{\boldsymbol{k}'\sigma'}(\tau_4)\right\rangle_0\\ &\quad - \left\langle \mathcal{T}c_{\boldsymbol{k}\sigma}(\tau_1)c^\dagger_{\boldsymbol{k}+\boldsymbol{q}\sigma}(\tau_2)\right\rangle_0\left\langle \mathcal{T}c_{\boldsymbol{k}'+\boldsymbol{q}\sigma'}(\tau_3)c^\dagger_{\boldsymbol{k}'\sigma'}(\tau_4)\right\rangle_0. \end{aligned} \tag{95}$$

The associated imaginary-time magnetic susceptibility is then given by

$$\chi_{zz}(\boldsymbol{q};\boldsymbol{\tau}) = (g\mu_B)^2\frac{1}{4}\sum_{\sigma\sigma'} s_\sigma s_{\sigma'}\underbrace{\frac{1}{\beta}\frac{1}{N^2_{\boldsymbol{k}}}\sum_{\boldsymbol{k}\boldsymbol{k}'}\left[\chi(\boldsymbol{q};\boldsymbol{\tau})\right]_{\boldsymbol{k}\sigma,\boldsymbol{k}'\sigma'}}_{\chi_{\sigma\sigma\sigma'\sigma'}(\boldsymbol{q};\boldsymbol{\tau})}. \tag{96}$$

After we Fourier transform with respect to imaginary time and sum over the fermionic Matsubara frequencies, we have

$$\chi_{zz}(\boldsymbol{q}; i\omega_m) = (g\mu_B)^2\frac{1}{4}\sum_{\sigma\sigma'} s_\sigma s_{\sigma'}\frac{1}{\beta^2}\sum_{nn'}\chi^{n,n'}_{\sigma\sigma\sigma'\sigma'}(\boldsymbol{q}; i\omega_m), \tag{97}$$

where

$$\chi^{n,n'}_{\sigma\sigma\sigma'\sigma'}(\boldsymbol{q}; i\omega_m) = \frac{1}{16}\iiiint d\boldsymbol{\tau}\; e^{i\boldsymbol{\nu}\cdot\boldsymbol{\tau}}\chi_{\sigma\sigma\sigma'\sigma'}(\boldsymbol{q};\boldsymbol{\tau}). \tag{98}$$

For $\omega_n = 0$ we obtain the static response function.

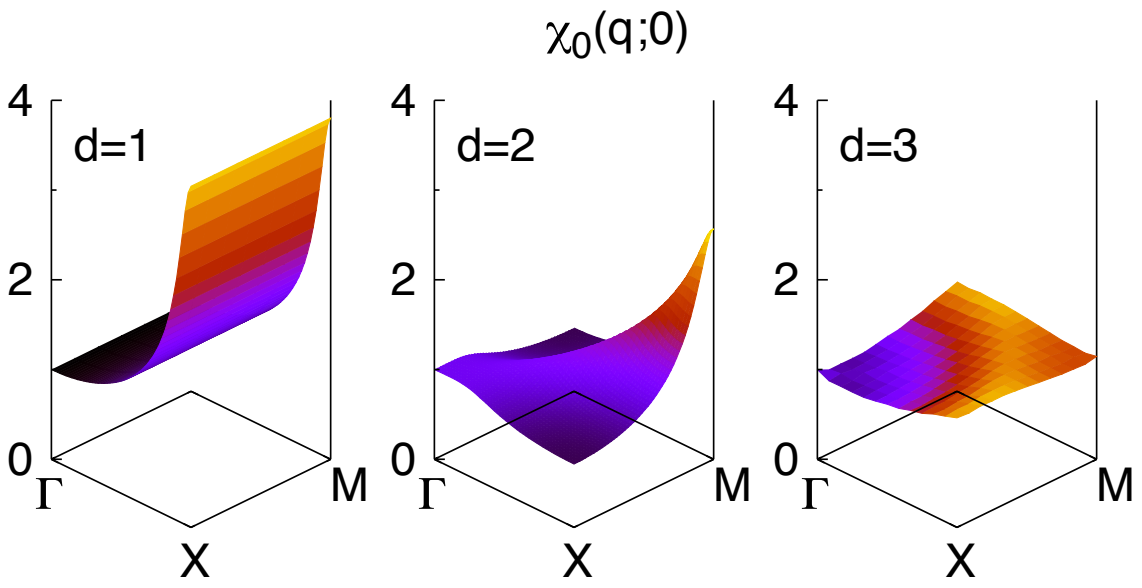


**Fig. 15:** *The ratio $\chi_0(\boldsymbol{q};0)/\chi_0(\boldsymbol{0};0)$ in the $x$-$y$ plane for a hypercubic lattice with $t = 0.4$ eV ($T \sim 230$ K) at half filling. From left to right: one, two, and three dimensions.*

### 3.4.1 Non-interacting limit

In the non-interacting limit we can use Wick's theorem to simplify Eq. (95). It follows that the elements of the two-particle Green function tensor vanish if $\boldsymbol{k} \neq \boldsymbol{k}'$. Thus Eq. (96) becomes

$$\chi_{zz}(\boldsymbol{q};\boldsymbol{\tau}) = -(g\mu_B)^2 \frac{1}{4}\frac{1}{\beta}\frac{1}{N_{\boldsymbol{k}}} \sum_{\boldsymbol{k}} \sum_{\sigma} \mathcal{G}_{\boldsymbol{k}\sigma}(\tau_{14}) \mathcal{G}_{\boldsymbol{k}+\boldsymbol{q}\sigma}(-\tau_{23}).$$

For the frequency-dependent magnetic susceptibility Eq. (97) we have instead

$$\chi_{zz}(\boldsymbol{q};i\omega_m) = (g\mu_B)^2 \frac{1}{4}\frac{1}{\beta^2} \sum_{nn'} \sum_{\sigma} \chi^{n,n'}_{\sigma\sigma\sigma\sigma}(\boldsymbol{q};i\omega_m),$$

where

$$\sum_{\sigma} \chi^{n,n'}_{\sigma\sigma\sigma\sigma}(\boldsymbol{q};i\omega_m) = -\frac{\beta}{N_{\boldsymbol{k}}} \sum_{\boldsymbol{k}} \sum_{\sigma} \mathcal{G}_{\boldsymbol{k}\sigma}(i\nu_n)\, \mathcal{G}_{\boldsymbol{k}+\boldsymbol{q}\sigma}(i\nu_n + i\omega_m)\, \delta_{n,n'}. \tag{99}$$

The actual dynamical susceptibility is then given by

$$\chi_{zz}(\boldsymbol{q};i\omega_m) = -\,(g\mu_B)^2\, \frac{1}{4}\frac{1}{N_{\boldsymbol{k}}} \sum_{\boldsymbol{k}} \sum_{\sigma} \frac{n_\sigma(\varepsilon_{\boldsymbol{k}+\boldsymbol{q}}) - n_\sigma(\varepsilon_{\boldsymbol{k}})}{\varepsilon_{\boldsymbol{k}+\boldsymbol{q}} - \varepsilon_{\boldsymbol{k}} + i\omega_m},$$

where $n_\sigma(x) = n_F(x)$ is the Fermi distribution function. Figure 15 shows the static spin susceptibility for a $d$-dimensional hypercubic lattice. For $T \to 0$, it diverges at the antiferromagnetic vector $\boldsymbol{q}_C$, which in two dimension is the M point. Indeed, since $\varepsilon_{\boldsymbol{k}+\boldsymbol{q}_C} = -\varepsilon_{\boldsymbol{k}}$ (perfect nesting) we have

$$\chi_0(\boldsymbol{q}_C;0) \propto \frac{1}{4}\int_{-\infty}^{\varepsilon_F} d\varepsilon\, \frac{\rho(\varepsilon)}{\varepsilon}.$$

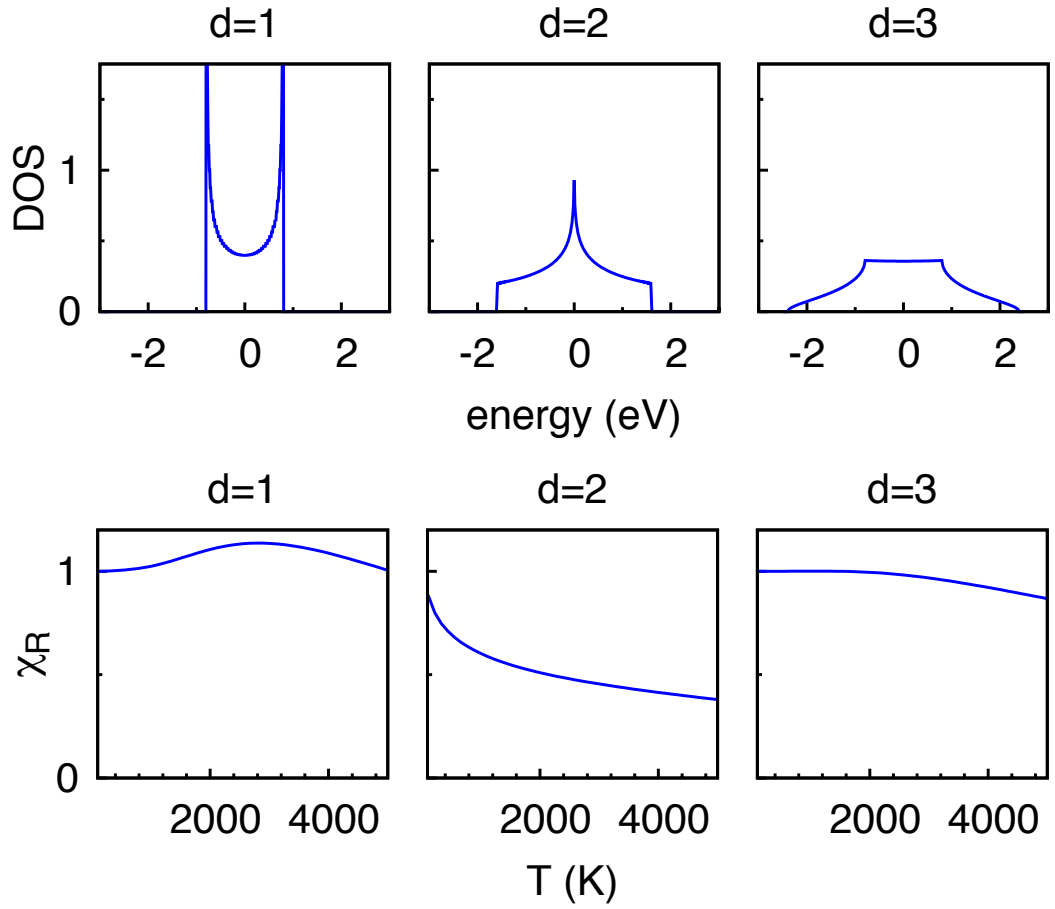


**Fig. 16:** *Effect of $\rho(\varepsilon_F)$ on the temperature dependence of $\chi_R = \chi_P(T)/\chi_P(0)$ for a hypercubic lattice with $t = 0.4$ eV and at half filling. Up to $\sim 1000$ K only the logarithmic Van-Hove singularity (two-dimensional case) yields a sizable effect.*

In the $\boldsymbol{q} \to 0$ and $T \to 0$ limit, setting $\omega_m = 0$ we recover the Pauli susceptibility

$$\chi_{zz}(\mathbf{0};0) = \frac{1}{4}\left(g\mu_B\right)^2 \rho(\varepsilon_F),$$

$$\rho(\varepsilon_F) = -\sum_\sigma \frac{1}{N_{\boldsymbol{k}}} \sum_{\boldsymbol{k}} \left.\frac{dn_\sigma(\varepsilon_{\boldsymbol{k}})}{d\varepsilon_{\boldsymbol{k}}}\right|_{T=0}.$$

Fig. 16 shows that, assuming the dispersion given in Eq. (93), the Pauli susceptibility is weakly temperature dependent in three dimensions, but not when a van-Hove singularity is close to the Fermi level, as it happens for the $d = 2$ case.

### 3.4.2 Small $U/t$ limit: Hartree Fock approximation and Stoner model

In the small $U/t$ limit one can expand around the non-interacting susceptibility and treat the effect of Coulomb repulsion in the static mean-field or Hartree-Fock approximation. We have previously seen (Section 2.4 and Fig. 6) that in the ferromagnetic case this means that the band for spin up and spin down electrons acquire different energy. The energy splitting equals

the one obtained in the presence of an effective magnetic field $h_{\rm eff} = 2mU$, where $m$ is the magnetization. We can generalize this result to a magnetic structure characterized by a vector $\boldsymbol{q}$; in this case we have $h_{\rm eff}(\boldsymbol{q}) = 2m(\boldsymbol{q})U$, where $m(\boldsymbol{q})$ is the associated order parameter. The associated static magnetic response function is thus

$$\chi(\boldsymbol{q};0) = \frac{\chi_0(\boldsymbol{q};0)}{1 - \Gamma\chi_0(\boldsymbol{q};0)}, \tag{100}$$

where $\Gamma{=}2U$. This is a simplified version of the Bethe-Salpeter equation obtained in standard many-body perturbation theory, with, however, a first-order frequency- and momentum-independent vertex. In the case of a hypercubic lattice with dispersion (93) the susceptibility $\chi_0(\boldsymbol{q};0)$ is larger at the nesting vector; this favors instabilities towards antiferromagnetism.

### 3.4.3 Atomic limit

Let us now consider the opposite extreme, the atomic limit. First we adopt a simple approach. Since all atoms are decoupled, only on-site terms $i = i'$ contribute. We then can calculate the right-hand side of Eq. (92) by summing up the contributions of the four atomic states, $|0\rangle$, $c^\dagger_\uparrow|0\rangle$, $c^\dagger_\downarrow|0\rangle$, $c^\dagger_\uparrow c^\dagger_\downarrow|0\rangle$, obtaining at half filling

$$\chi_{zz}(\boldsymbol{q};i\omega_m) = (g\mu_B)^2 \frac{1}{4k_BT} \frac{e^{\beta U/2}}{1+e^{\beta U/2}} \delta_{\omega_m,0}. \tag{101}$$

The same expression can be derived following the general procedure outlined in the previous pages, i.e., starting from the two-particle Green function tensor $\chi_{\sigma\sigma\sigma'\sigma'}(\boldsymbol{q};\boldsymbol{\tau})$, defined in Eq. (96). In the atomic limit, it is convenient to work in real space, since

$$\chi_{\sigma\sigma\sigma'\sigma'}(\boldsymbol{q};\boldsymbol{\tau}) = \frac{1}{\beta} \sum_i \chi_{i\sigma\sigma,i\sigma'\sigma'}(\boldsymbol{\tau}).$$

Thanks to the symmetries of the tensor in imaginary time, it is sufficient to calculate $\chi_{i\sigma\sigma,i\sigma'\sigma'}(\boldsymbol{\tau})$ for positive times $0 < \tau_{j4} < \beta$, where $\tau_{j4} = \tau_j - \tau_4$ with $j = 1,2,3$. Due to the time ordering operator we have, however, to consider separately six different imaginary-time sectors. In the Appendix one can find a list of all these sectors and their contributions. For simplicity, we discuss here explicitly only the case $\tau_{14} > \tau_{24} > \tau_{34} > 0$ and label the corresponding $\boldsymbol{\tau}$-vector as $\boldsymbol{\tau}^+$. Calculating the trace we obtain

$$\chi_{i\sigma\sigma,i\sigma'\sigma'}(\boldsymbol{\tau}^+) = \frac{e^{\tau_{12}U/2+\tau_{34}U/2} + \delta_{\sigma\sigma'} e^{(\beta-\tau_{12})U/2-\tau_{34}U/2}}{2(1+e^{\beta U/2})} - G^\sigma_{i,i}(\tau_{12})\, G^{\sigma'}_{i,i}(\tau_{34}).$$

The mean-field terms $G^\sigma_{i,i}(\tau_{12})\, G^{\sigma'}_{i,i}(\tau_{34})$ cancel out in the actual magnetic linear response function, so here we do not give their form explicitly and we will neglect them in the rest of the calculations. For a single atom, the contribution of the $\boldsymbol{\tau}^+$ sector to the imaginary-time magnetic susceptibility is

$$\chi_{zz}(\boldsymbol{\tau}^+) = (g\mu_B)^2 \frac{1}{4}\frac{1}{\beta} \sum_{\sigma\sigma'} s_\sigma s_{\sigma'} \chi_{i\sigma\sigma,i\sigma'\sigma'}(\boldsymbol{\tau}^+) = \frac{(g\mu_B)^2}{4\beta} \frac{1}{(1+e^{\beta U/2})} e^{(\beta-\tau_{12}-\tau_{34})U/2}.$$

Summing up the contributions of all imaginary-time sectors and performing the Fourier transform we obtain $\chi^{n,n'}_{\sigma\sigma\sigma'\sigma'}(i\omega_n)$, defined in Eq. (98). For $U \neq 0$ this tensor is non-diagonal in the fermionic Matsubara frequencies. For $\omega_n = 0$ we have [11]

$$\sum_{\sigma\sigma'} \sigma\sigma' \, \chi^{n,n'}_{i\sigma\sigma,i\sigma'\sigma'}(0) = M_{n'}\frac{dM_n}{dy} + M_n\frac{dM_{n'}}{dy} - \beta n(y)\left[\delta_{n,n'} + \delta_{n,-n'}\right]\frac{dM_n}{dy} + \beta n(-y) M_n M_{n'} - \frac{1}{y}\left\{ M_{n'} - \beta\left[ n(y)\delta_{n,-n'} - n(-y)\delta_{n,n'}\right]\right\} M_n \tag{102}$$

where

$$M_n = \frac{1}{i\nu_n - y} - \frac{1}{i\nu_n + y}. \tag{103}$$

We can now calculate the magnetic susceptibility via Eq. (97), recovering the expected result, Eq. (101). The resulting atomic magnetic susceptibility is thus proportional to $1/k_B T$, i.e., has a Curie-like behavior; furthermore it is zero at finite frequency. The temperature dependence can be remarkably different from the $U = 0$ limit. Indeed, if the density of states is flat around the Fermi level, as it is often the case in three-dimensional lattices, the non-interacting Pauli susceptibility $\chi_{zz}(\mathbf{0}; 0)$ is weakly temperature dependent. As we have seen, a strong temperature dependence can be found, however, if, e.g., a logarithmic van-Hove singularity is at the Fermi level, as in the case of the square lattice at half filling shown in Fig. 16.

### 3.4.4 DMFT: $\chi_0(\mathbf{q};\omega)$ and the Bethe-Salpeter equation

In order to calculate the magnetic susceptibility with DMFT we need, first of all, $\chi_0(\mathbf{q};\omega)$, the bubble term calculated from the DMFT Green functions. We consider here the small $t/U$ or Mott insulating regime. In this case we can derive an approximate local self-energy starting from the atomic limit. The $t$=0 local Green function is

$$G^\sigma_{i,i}(i\nu_n) = \frac{1}{i\nu_n + \mu - \varepsilon_d - \Sigma^\sigma_l(i\nu_n)},$$

where the local self-energy is given by

$$\Sigma^\sigma_l(i\nu_n) = \frac{U}{2} + \frac{U^2}{4}\frac{1}{i\nu_n + \mu - \varepsilon_d - \frac{U}{2}}, \tag{104}$$

and $\mu = \varepsilon_d + \frac{U}{2}$. In the Mott insulating regime we can assume that the local self-energy has the same form (104), with $U^2/4$ replaced by a quantity which plays the role of a dimensionless *order parameter* [17] for the insulating phase

$$\frac{1}{r_U}\frac{4}{U^2} = \int_{-\infty}^{+\infty} d\varepsilon \, \frac{\rho(\varepsilon)}{\varepsilon^2}. \tag{105}$$

Here $\rho(\varepsilon)$ is the density of states per spin. The integral in Eq. (105) diverges in the metallic phase. The Green function can then be rewritten as

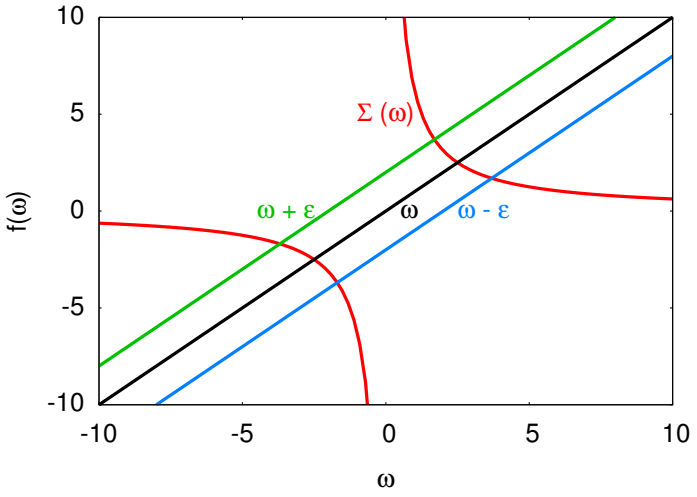


**Fig. 17:** *Graphical solution of the equation $\omega - \varepsilon_{\boldsymbol{k}} = \Sigma_l^\sigma(\omega)$ yielding the poles $E_{\boldsymbol{k}}^+$ and $E_{\boldsymbol{k}}^-$ of the Green function defined in Eq. (106).*

$$G^\sigma(\boldsymbol{k}; i\nu_n) = \frac{1}{i\nu_n - \Sigma_l^\sigma(i\nu_n) - \varepsilon_{\boldsymbol{k}}} = \frac{1}{E_{\boldsymbol{k}}^+ - E_{\boldsymbol{k}}^-}\left[\frac{E_{\boldsymbol{k}}^+}{i\nu_n - E_{\boldsymbol{k}}^+} - \frac{E_{\boldsymbol{k}}^-}{i\nu_n - E_{\boldsymbol{k}}^-}\right] \tag{106}$$

where $E_{\boldsymbol{k}}^+$ and $E_{\boldsymbol{k}}^-$ are the two roots of the equation $\omega - \Sigma_l^\sigma(\omega) - \varepsilon_{\boldsymbol{k}} = 0$,

$$E_{\boldsymbol{k}}^\pm = \frac{1}{2}\varepsilon_{\boldsymbol{k}} \pm \frac{1}{2}\sqrt{\varepsilon_{\boldsymbol{k}}^2 + r_U\, U^2}.$$

By performing the Matsubara sums, one finds

$$\begin{aligned}\chi_{zz}^0(\boldsymbol{q}; 0) &= (g\mu_B)^2 \frac{1}{4}\sum_\sigma \frac{1}{\beta^2}\sum_n \chi_{\sigma\sigma\sigma\sigma}^{n,n}(0) \\ &= (g\mu_B)^2 \frac{1}{2}\frac{1}{N_{\boldsymbol{k}}}\sum_{\boldsymbol{k}}\Big[\underbrace{-I_{\boldsymbol{k},\boldsymbol{q}}^{++} - I_{\boldsymbol{k},\boldsymbol{q}}^{--}}_{A_{\boldsymbol{k},\boldsymbol{q}}} + \underbrace{I_{\boldsymbol{k},\boldsymbol{q}}^{+-} + I_{\boldsymbol{k},\boldsymbol{q}}^{-+}}_{B_{\boldsymbol{k},\boldsymbol{q}}},\Big]\end{aligned}$$

where, setting $\alpha = \pm$ and $\gamma = \pm$,

$$I_{\boldsymbol{k},\boldsymbol{q}}^{\alpha\gamma} = \frac{E_{\boldsymbol{k}}^\alpha\, E_{\boldsymbol{k}+\boldsymbol{q}}^\gamma}{\big(E_{\boldsymbol{k}}^+ - E_{\boldsymbol{k}}^-\big)\big(E_{\boldsymbol{k}+\boldsymbol{q}}^+ - E_{\boldsymbol{k}+\boldsymbol{q}}^-\big)}\frac{n(E_{\boldsymbol{k}}^\alpha) - n(E_{\boldsymbol{k}+\boldsymbol{q}}^\gamma)}{E_{\boldsymbol{k}}^\alpha - E_{\boldsymbol{k}+\boldsymbol{q}}^\gamma}.$$

In the $\boldsymbol{q} \to \boldsymbol{0}$ limit

$$\begin{aligned}A_{\boldsymbol{k},\boldsymbol{0}} &= \beta\,\left[\frac{(E_{\boldsymbol{k}}^+)^2}{\varepsilon_{\boldsymbol{k}}^2 + r_U\, U^2}\, n(E_{\boldsymbol{k}}^+)\big(1 - n(E_{\boldsymbol{k}}^+)\big) + \frac{(E_{\boldsymbol{k}}^-)^2}{\varepsilon_{\boldsymbol{k}}^2 + r_U\, U^2}\, n(E_{\boldsymbol{k}}^-)\big(1 - n(E_{\boldsymbol{k}}^-)\big)\right] \\ B_{\boldsymbol{k},\boldsymbol{0}} &= \frac{r_U\, U^2}{2(\varepsilon_{\boldsymbol{k}}^2 + r_U\, U^2)^{3/2}}\,\big(n(E_{\boldsymbol{k}}^-) - n(E_{\boldsymbol{k}}^+)\big)\,.\end{aligned}$$

In the large $\beta U$ limit, the $A_{\boldsymbol{k},\boldsymbol{0}}$ term, proportional to the density of states at the Fermi level, vanishes exponentially; the $B_{\boldsymbol{k},\boldsymbol{0}}$ term yields the dominant contribution. Hence

$$\chi_{zz}^0(\boldsymbol{0}; 0) \sim (g\mu_B)^2 \frac{1}{4}\frac{1}{N_{\boldsymbol{k}}}\sum_{\boldsymbol{k}} \frac{r_U\, U^2}{(\varepsilon_{\boldsymbol{k}}^2 + r_U\, U^2)^{3/2}} \sim (g\mu_B)^2 \frac{1}{4\sqrt{r_U}\, U}\left[1 - \frac{3}{2}\frac{1}{N_{\boldsymbol{k}}}\sum_{\boldsymbol{k}} \frac{\varepsilon_{\boldsymbol{k}}^2}{r_U\, U^2} + \ldots\right].$$

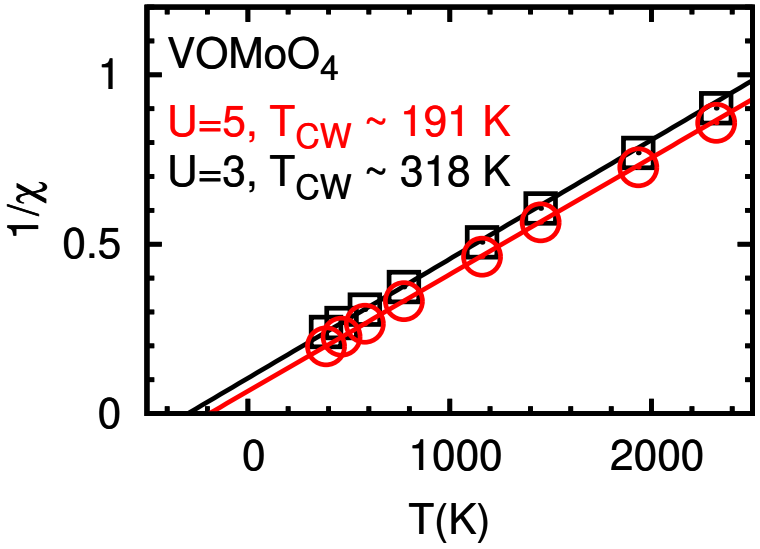


**Fig. 18:** *$VOMoO_4$: The Curie-Weiss behavior of the uniform magnetic susceptibility at half filling, obtained with the LDA+DMFT approach. Rearranged from Ref. [11].*

The right-hand side is equal to the atomic term $\chi^0_{zz}(0)$ minus a correction of order $t^2/U^3$. As we can see, $\chi^0_{zz}(\mathbf{0};0)$ is small and weakly dependent on the temperature. Here for simplicity we will discuss only the case of the two-dimensional square lattice at half filling. In the Mott-insulating regime, due to the superexchange interaction, this model exhibits an antiferromagnetic instability at $\boldsymbol{q}_C = (\pi/a, \pi/a, 0)$. Let us then calculate $\chi^0_{zz}(\boldsymbol{q}_C;0)$ and compare it with $\chi^0_{zz}(\mathbf{0};0)$. Since, as we have seen, $\varepsilon_{\boldsymbol{k}+\boldsymbol{q}_C} = -\varepsilon_{\boldsymbol{k}}$, we find

$$A_{\boldsymbol{k},\boldsymbol{q}_C} = \frac{1}{2}\frac{r_U\,U^2}{\varepsilon^2_{\boldsymbol{k}} + r_U\,U^2}\frac{n(E^+_{\boldsymbol{k}}-\varepsilon_{\boldsymbol{k}}) - n(E^+_{\boldsymbol{k}})}{\varepsilon_{\boldsymbol{k}}}$$
$$B_{\boldsymbol{k},\boldsymbol{q}_C} = \frac{1}{2}\frac{\varepsilon^2_{\boldsymbol{k}}}{\varepsilon^2_{\boldsymbol{k}} + r_U\,U^2}\frac{n(E^+_{\boldsymbol{k}}-\varepsilon_{\boldsymbol{k}}) - n(E^+_{\boldsymbol{k}})}{\varepsilon_{\boldsymbol{k}}} - \frac{1}{2}\frac{1}{\sqrt{\varepsilon^2_{\boldsymbol{k}} + r_U\,U^2}}\left(n(E^+_{\boldsymbol{k}}) - n(E^-_{\boldsymbol{k}})\right),$$

and therefore

$$\chi_0(\boldsymbol{q}_C;0) \sim (g\mu_B)^2\frac{1}{4\sqrt{r_U}U}\left(1 - \frac{1}{2}\frac{1}{N_{\boldsymbol{k}}}\sum_{\boldsymbol{k}}\frac{\varepsilon^2_{\boldsymbol{k}}}{r_U U^2}\right).$$

Thus $\chi_0(\boldsymbol{q};0)$ is indeed larger at $\boldsymbol{q} = \boldsymbol{q}_C$ than at $\boldsymbol{q} = \mathbf{0}$; it is however weakly temperature dependent and does not exhibit Curie-Weiss instabilities. The calculation presented above can be generalized to any $\boldsymbol{q}$ vector [11], obtaining the expression

$$\chi_0(\boldsymbol{q};0) \sim (g\mu_B)^2\frac{1}{4\sqrt{r_U}U}\left(1 - \frac{1}{2}\frac{J_{\mathbf{0}}}{\sqrt{r_U}U} - \frac{1}{4}\frac{J_{\boldsymbol{q}}}{\sqrt{r_U}U}\right), \tag{107}$$

where $J_{\boldsymbol{q}} = J\big(\cos q_x + \cos q_y\big)$, and the super-exchange coupling is $J = 4t^2/U$. For the next step we need to calculate the local vertex. This requires, as we have seen, the solution of the self-consistent quantum-impurity model via the quantum-impurity solver. Here, for the purpose of illustrating how the approach works, we approximate the local susceptibility with the atomic

susceptibility in the large $\beta U$ limit. Furthermore we work with the susceptibilities obtained *after* the Matsubara sums have been performed. Thus

$$\chi^0_{zz}(0) \sim (g\mu_B)^2 \frac{1}{4\sqrt{r_U}U}, \qquad \chi_{zz}(0) \sim \frac{1}{4k_BT}.$$

The local vertex is then approximately given by

$$\Gamma \sim \frac{1}{\chi^0_{zz}(0)} - \frac{1}{\chi_{zz}(0)} \sim \frac{1}{(g\mu_B)^2}\left[4\sqrt{r_U}U\left(1+\frac{1}{2}\frac{J_{\mathbf{0}}}{\sqrt{r_U}U}\right) - 4k_BT\right].$$

The last step consists in solving the Bethe-Salpeter equation

$$\chi_{zz}(\boldsymbol{q};0) = \frac{1}{(\chi^0_{zz}(\boldsymbol{q};0))^{-1} - \Gamma} \sim \frac{(g\mu_B)^2}{4}\frac{1}{k_BT + J_{\boldsymbol{q}}/4} = \frac{(g\mu_B)^2}{4k_B}\,\frac{1}{T - T_{\boldsymbol{q}}}.$$

This shows that including the local vertex correction we recover the Curie-Weiss behavior, as expected for a system described by local spins coupled by a Heisenberg-like exchange; we also correctly find the antiferromagnetic instability, since $\boldsymbol{q}_C$ is the vector for which the critical temperature $T_{\boldsymbol{q}}$ is the largest. In conclusion, we have seen that $\Gamma(i\omega_m)$ is essential to properly describe the magnetic response function of strongly-correlated systems. This can be seen in Fig. 14 for the Mott insulator $VOMoO_4$. In the figure we can compare the very weak linear magnetic response $\chi_0(\boldsymbol{q};0)$ (upper panels) with the LDA+DMFT result $\chi(\boldsymbol{q};0)$ (lower panels). The latter is not only strongly enhanced with respect to $\chi_0(\boldsymbol{q};0)$, but also exhibits the expected Curie-Weiss like behavior, as can be seen in Fig. 18 for $\boldsymbol{q} = \mathbf{0}$.

### 3.4.5 DMFT: Static and dynamical susceptibility below the critical temperature

In this section we will discuss the magnetic response in the anti-ferromagnetic phase, i.e., for $T \ll T_N$, where $T_N$ is the transition temperature in DMFT. We will consider as representative case the single-band Hubbard model on a square lattice with dispersion

$$\varepsilon_{\boldsymbol{k}} = \underbrace{-2t(\cos k_x + \cos k_y)}_{\alpha_{\boldsymbol{k}}} + \underbrace{4t' \cos k_x \cos k_y}_{\gamma_{\boldsymbol{k}}} + \dots . \tag{108}$$

a model typically adopted for describing the Cu $3d$ $x^2{-}y^2$ states at the Fermi level in high-temperature superconducting cuprates. We consider again the half-filled case in the small $t/U$ and $t'/U$ limit, yielding an insulating ground state. The DMFT results presented for this model are from Ref. [19], where more details can be found. In the paramagnetic phase, the static susceptibility exhibits a Curie-Weiss behavior, for the same reasons we discussed in the previous section. This can be seen in Fig. 19.

In the antiferromagnetic phase, the square lattice can be divided into two sublattices, $A$ and $B$, describing sites with opposite magnetic moment, $m$ (sub-lattice $A$) and $-m$ (sub-lattice $B$); the unit cell contains $n_s{=}2$ Cu atoms, labeled with $i_c = 1, 2$. In this case the local self-energy can be approximated by the site-dependent static Hartree-Fock term

$$\Sigma^{\sigma}_{i_c,i'_c}(i\nu_n) \approx \left(-\mu + (-1)^{i_c-1} s_\sigma m U\right)\delta_{i_c,i'_c}. \tag{109}$$

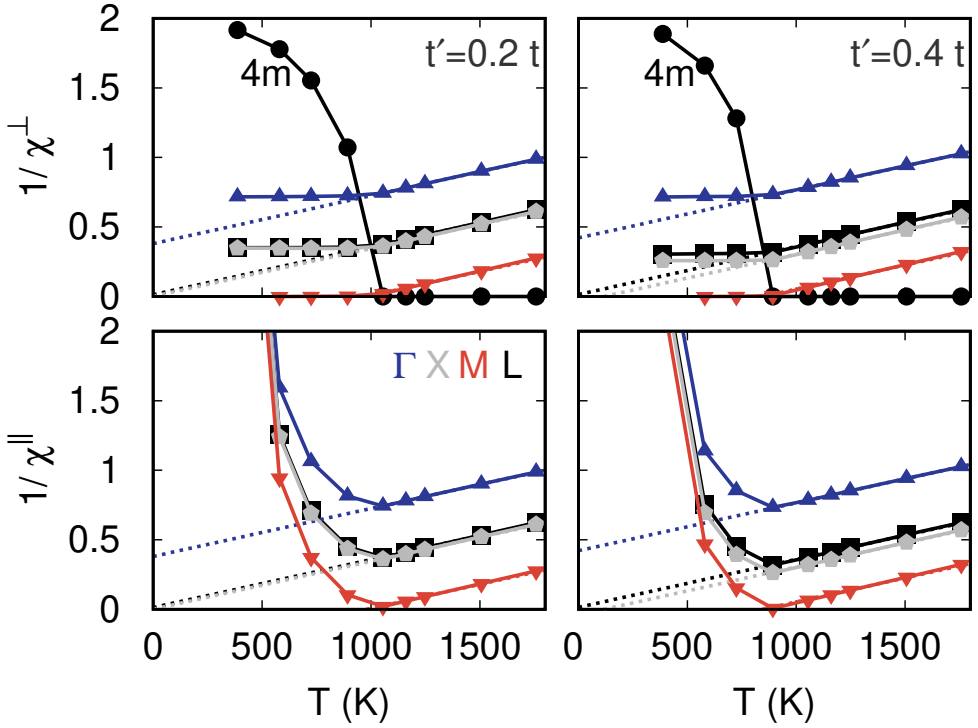


**Fig. 19:** *Static inverse transverse and longitudinal susceptibility $\chi(\boldsymbol{q};0)$ as a function of temperature. Triangles: $\Gamma$ and $M$ point. Gray pentagons: $X$ point. Black circles: local (L) susceptibility. Rearranged from Ref. [19].*

For a given spin we can thus write the associated $n_s \times n_s$ Green function matrix as

$$G^{\sigma}(\boldsymbol{k};i\nu_n) \approx \frac{1}{D_{\boldsymbol{k}}(i\nu_n)} \begin{pmatrix} i\nu_n - \gamma_{\boldsymbol{k}} - s_\sigma mU & \alpha_{\boldsymbol{k}} e^{-ik_x a} \\ \alpha_{\boldsymbol{k}} e^{ik_x a} & i\nu_n - \gamma_{\boldsymbol{k}} + s_\sigma mU \end{pmatrix}, \tag{110}$$

where $D_{\boldsymbol{k}}(i\nu_n) = (i\nu_n - \gamma_{\boldsymbol{k}})^2 - \alpha_{\boldsymbol{k}}^2 - (mU)^2$. The elements of $G^{\sigma}(\boldsymbol{k};i\nu_n)$ can be re-expressed as

$$G^{\sigma}_{i_c,i'_c}(\boldsymbol{k};i\nu_n) = \sum_{p=\pm} \frac{w^{i_c i'_c}_{\sigma \boldsymbol{k} p}}{i\nu_n - E^p_{\boldsymbol{k}}}, \tag{111}$$

where the poles corresponds to the Hartree-Fock energies $E^{\pm}_{\mathbf{k}} = \gamma_{\boldsymbol{k}} \pm \sqrt{\alpha^2_{\mathbf{k}} + (mU)^2} = \gamma_{\boldsymbol{k}} \pm \Delta\alpha_{\boldsymbol{k}}$, shown in Fig. 20 for $\gamma_{\boldsymbol{k}} = 0$. The weights are

$$w^{11}_{\sigma \boldsymbol{k} p} = \frac{1}{2}\left(1 - p\frac{s_\sigma mU}{\sqrt{\alpha^2_{\boldsymbol{k}} + (mU)^2}}\right) = w^{22}_{-\sigma \mathbf{k} p}, \tag{112}$$

$$w^{12}_{\sigma \boldsymbol{k} p} = \frac{p}{2}\frac{\alpha_{\boldsymbol{k}}}{\sqrt{\alpha^2_{\mathbf{k}} + (mU)^2}} e^{-i\boldsymbol{k}\cdot(\boldsymbol{T}_1 - \boldsymbol{T}_2)} = \left[w^{21}_{\sigma \boldsymbol{k} p}\right]^*. \tag{113}$$

Performing the Matsubara sum

$$\chi^{0;i_c i'_c}_{\sigma\sigma'\sigma'\sigma}(\mathbf{q};i\omega_m) = -\frac{1}{\beta N_{\boldsymbol{k}}} \sum_{\boldsymbol{k}n} G^{\sigma}_{i_c,i'_c}(\boldsymbol{k};i\nu_n)\, G^{\sigma'}_{i'_c,i_c}(\boldsymbol{k}+\boldsymbol{q};i\nu_n + i\omega_m) \tag{114}$$

$$\approx \frac{1}{N_{\boldsymbol{k}}} \sum_{\boldsymbol{k}} \sum_{pp'} w^{i_c i'_c}_{\sigma \boldsymbol{k} p}\, w^{i'_c i_c}_{\sigma' \boldsymbol{k}+\boldsymbol{q} p'}\, \mathcal{I}^{pp'}_{\mathbf{k},\boldsymbol{q}}(i\omega_m), \tag{115}$$

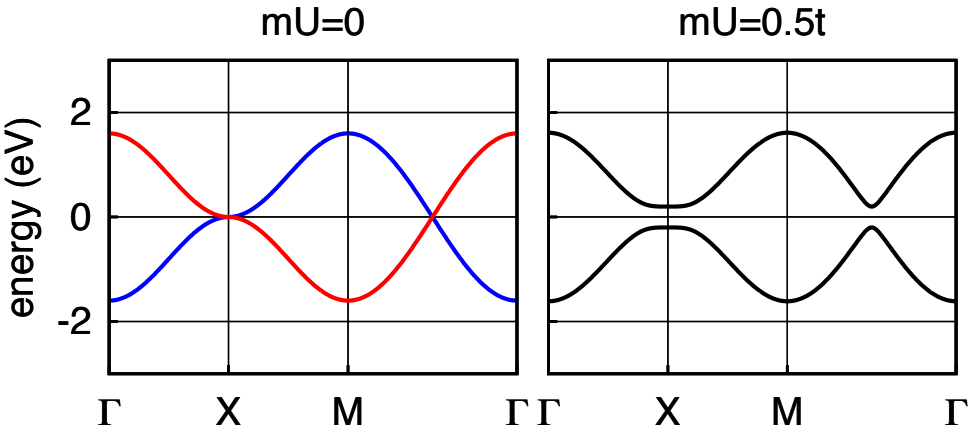


**Fig. 20:** *The metal-insulator transition in anti-ferromagnetic Hartree-Fock. The calculation is for a square lattice tight-binding model with dispersion* $\varepsilon_{\boldsymbol{k}} = -2t(\cos k_x + \cos k_y)$.

with

$$\mathcal{I}^{pp'}_{\boldsymbol{k},\boldsymbol{q}}(i\omega_m) = -\frac{n_F(E^p_{\boldsymbol{k}}) - n_F(E^{p'}_{\boldsymbol{k}+\boldsymbol{q}})}{i\omega_m + E^p_{\mathbf{k}} - E^{p'}_{\boldsymbol{k}+\boldsymbol{q}}}. \tag{116}$$

Below the critical temperature we have to distinguish two types $(T)$ of response. Assuming that the ordered magnetic moments are along $\hat{z}$, a magnetic field parallel to $\hat{z}$ yields the longitudinal ($T = \parallel$) linear response, and one perpendicular to $\hat{z}$ the transverse ($T = \perp$) linear susceptibility. They can be expressed in a compact way as

$$\chi^T_0(\mathbf{q}; i\omega_m) = \frac{(g\mu_B)^2}{4} \sum_{\sigma\sigma'} \frac{1}{2} \sum_{i_c i'_c} f^T_{\sigma\sigma'}\, \chi^{0;i_c i'_c}_{\sigma\sigma'\sigma'\sigma}(\mathbf{q}; i\omega_m) e^{i\boldsymbol{q}\cdot(\boldsymbol{T}_{i_c} - \boldsymbol{T}_{i'_c})} \tag{117}$$

$$\approx \frac{(g\mu_B)^2}{4} \frac{1}{N_{\boldsymbol{k}}} \sum_{\boldsymbol{k}} \sum_{pp'} v^{T,pp'}_{\boldsymbol{k},\mathbf{q}} \mathcal{I}^{pp'}_{\boldsymbol{k},\boldsymbol{q}}(i\omega_m) \tag{118}$$

where $f^{\parallel}_{\sigma\sigma'} = \delta_{\sigma,\sigma'}$ and $f^{\perp}_{\sigma\sigma'} = \delta_{\sigma,-\sigma'}$, while

$$v^{T,pp'}_{\boldsymbol{k},\mathbf{q}} = \frac{1}{2} \sum_{\sigma\sigma'} \sum_{i_c i'_c} w^{i_c i'_c}_{\sigma\boldsymbol{k}p} w^{i'_c i_c}_{\sigma'\boldsymbol{k}+\mathbf{q}p'} f^T_{\sigma\sigma'} e^{i\varphi^{i_c i'_c}_{\boldsymbol{q}}} \tag{119}$$

$$= \frac{1}{2}\left(1 + pp' \frac{\alpha_{\boldsymbol{k}}\alpha_{\boldsymbol{k}+\boldsymbol{q}} + f^T_{\sigma\sigma'} s_\sigma s_{\sigma'} (mU)^2}{\Delta\alpha_{\mathbf{k}} \Delta\alpha_{\boldsymbol{k}+\boldsymbol{q}}}\right). \tag{120}$$

We note that $v^{\parallel,pp}_{\boldsymbol{k},\mathbf{0}} = 1$ and $v^{\parallel,p-p}_{\boldsymbol{k},\mathbf{0}} = 0$, while $v^{\perp,p-p}_{\boldsymbol{k},M} = 1$ and $v^{\parallel,pp}_{\boldsymbol{k},M} = 0$. For simplicity in the discussion that follows we set $t' = 0$. In the low-temperature limit only the terms with $p = -p'$ contribute. For $t \ll U$ we have

$$\chi^T_0(\boldsymbol{q}; i\omega_m) \approx \frac{(g\mu_B)^2}{4} \frac{1}{N_{\boldsymbol{k}}} \sum_{\boldsymbol{k}} v^{T,+-}_{\boldsymbol{k},\boldsymbol{q}} \left(\frac{1}{i\omega_m + U} - \frac{1}{i\omega_m - U}\right). \tag{121}$$

Here we can see that the excitation energies are of order $U$, and not of the order of the superexchange couplings as we would expect for the Hubbard model.

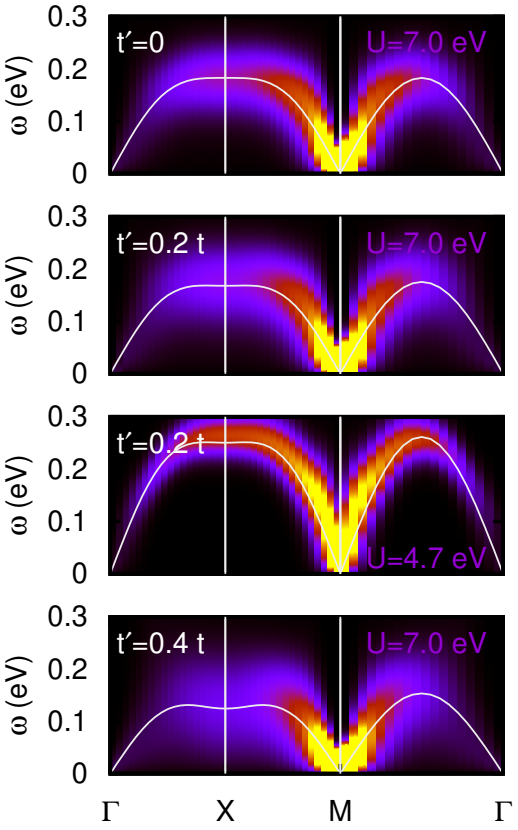


**Fig. 21:** *DMFT spin-wave spectra for fixed* $t$ *and representative values of* $t'$*. The white lines are linear spin-wave curves calculated using super-exchange couplings* $J_1 = \frac{4t^2}{U}$ *and* $J_2 = \frac{4(t')^2}{U}$*. Rearranged from Ref. [19].*

In order to recover the correct behavior we have to solve the Bethe-Salpeter equation. To this end we have first to return to the site-dependent tensor, since we have to invert the associated $n_s \times n_s$ matrices. Using the transverse susceptibility as representative case, the relevant matrix elements in the ordered phase are

$$\chi^{0;i_c i'_c}_{\sigma-\sigma-\sigma\sigma}(\boldsymbol{q}; i\omega_m) \approx \left( -\frac{a^{i_c i'_c}_{\sigma}(\boldsymbol{q})}{i\omega_n - U} + \frac{a^{i_c i'_c}_{-\sigma}(\boldsymbol{q})}{i\omega_n + U} \right) e^{-i\boldsymbol{q}\cdot(\boldsymbol{T}_{i_c} - \boldsymbol{T}_{i'_c})}, \tag{122}$$

where

$$a^{i_c i'_c}_{\sigma}(\boldsymbol{q}) = \frac{1}{N_{\boldsymbol{k}}} \sum_{\boldsymbol{k}} \sum_{pp'} w^{i_c i'_c}_{\sigma \boldsymbol{k} p} w^{i'_c i_c}_{-\sigma \boldsymbol{k}+\boldsymbol{q} p'} \delta_{p,+} \delta_{p,-}. \tag{123}$$

In the $t \ll U$ limit, at linear order in $J_1/U$ we have

$$a^{11}_{\sigma}(\boldsymbol{q}) = a^{22}_{-\sigma}(\boldsymbol{q}) \approx \frac{1}{4}(1-s_\sigma)^2 + s_\sigma(1-s_\sigma)\frac{J_1}{U}, \tag{124}$$

$$a^{12}_{\sigma}(\boldsymbol{q}) = a^{21}_{-\sigma}(\boldsymbol{q}) \approx -\frac{J_1}{U} f_{\boldsymbol{q}}, \tag{125}$$

where $f_{\boldsymbol{q}} = (\cos q_x + \cos q_y)/2$. The $i_c{=}i'_c$ elements are therefore independent on $\boldsymbol{q}$ at order $J_1/U$. By inverting the susceptibility matrix with the elements defined above we thus obtain, at

sufficiently low frequency

$$\left[\frac{1}{\chi^0(\boldsymbol{q};i\omega_m)}-\frac{1}{\chi^0(i\omega_m)}\right]^{i_c i'_c}_{\sigma-\sigma-\sigma\sigma}\approx 2J_1 f_{\boldsymbol{q}}(1-\delta_{i_c i'_c})e^{-i\boldsymbol{q}\cdot(\boldsymbol{T}_{i_c}-\boldsymbol{T}_{i'_c})} \tag{126}$$

By adding to this the inverse of the local susceptibility matrix

$$\chi^{i_c i'_c}_{\sigma-\sigma-\sigma\sigma}(i\omega_m)\approx\left(-\frac{a^{i_c i'_c}_{\sigma}}{i\omega_n-2J_1}+\frac{a^{i_c i'_c}_{-\sigma}}{i\omega_n+2J_1}\right)\delta_{i_c,i'_c}$$

with $a^{i_c i'_c}_{\sigma}=\frac{1}{N_{\boldsymbol{q}}}\sum_{\boldsymbol{q}}a^{i_c i'_c}_{\sigma}(\boldsymbol{q})$. Inverting again, we finally obtain

$$\chi^{\perp}(\boldsymbol{q};i\omega_m)=\frac{(g\mu_B)^2}{4}\sum_{\sigma}\frac{1}{2}\sum_{i_c i'_c}\chi^{i_c i'_c}_{\sigma-\sigma-\sigma\sigma}(\mathbf{q};i\omega_m)e^{i\boldsymbol{q}\cdot(\boldsymbol{T}_{i_c}-\boldsymbol{T}_{i'_c})} \tag{127}$$

$$\approx(g\mu_B)^2\frac{J_1(1-f_{\boldsymbol{q}})}{\omega_m^2+4J_1^2(1-f_{\boldsymbol{q}}^2)}, \tag{128}$$

which is the expected behavior for a Heisenberg antiferromagnet. The result of actual DMFT calculations is shown in Fig. 19 and Fig. 21. More details can be found in Ref. [19].

# 4 Conclusion

The LDA+DMFT approach and its extension has proved very successful for describing correlated materials. It has shown us that materials details do matter, contrarily to what often was assumed in the past; for example a crystal field much smaller than the bandwidth can favor the Mott metal-insulator transition [18]. The method is becoming progressively more and more versatile. It is now possible, e.g., to study multi-orbital Hubbard-like models including the full Coulomb vertex and the spin-orbit interaction. Successful extension schemes, e.g., cluster methods, account, at least in part, for the $\boldsymbol{q}$-dependence of the self-energy. In this lecture, we have seen how to use the LDA+DMFT approach to calculate not only Green and spectral functions but also linear-response functions. In the scheme presented, the local susceptibility is obtained via the quantum-impurity solver at the end of the self-consistency loop; the $\boldsymbol{q}$-dependent susceptibility is, instead, calculated solving in addition the Bethe-Salpeter equation in the local-vertex approximation. As representative case we have studied the magnetic susceptibility of the one-band Hubbard model at half filling. The extension of the LDA+DMFT approach to the calculation of generalized susceptibilities makes it possible to put the method and the approximations adopted to more stringent tests. This is key for further advancing the theoretical tools for the description of strong correlation effects in real materials.

# Appendix

## A Eigenstates of Hubbard dimer and Anderson molecule

The Hamiltonian of the **Hubbard dimer** is given by

$$\hat{H} = \varepsilon_d \sum_\sigma \sum_{i=1,2} \hat{n}_{i\sigma} - t \sum_\sigma \left( c^\dagger_{1\sigma} c_{2\sigma} + c^\dagger_{2\sigma} c_{1\sigma} \right) + U \sum_{i=1,2} \hat{n}_{i\uparrow} \hat{n}_{i\downarrow}.$$

It commutes with the number of electron operator $\hat{N}$, with the total spin $\hat{S}$ and with $\hat{S}_z$. Thus we can express the many-body states in the atomic limit as

| $\|N,S,S_z\rangle$ | | | $N$ | $S$ | $E(N,S)$ |
|---|---|---|---|---|---|
| $\|0,0,0\rangle$ | $=$ | $\|0\rangle$ | 0 | 0 | 0 |
| $\|1,1/2,\sigma\rangle_1$ | $=$ | $c^\dagger_{1\sigma}\|0\rangle$ | 1 | $1/2$ | $\varepsilon_d$ |
| $\|1,1/2,\sigma\rangle_2$ | $=$ | $c^\dagger_{2\sigma}\|0\rangle$ | 1 | $1/2$ | $\varepsilon_d$ |
| $\|2,1,1\rangle$ | $=$ | $c^\dagger_{2\uparrow}c^\dagger_{1\uparrow}\|0\rangle$ | 2 | 1 | $2\varepsilon_d$ |
| $\|2,1,-1\rangle$ | $=$ | $c^\dagger_{2\downarrow}c^\dagger_{1\downarrow}\|0\rangle$ | 2 | 1 | $2\varepsilon_d$ |
| $\|2,1,0\rangle$ | $=$ | $\frac{1}{\sqrt{2}}\left(c^\dagger_{1\uparrow}c^\dagger_{2\downarrow} + c^\dagger_{1\downarrow}c^\dagger_{2\uparrow}\right)\|0\rangle$ | 2 | 1 | $2\varepsilon_d$ |
| $\|2,0,0\rangle_0$ | $=$ | $\frac{1}{\sqrt{2}}\left(c^\dagger_{1\uparrow}c^\dagger_{2\downarrow} - c^\dagger_{1\downarrow}c^\dagger_{2\uparrow}\right)\|0\rangle$ | 2 | 0 | $2\varepsilon_d$ |
| $\|2,0,0\rangle_1$ | $=$ | $c^\dagger_{1\uparrow}c^\dagger_{1\downarrow}\|0\rangle$ | 2 | 0 | $2\varepsilon_d + U$ |
| $\|2,0,0\rangle_2$ | $=$ | $c^\dagger_{2\uparrow}c^\dagger_{2\downarrow}\|0\rangle$ | 2 | 0 | $2\varepsilon_d + U$ |
| $\|3,1/2,\sigma\rangle_1$ | $=$ | $c^\dagger_{1\sigma}c^\dagger_{2\uparrow}c^\dagger_{2\downarrow}\|0\rangle$ | 3 | $1/2$ | $3\varepsilon_d + U$ |
| $\|3,1/2,\sigma\rangle_2$ | $=$ | $c^\dagger_{2\sigma}c^\dagger_{1\uparrow}c^\dagger_{1\downarrow}\|0\rangle$ | 3 | $1/2$ | $3\varepsilon_d + U$ |
| $\|4,0,0\rangle$ | $=$ | $c^\dagger_{1\uparrow}c^\dagger_{1\downarrow}c^\dagger_{2\uparrow}c^\dagger_{2\downarrow}\|0\rangle$ | 4 | 0 | $4\varepsilon_d + 2U$ |

Let us order the $N = 1$ states as in the table above, first the spin up and then spin down block. For finite $t$ the Hamiltonian matrix for $N = 1$ electrons takes then the form

$$\hat{H}_1 = \begin{pmatrix} \varepsilon_d & -t & 0 & 0 \\ -t & \varepsilon_d & 0 & 0 \\ 0 & 0 & \varepsilon_d & -t \\ 0 & 0 & -t & \varepsilon_d \end{pmatrix}.$$

This matrix can be easily diagonalized and yields the *bonding* $(-)$ and *antibonding* $(+)$ states

| $\|1,S,S_z\rangle_\alpha$ | $E_\alpha(1,S)$ | $d_\alpha(1,S)$ |
|---|---|---|
| $\|1,1/2,\sigma\rangle_+ = \frac{1}{\sqrt{2}}\big(\|1,1/2,\sigma\rangle_1 - \|1,1/2,\sigma\rangle_2\big)$ | $\varepsilon_d{+}t$ | 2 |
| $\|1,1/2,\sigma\rangle_- = \frac{1}{\sqrt{2}}\big(\|1,1/2,\sigma\rangle_1 + \|1,1/2,\sigma\rangle_2\big)$ | $\varepsilon_d{-}t$ | 2 |

where $d_\alpha(N)$ is the spin degeneracy of the $\alpha$ manifold.
For $N=2$ electrons (half filling), the hopping integrals only couple the three $S=0$ states, and therefore the Hamiltonian matrix is given by

$$\hat{H}_2 = \begin{pmatrix} 2\varepsilon_d & 0 & 0 & 0 & 0 & 0 \\ 0 & 2\varepsilon_d & 0 & 0 & 0 & 0 \\ 0 & 0 & 2\varepsilon_d & 0 & 0 & 0 \\ 0 & 0 & 0 & 2\varepsilon_d & -\sqrt{2}t & -\sqrt{2}t \\ 0 & 0 & 0 & -\sqrt{2}t & 2\varepsilon_d+U & 0 \\ 0 & 0 & 0 & -\sqrt{2}t & 0 & 2\varepsilon_d+U \end{pmatrix}.$$

The eigenvalues and the corresponding eigenvectors are

| $\|2,S,S_z\rangle_\alpha$ | $E_\alpha(2,S)$ | $d_\alpha(2,S)$ |
|---|---|---|
| $\|2,0,0\rangle_+ = a_1\|2,0,0\rangle_0 - \frac{a_2}{\sqrt{2}}\big(\|2,0,0\rangle_1 + \|2,0,0\rangle_2\big)$ | $2\varepsilon_d + \frac{1}{2}\big(U{+}\Delta(t,U)\big)$ | 1 |
| $\|2,0,0\rangle_o = \frac{1}{\sqrt{2}}\big(\|2,0,0\rangle_1 - \|2,0,0\rangle_2\big)$ | $2\varepsilon_d + U$ | 1 |
| $\|2,1,m\rangle_o = \|2,1,m\rangle$ | $2\varepsilon_d$ | 3 |
| $\|2,0,0\rangle_- = a_2\|2,0,0\rangle_0 + \frac{a_1}{\sqrt{2}}\big(\|2,0,0\rangle_1 + \|2,0,0\rangle_2\big)$ | $2\varepsilon_d + \frac{1}{2}\big(U{-}\Delta(t,U)\big)$ | 1 |

where

$$\Delta(t,U) = \sqrt{U^2+16t^2},$$

and

$$a_1^2 = a_1^2(t,U) = \frac{1}{\Delta(t,U)}\frac{\Delta(t,U)-U}{2} \qquad a_2^2 = a_2^2(t,U) = \frac{4t^2}{\Delta(t,U)}\frac{2}{(\Delta(t,U)-U)},$$

so that $a_1 a_2 = 2t/\Delta(t,U)$. For $U=0$ we have $a_1 = a_2 = 1/\sqrt{2}$, and the two states $|2,0,0\rangle_-$ and $|2,0,0\rangle_+$ become, respectively, the state with two electrons in the bonding orbital and the state with two electrons in the antibonding orbital; they have energy $E_\pm(2,0) = 2\varepsilon_d \pm 2t$; the remaining states have energy $2\varepsilon_d$ and are non-bonding. For $t>0$, the ground state is unique and it is always the singlet $|2,0,0\rangle_-$; in the large $U$ limit its energy is

$$E_-(2,0) \sim 2\varepsilon_d - 4t^2/U.$$

In this limit the energy difference between the first excited state, a triplet state, and the singlet ground state is thus equal to the Heisenberg antiferromagnetic coupling

$$E_o(2,1) - E_-(2,0) \sim 4t^2/U = \Gamma.$$

Finally, for $N = 3$ electrons, eigenstates and eigenvectors are

| $\|3,S,S_z\rangle_\alpha$ | | $E_\alpha(3)$ | $d_\alpha(3,S)$ |
|---|---|---|---|
| $\|3,1/2,\sigma\rangle_+$ | $= \frac{1}{\sqrt{2}}\big(\|1,1/2,\sigma\rangle_1 + \|1,1/2,\sigma\rangle_2\big)$ | $3\varepsilon_d + U + t$ | 2 |
| $\|3,1/2,\sigma\rangle_-$ | $= \frac{1}{\sqrt{2}}\big(\|1,1/2,\sigma\rangle_1 - \|1,1/2,\sigma\rangle_2\big)$ | $3\varepsilon_d + U - t$ | 2 |

If we exchange holes and electrons, the $N = 3$ case is identical to the $N = 1$ electron case. This is due to the particle-hole symmetry of the model.

The Hamiltonian of the **Anderson molecule** is given by

$$\hat{H} = \varepsilon_s \sum_\sigma \hat{n}_{2\sigma} - t \sum_\sigma \left(c^\dagger_{1\sigma} c_{2\sigma} + c^\dagger_{2\sigma} c_{1\sigma}\right) + \varepsilon_d \sum_\sigma \hat{n}_{1\sigma} + U \hat{n}_{1\uparrow}\hat{n}_{1\downarrow}.$$

In the atomic limit, its eigenstates states can be classified as

| $\|N,S,S_z\rangle$ | | | $N$ | $S$ | $E(N,S)$ |
|---|---|---|---|---|---|
| $\|0,0,0\rangle$ | $=$ | $\|0\rangle$ | 0 | 0 | 0 |
| $\|1,1/2,\sigma\rangle_1$ | $=$ | $c^\dagger_{1\sigma}\|0\rangle$ | 1 | 1/2 | $\varepsilon_d$ |
| $\|1,1/2,\sigma\rangle_2$ | $=$ | $c^\dagger_{2\sigma}\|0\rangle$ | 1 | 1/2 | $\varepsilon_s$ |
| $\|2,1,1\rangle$ | $=$ | $c^\dagger_{2\uparrow}c^\dagger_{1\uparrow}\|0\rangle$ | 2 | 1 | $\varepsilon_d + \varepsilon_s$ |
| $\|2,1,-1\rangle$ | $=$ | $c^\dagger_{2\downarrow}c^\dagger_{1\downarrow}\|0\rangle$ | 2 | 1 | $\varepsilon_d + \varepsilon_s$ |
| $\|2,1,0\rangle$ | $=$ | $\frac{1}{\sqrt{2}}\left(c^\dagger_{1\uparrow}c^\dagger_{2\downarrow} + c^\dagger_{1\downarrow}c^\dagger_{2\uparrow}\right)\|0\rangle$ | 2 | 1 | $\varepsilon_d + \varepsilon_s$ |
| $\|2,0,0\rangle_0$ | $=$ | $\frac{1}{\sqrt{2}}\left(c^\dagger_{1\uparrow}c^\dagger_{2\downarrow} - c^\dagger_{1\downarrow}c^\dagger_{2\uparrow}\right)\|0\rangle$ | 2 | 0 | $\varepsilon_d + \varepsilon_s$ |
| $\|2,0,0\rangle_1$ | $=$ | $c^\dagger_{1\uparrow}c^\dagger_{1\downarrow}\|0\rangle$ | 2 | 0 | $2\varepsilon_d + U$ |
| $\|2,0,0\rangle_2$ | $=$ | $c^\dagger_{2\uparrow}c^\dagger_{2\downarrow}\|0\rangle$ | 2 | 0 | $2\varepsilon_s$ |
| $\|3,1/2,\sigma\rangle_1$ | $=$ | $c^\dagger_{1\sigma}c^\dagger_{2\uparrow}c^\dagger_{2\downarrow}\|0\rangle$ | 3 | 1/2 | $\varepsilon_d + 2\varepsilon_s$ |
| $\|3,1/2,\sigma\rangle_2$ | $=$ | $c^\dagger_{2\sigma}c^\dagger_{1\uparrow}c^\dagger_{1\downarrow}\|0\rangle$ | 3 | 1/2 | $2\varepsilon_d + \varepsilon_s + U$ |
| $\|4,0,0\rangle$ | $=$ | $c^\dagger_{1\uparrow}c^\dagger_{1\downarrow}c^\dagger_{2\uparrow}c^\dagger_{2\downarrow}\|0\rangle$ | 4 | 0 | $2\varepsilon_d + 2\varepsilon_s + U$ |

For $N = 1$ electrons the Hamiltonian can be written in the matrix form

$$\hat{H}_1 = \begin{pmatrix} \varepsilon_d & -t & 0 & 0 \\ -t & \varepsilon_s & 0 & 0 \\ 0 & 0 & \varepsilon_d & -t \\ 0 & 0 & -t & \varepsilon_s \end{pmatrix}.$$

The eigenstates are thus

| $\lvert 1, S, S_z\rangle_\alpha$ | $E_\alpha(1,S)$ | $d_\alpha(1,S)$ |
|---|---|---|
| $\lvert 1,1/2,\sigma\rangle_+ = \alpha_1\lvert 1,1/2,\sigma\rangle_1 - \alpha_2\lvert 1,1/2,\sigma\rangle_2$ | $\frac{1}{2}\big(\varepsilon_d+\varepsilon_s+\sqrt{(\varepsilon_d-\varepsilon_s)^2+4t^2}\big)$ | 2 |
| $\lvert 1,1/2,\sigma\rangle_- = \alpha_2\lvert 1,1/2,\sigma\rangle_1 + \alpha_1\lvert 1,1/2,\sigma\rangle_2$ | $\frac{1}{2}\big(\varepsilon_d+\varepsilon_s-\sqrt{(\varepsilon_d-\varepsilon_s)^2+4t^2}\big)$ | 2 |

where $d_\alpha(N)$ is the spin degeneracy of the $\alpha$ manifold. For $\varepsilon_s = \varepsilon_d + U/2$ the eigenvalues are

$$E_\pm(1,S) = \varepsilon_d + \frac{1}{4}\big(U \pm \Delta(t,U)\big),$$

while the coefficients are $\alpha_1 = a_1(t,U)$ and $\alpha_2 = a_2(t,U)$.
For $N$=2 electrons, the hopping integrals only couple the $S$=0 states. The Hamiltonian is

$$\hat{H}_2 = \begin{pmatrix} \varepsilon_d{+}\varepsilon_s & 0 & 0 & 0 & 0 & 0 \\ 0 & \varepsilon_d{+}\varepsilon_s & 0 & 0 & 0 & 0 \\ 0 & 0 & \varepsilon_d{+}\varepsilon_s & 0 & 0 & 0 \\ 0 & 0 & 0 & \varepsilon_d{+}\varepsilon_s & -\sqrt{2}t & -\sqrt{2}t \\ 0 & 0 & 0 & -\sqrt{2}t & 2\varepsilon_d{+}U & 0 \\ 0 & 0 & 0 & -\sqrt{2}t & 0 & 2\varepsilon_s \end{pmatrix}$$

For $\varepsilon_s = \varepsilon_d + U/2$ the eigenvalues and the corresponding eigenvectors are

| $\lvert 2, S, S_z\rangle_\alpha$ | $E_\alpha(2,S)$ | $d_\alpha(2,S)$ |
|---|---|---|
| $\lvert 2,0,0\rangle_+ = b_1\lvert 2,0,0\rangle_0 - \frac{b_2}{\sqrt{2}}\big(\lvert 2,0,0\rangle_1 + \lvert 2,0,0\rangle_2\big)$ | $2\varepsilon_d + \frac{U}{2} + \frac{1}{4}\big(U{+}2\Delta(t,\frac{U}{2})\big)$ | 1 |
| $\lvert 2,0,0\rangle_o = \frac{1}{\sqrt{2}}\big(\lvert 2,0,0\rangle_1 - \lvert 2,0,0\rangle_2\big)$ | $2\varepsilon_d + U$ | 1 |
| $\lvert 2,1,m\rangle_o = \lvert 2,1,m\rangle$ | $2\varepsilon_d + \frac{U}{2}$ | 3 |
| $\lvert 2,0,0\rangle_- = b_2\lvert 2,0,0\rangle_0 + \frac{b_1}{\sqrt{2}}\big(\lvert 2,0,0\rangle_1 + \lvert 2,0,0\rangle_2\big)$ | $2\varepsilon_d + \frac{U}{2} + \frac{1}{4}\big(U{-}2\Delta(t,\frac{U}{2})\big)$ | 1 |

where $b_1 = a_1(t,U/2)$ and $b_2 = a_2(t,U/2)$. These states have the same form as in the case of the Hubbard dimer; the ground state energy and the weight of doubly occupied states in $\lvert 2,0,0\rangle_-$ differ, however. Finally, for $N = 3$ electrons, the eigenstates are

| $\lvert 3, S, S_z\rangle_\alpha$ | $E_\alpha(3,S)$ | $d_\alpha(3,S)$ |
|---|---|---|
| $\lvert 3,1/2,\sigma\rangle_+ = \alpha_2\lvert 1,1/2,\sigma\rangle_1 + \alpha_1\lvert 1,1/2,\sigma\rangle_2$ | $3\varepsilon_d + U + \frac{1}{4}\big(U{+}\Delta(t,U)\big)$ | 2 |
| $\lvert 3,1/2,\sigma\rangle_- = \alpha_1\lvert 1,1/2,\sigma\rangle_1 - \alpha_2\lvert 1,1/2,\sigma\rangle_2$ | $3\varepsilon_d + U + \frac{1}{4}\big(U{-}\Delta(t,U)\big)$ | 2 |

# B Lehmann representation of the local Green function

For a single-orbital model, the local Matsubara Green function for a given site $i$ is defined as

$$G^{\sigma}_{i,i}(i\nu_n) = -\int_0^{\beta} d\tau e^{i\nu_n\tau}\big\langle \mathcal{T} c_{i\sigma}(\tau)c^{\dagger}_{i\sigma}(0)\big\rangle,$$

where $\mathcal{T}$ is the time-ordering operator, $\beta = 1/k_BT$, and $\nu_n$ a fermionic Matsubara frequency. Let us assume we know all eigenstates $|N_l\rangle$ and their energy $E_l(N)$, for arbitrary number of electrons $N$. Thus, formally

$$G^{\sigma}_{i,i}(i\nu_n) = -\frac{1}{Z}\sum_{Nl}\int_0^{\beta} d\tau e^{i\nu_n\tau}e^{-\Delta E_l(N)\beta}\big\langle N_l\big|c_{i\sigma}(\tau)c^{\dagger}_{i\sigma}(0)\big|N_l\big\rangle,$$

where $Z = \sum_{Nl} e^{-\Delta E_l(N)\beta}$ is the partition function, $\Delta E_l(N) = E_l(N) - \mu N$ with $\mu$ the chemical potential, and $c^{\dagger}_{i\sigma}(0) = c^{\dagger}_{i\sigma}$. We now insert a complete set of states, obtaining

$$\begin{aligned} G^{\sigma}_{i,i}(i\nu_n) &= -\frac{1}{Z}\sum_{ll'NN'}\int_0^{\beta} d\tau e^{i\nu_n\tau}e^{-\Delta E_l(N)\beta}\big\langle N_l\big|c_{i\sigma}(\tau)|N'_{l'}\big\rangle\big\langle N'_{l'}\big|c^{\dagger}_{i\sigma}\big|N_l\big\rangle \\ &= -\frac{1}{Z}\sum_{ll'NN'}\int_0^{\beta} d\tau e^{-\Delta E_l(N)\beta}e^{(i\nu_n+\Delta E_l(N)-\Delta E_{l'}(N'))\tau}\big|\langle N'_{l'}|c^{\dagger}_{i\sigma}|N_l\rangle\big|^2 \\ &= \frac{1}{Z}\sum_{ll'NN'}\frac{e^{-\Delta E_{l'}(N')\beta}+e^{-\Delta E_l(N)\beta}}{i\nu_n+\Delta E_l(N)-\Delta E_{l'}(N')}\big|\langle N'_{l'}|c^{\dagger}_{i\sigma}|N_l\rangle\big|^2. \end{aligned}$$

Due to the weight $\big|\langle N'_{l'}|c^{\dagger}_{i\sigma}(0)|N_l\rangle\big|^2$ only the terms for which $N' = N+1$ contribute. Thus, after exchanging the labels $l'N' \leftrightarrow lN$ in the first addend, we obtain the Lehmann representation

$$G^{\sigma}_{i,i}(i\nu_n)=\sum_{ll'N}\frac{e^{-\beta\Delta E_l(N)}}{Z}\left(\frac{\big|\langle(N-1)_{l'}|c_{i\sigma}|N_l\rangle\big|^2}{i\nu_n-\Delta E_l(N)+\Delta E_{l'}(N-1)}+\frac{\big|\langle(N+1)_{l'}|c^{\dagger}_{i\sigma}|N_l\rangle\big|^2}{i\nu_n-\Delta E_{l'}(N+1)+\Delta E_l(N)}\right).$$

Let us consider as example the atomic limit of the Hubbard model at half filling. In this case all sites are decoupled; there are four eigenstates per site, the vacuum $|0\rangle$, with $\Delta E(0) = 0$, the doublet $|1_\sigma\rangle = c^{\dagger}_{i\sigma}|0\rangle$, with $\Delta E_\sigma(1) = -U/2$, and the doubly-occupied singlet $|2\rangle = c^{\dagger}_{i\uparrow}c^{\dagger}_{i\downarrow}|0\rangle$, with $\Delta E(2) = 0$. Furthermore, $Z = 2(1+e^{\beta U/2})$ and

$$\big|\langle(N-1)_{l'}|c_{i\sigma}|N_l\rangle\big|^2=\begin{cases}1 & \text{if } |N_l\rangle=|2\rangle\vee|1_\sigma\rangle\\ 0 & \text{otherwise}\end{cases}\qquad \big|\langle(N+1)_{l'}|c^{\dagger}_{i\sigma}|N_l\rangle\big|^2=\begin{cases}1 & \text{if } |N_l\rangle=|0\rangle\vee|1_{-\sigma}\rangle\\ 0 & \text{otherwise}\end{cases}$$

Thus, after summing up the four non-zero contributions, we find

$$G^{\sigma}_{i,i}(\nu_n) = \frac{1}{2}\left(\frac{1}{i\nu_n+U/2}+\frac{1}{i\nu_n-U/2}\right).$$

# C Atomic magnetic susceptibility

Let us consider an idealized single-level atom described by the Hamiltonian

$$\hat{H} = \varepsilon_d\big(\hat{n}_\uparrow + \hat{n}_\downarrow\big) + U n_\uparrow n_\downarrow.$$

The eigenstates of this system, $|\Psi_i^N\rangle$, as well as their expectation values at half filling are

| $\lvert\Psi_i^N\rangle$ | $N$ | $\Delta E_i = \langle\Psi_i^N\lvert\hat{H}-\mu\hat{N}\rvert\Psi_i^N\rangle$ |
|---|---|---|
| $\lvert 0\rangle$ | 0 | 0 |
| $c_\sigma^\dagger\lvert 0\rangle$ | 1 | $-\frac{U}{2}$ |
| $c_\uparrow^\dagger c_\downarrow^\dagger\lvert 0\rangle$ | 2 | 0 |

The magnetic susceptibility in Matsubara space is given by

$$\Big[\chi_{zz}(i\omega_m)\Big]_{nn'} = \beta\frac{1}{4}(g\mu_B)^2\sum_P \mathrm{sign}(P) f_P$$

$$f_P(i\omega_{P_1}, i\omega_{P_2}, i\omega_{P_3}) = \int_0^\beta d\tau_{14}\int_0^{\tau_{14}} d\tau_{24}\int_0^{\tau_{24}} d\tau_{34}\; e^{i\omega_{P_1}\tau_{14}+i\omega_{P_2}\tau_{24}+i\omega_{P_3}\tau_{34}} f_P(\tau_{14},\tau_{24},\tau_{34})$$

where $P = A, B, \ldots$ are the six possible permutations of the indices $(123)$ and

$$\begin{aligned} f_P(\tau_{14},\tau_{24},\tau_{34}) &= \frac{1}{Z}\sum_{\sigma\sigma'}\sigma\sigma'\mathrm{Tr}\; e^{-\beta(\hat{H}-\mu\hat{N})}\left[\hat{o}_{P_1}(\tau_{14})\hat{o}_{P_2}(\tau_{24})\hat{o}_{P_3}(\tau_{34})c_{\sigma'}^\dagger\right] \\ &= \frac{1}{Z}\sum_{\sigma\sigma'}\sigma\sigma'\sum_{ijkl} e^{-\beta\Delta E_i}\langle i|\hat{o}_{P_1}|j\rangle\langle j|\hat{o}_{P_2}|k\rangle\langle k|\hat{o}_{P_3}|l\rangle\langle l|c_{\sigma'}^\dagger|i\rangle \\ &\quad\times\left[e^{\Delta E_{ij}\tau_{14}+\Delta E_{jk}\tau_{24}+\Delta E_{kl}\tau_{34}}\right], \end{aligned}$$

where $\Delta E_{ij} = \Delta E_i - \Delta E_j$. For the identity permutation the operators are $\hat{o}_{P_1} = c_\sigma$, $\hat{o}_{P_2} = c_\sigma^\dagger$, and $\hat{o}_{P_3} = c_{\sigma'}$ and the frequencies are $\omega_1 = \nu_n$, $\omega_2 = -\omega_m - \nu_n$, $\omega_3 = \omega_m + \nu_{n'}$. This expression can be used to calculate the magnetic susceptibility of any one-band system whose eigenvalues and eigenvectors are known, e.g., via exact diagonalization. In the case of our idealized atom

$$f_E(\tau_{14},\tau_{24},\tau_{34}) = \frac{1}{(1+e^{\beta U/2})}\; e^{\beta U/2}\; e^{-(\tau_{12}+\tau_{34})U/2} = \frac{1}{(1+e^{\beta U/2})}\; g_E(\tau_{14},\tau_{24},\tau_{34}).$$

The frequencies and functions $f_P(\tau_{14},\tau_{24},\tau_{34})$ for all permutations are given in the table below

| | $\omega_{P_1}$ | $\omega_{P_2}$ | $\omega_{P_3}$ | $g_P(\tau_{14},\tau_{24},\tau_{34})$ | $\mathrm{sign}(P)$ |
|---|---|---|---|---|---|
| $E(123)$ | $\nu_n$ | $-\omega_m-\nu_n$ | $\omega_m+\nu_{n'}$ | $e^{\beta U/2}\; e^{-(\tau_{12}+\tau_{34})U/2}$ | $+$ |
| $A(231)$ | $-\omega_m-\nu_n$ | $\omega_m+\nu_{n'}$ | $\nu_n$ | $e^{\beta U/2}\; e^{-(\tau_{12}+\tau_{34})U/2}$ | $+$ |
| $B(312)$ | $\omega_m+\nu_{n'}$ | $\nu_n$ | $-\omega_m-\nu_n$ | $-e^{+(\tau_{12}+\tau_{34})U/2}$ | $+$ |
| $C(213)$ | $-\omega_m-\nu_n$ | $\nu_n$ | $\omega_m+\nu_{n'}$ | $-e^{\beta U/2}e^{-(\tau_{12}+\tau_{34})U/2}$ | $-$ |
| $D(132)$ | $\nu_n$ | $\omega_m+\nu_{n'}$ | $-\omega_m-\nu_n$ | $e^{+(\tau_{12}+\tau_{34})U/2}$ | $-$ |
| $F(321)$ | $\omega_m+\nu_{n'}$ | $-\omega_m-\nu_n$ | $\nu_n$ | $e^{+(\tau_{12}+\tau_{34})U/2}$ | $-$ |

The missing ingredient is the integral

$$
\begin{aligned}
I_P(x,-x,x;i\omega_{P_1},i\omega_{P_2},i\omega_{P_3}) &= \int_0^\beta d\tau_{14}\int_0^{\tau_{14}} d\tau_{24}\int_0^{\tau_{24}} d\tau_{34}\, e^{i\omega_{P_1}\tau_{14}+i\omega_{P_2}\tau_{24}+i\omega_{P_3}\tau_{34}} e^{x(\tau_{14}-\tau_{24}+\tau_{34})} \\
&= +\int_0^\beta d\tau_{14}\int_0^{\tau_{14}} d\tau\int_0^{\tau_{14}-\tau} d\tau'\, e^{(i\omega_{P_1}+i\omega_{P_2}+i\omega_{P_3}+x)\tau_{14}-i(\omega_{P_2}+\omega_{P_3})\tau} e^{-(i\omega_{P_3}+x)\tau'} \\
&= +\frac{1}{i\omega_{P_3}+x}\frac{1}{-i\omega_{P_2}+x}\left[\frac{1}{i\omega_{P_1}+x}\,\frac{1}{n(x)}+\beta\delta_{\omega_{P_1}+\omega_{P_2}}\right] \\
&\quad +\frac{1}{i\omega_{P_3}+x}\frac{1-\delta_{\omega_{P_2}+\omega_{P_3}}}{i(\omega_{P_2}+\omega_{P_3})}\left[\frac{1}{i\omega_{P_1}+x}-\frac{1}{i(\omega_{P_1}+\omega_{P_2}+\omega_{P_3})+x}\right]\frac{1}{n(x)} \\
&\quad +\delta_{\omega_{P_2}+\omega_{P_3}}\frac{1}{i\omega_{P_3}+x}\left\{\left[\frac{1}{(i\omega_{P_1}+x)}\right]^2\frac{1}{n(x)}-\beta\left[\frac{1}{(i\omega_{P_1}+x)}\right]\frac{1-n(x)}{n(x)}\right\}.
\end{aligned}
$$

where $x=\pm U/2$, depending on the permutation. Summing up all terms we obtain the final expression for $\omega_m=0$. Setting $y=U/2$ we have in total [11]

$$
\begin{aligned}
\sum_{\sigma\sigma'}\sigma\sigma'\,\chi^{n,n'}_{i\sigma\sigma,i\sigma'\sigma'}(0) =& M_{n'}\frac{dM_n}{dy}+M_n\frac{dM_{n'}}{dy}-\beta n(y)\left[\delta_{n,n'}+\delta_{n,-n'}\right]\frac{dM_n}{dy}+\beta n(-y)M_nM_{n'} \\
&-\frac{1}{y}\left\{M_{n'}-\beta\left[n(y)\delta_{n,-n'}-n(-y)\delta_{n,n'}\right]\right\}M_n
\end{aligned}
\tag{129}
$$

where

$$
M_n=\frac{1}{i\nu_n-y}-\frac{1}{i\nu_n+y}. \tag{130}
$$

The finite frequency term (not given here) vanishes once we sum over $n,n'$.

# References


[1] W. Metzner and D. Vollhardt, Phys. Rev. Lett. **62**, 324 (1989)

[2] E. Müller-Hartmann, Z. Phys. B **74**, 507 (1989); Z. Phys. B **76**, 211 (1989); Int. J. Mod. Phys. B **3**, 2169 (1989)

[3] A. Georges and G. Kotliar, Phys. Rev. B **45**, 6479 (1992)

[4] M. Jarrell, Phys. Rev. Lett. **69**, 168 (1992)

[5] E. Pavarini, E. Koch, D. Vollhardt, A. Lichtenstein (Eds.): *The LDA+DMFT approach to strongly-correlated materials*, Reihe Modeling and Simulation, Vol. 1 (Forschungszentrum Jülich, 2011) http://www.cond-mat.de/events/correl11

[6] E. Pavarini, E. Koch, A. Lichtenstein, D. Vollhardt (Eds.): *DMFT at 25: Infinite Dimensions*, Reihe Modeling and Simulation, Vol. 4 (Forschungszentrum Jülich, 2014) http://www.cond-mat.de/events/correl14

[7] E. Pavarini, E. Koch, A. Lichtenstein, D. Vollhardt (Eds.): *DMFT: From Infinite Dimensions to Real Materials*, Reihe Modeling and Simulation, Vol. 8 (Forschungszentrum Jülich, 2018) http://www.cond-mat.de/events/correl18

[8] E. Koch, G. Sangiovanni, and O. Gunnarsson, Phys. Rev. B **78**, 115102 (2008)

[9] E. Gull, A.J. Millis, A.I. Lichtenstein, A.N. Rubtsov, M. Troyer, and P. Werner, Rev. Mod. Phys. **83**, 349 (2011)

[10] A. Flesch, E. Gorelov, E. Koch, E. Pavarini, Phys. Rev. B **87**, 195141 (2013)

[11] A. Kiani and E. Pavarini, Phys. Rev. B **94**, 075112 (2016)

[12] E. Pavarini, A. Yamasaki, J. Nuss, and O.K. Andersen, New. J. Phys **7**, 188 (2005)

[13] N. Marzari *et al.*, Rev. Mod. Phys. **84**, 1419 (2012)

[14] V. Slatić and B. Horvatić, Sol. Stat. Comm. **75**, 263 (1990)

[15] L. Boehnke, H. Hafermann, M. Ferrero, F. Lechermann and O. Parcollet, Phys. Rev. B **84**, 075145 (2011)

[16] J. Musshoff, G. Zhang, E. Koch, and E. Pavarini, Phys. Rev. B **100**, 045116 (2019)

[17] A. Georges, G. Kotliar, W. Krauth and M.J. Rozenberg, Rev. Mod. Phys. **68**, 13 (1996)

[18] E. Pavarini *et al.*, Phys. Rev. Lett. **92**, 176403 (2004)

[19] J. Musshoff, A. Kiani and E. Pavarini, Phys. Rev. B **103**, 075136 (2021)